POSSIBLE MECHANISMS OF EXPLOSIVE MARITIME CYCLOGENESIS

by

PAUL JOSEPH ROEBBER

B. Sc. McGill University
(1981)

Submitted to the Department of Meteorology and Physical Oceanography
in partial fulfillment of the requirements of the
Degree of Master of Science
at the
Massachusetts Institute of Technology

June 1983

Signature of Author_____
Department of Meteorology and Physical Oceanography
May 6, 1983

Certified by_____
Thesis Supervisor

Accepted by_____
Chairman, Departmental Committee on Graduate Students

POSSIBLE MECHANISMS OF EXPLOSIVE MARITIME CYCLOGENESIS

by

PAUL JOSEPH ROEBBER

Submitted to the Department of Meteorology and Physical Oceanography on May 6, 1983 in partial fulfillment of the requirements for the Degree of Master of Science

ABSTRACT

A statistical analysis of 12 and 24 hour deepening rates for all surface lows analyzed on at least two successive NMC 12 hourly hemispheric surface charts was performed for one full year of data. The basis of the analysis was the Central Limit Theorem of Statistics, which would require an approximate Gaussian distribution of deepening rates, provided the mechanism(s) of deepening was (were) identical in all cases. Statistically significant deviations from the normal curve were found in both the 12 and 24 hour studies, with the largest deviations occurring along the tail of the distribution associated with most rapid deepening. An attempt was made to iteratively fit two normal curves of different means and standard deviations to the deepening spectra; the attempt was successful in both the 12 and 24 hour cases, suggesting that most cases of explosive cyclogenesis are the result of some physical mechanism in addition to or other than ordinary baroclinic instability.

The climatology of explosive cyclones (Sanders and Gyakum, 1980) was updated to include the 1979-82 cold seasons. In addition, a climatology of formation positions, maximum deepening positions, and dissipation positions for all cyclones in a one year data sample was compiled. These studies suggested that the preferred regions of explosive cyclogenesis are primarily baroclinic zones; the climatological and statistical evidence therefore suggests that the explosive mechanism is a combination of the baroclinic process and some other mechanism.

A quasi-geostrophic investigation of a particular formulation of the wave-CISK hypothesis was carried out on a sample of 18 explosively developing cyclones, using a modified version of the analytic baroclinic model suggested

by Sanders (1971) and Sanders and Gyakum (1980), with the CISK parameterization detailed in Mak (1982). An extrapolation of the instantaneous model results (with friction) was able to account for 67% of the sample variance in 12 hour deepening rates, and 14% at 24 hours. This was a significant improvement over the baroclinic model, which could account for only 2% of the 12 hour variance, and 27% at a range of 24 hours. It was suggested that the improvement in the baroclinic model at longer range was related to the problem of extrapolating instantaneous results rather than any improvement in forecast skill. Evidence was found to suggest that the postulated explosive forcing of atmospheric bombs, the CISK mechanism, is operative only for the period of most rapid deepening; subsequent balance is achieved between friction and the weaker, baroclinic forcing. A logical relationship between convective heating intensity and geographical location was established, with the axis of maximum heating intensity located slightly to the warm side of the mean Gulf Stream position.

An attempt was made to apply the model to the operational forecasting of explosive cyclogenesis, with generally poor results. It is suggested that this failure is related to the problem of forecasting the occurrence, duration, and intensity of the operative CISK mechanism, and that the key to forecasting explosive cyclogenesis is essentially in the better understanding of the initiation and continued evolution of cooperative convection embedded within the large scale flow.

Thesis Supervisor: Dr. Frederick Sanders

Title: Professor of Meteorology

TABLE OF CONTENTS

1.0 Introduction.....8

2.0 Statistical Analysis and Climatology of Cyclones...10

.1 Statistical Analysis.....12

.2 Climatology.....24

.1 Statistics of Deepening Cyclones.....24

.2 Geographic Distribution of Cyclones.....28

.3 Summary.....51

3.0 Application of an Analytic Model of Wave-CISK.....52

.1 Objectives.....52

.2 Review of Wave-CISK.....53

.3 Model Formulation.....56

.4 Model Climatology of Explosive Cyclones.....93

.5 Operational Forecasting of Explosive Cyclogenesis.108

4.0 Conclusions.....116

ACKNOWLEDGMENTS.....118

APPENDIX.....119

REFERENCES.....126

LIST OF FIGURES

2.01 12 hour deepening distribution (warm season)..... 16
.02 24 hour deepening distribution (warm season)..... 17
.03 12 hour deepening distribution (cold season)..... 18
.04 24 hour deepening distribution (cold season)..... 19
.05 24 hour deepening distribution / cold season sum.. 20
.06 12 hour deepening distribution (full year)..... 21
.07 24 hour deepening distribution (full year)..... 22
.08 24 hour deepening distribution / full year sum.... 23
.09 Table of confidence intervals
Table of deepening times (GMT)..... 26
.10 Length of deepening periods..... 27
.11 Formation positions (warm season)..... 32
.12 Formation positions (full year)..... 33
.13 Formation positions (Bombs)..... 34
.14 Maximum deepening positions (warm season)..... 35
.15 Maximum deepening positions (full year)..... 36
.16 Maximum deepening positions (Bombs)..... 37
.17 Maximum deepening positions, Bombs 1976-79..... 39
.18 Maximum deepening positions, Bombs 1979-82..... 40
.19 Maximum deepening positions, Bombs 1976-82..... 41
.20 Dissipation positions (warm season)..... 42
.21 Dissipation positions (full year)..... 43
.22 Dissipation positions (Bombs)..... 44

.23 700 mb height contours, May 1980.....47

.24 700 mb height contours, June 1980.....48

.25 700 mb height contours, July 1980.....49

.26 700 mb height contours, August 1980.....50

3.01 Model heating profiles.....61

.02 Model temperature profile.....64

.03 Model stability profile.....65

.04 Vertical motion profiles (baroclinic model).....67

.05 Vertical profile of friction.....70

.06 Vertical motion profile (CISK model).....73

.07 Vertical profile of frictional updraft.....74

.08 Type B CISK (geopotential tendency)

Type B CISK (phase speeds).....79

.09 Presidents' Day deepening profile (baroclinic)....85

.10 Presidents' Day deepening profile (CISK).....86

.11 Presidents' Day deepening profile (CISK cut off)..87

.12 Presidents' Day surface analysis (model).....88

.13 Presidents' Day 500 mb analysis (model).....89

.14 Presidents' Day surface analysis (observed).....90

.15 Presidents' Day 500 mb analysis (observed).....91

.16 Presidents' Day 500 mb vertical motion (observed).92

.17 Table of explosive cases modeled.....95

.18 Heating intensity distribution.....100

.19 Table of explosive cases (model results).....103

.20 Table of deepening periods (modeled/observed)....107

.21 Cases within satellite coverage 1980-81(Nov-Feb).111

.22 Cases within satellite coverage 1982-83(Nov-Feb). 112

.23 Table of operational forecasting results..... 115

1.0 Introduction

The emphasis of this research on explosively developing extratropical cyclones (bombs) has been twofold. The first goal has been to obtain some significant statistical evidence that such storms are in some way manifestations of a different physical process than ordinary baroclinic instability. Up to this point, there has been some question as to the actual existence of such phenomena as distinct physical entities, owing to inadequate data coverage over the oceans. The statistical approach provides a means of addressing this issue despite the minimal data available. The details of this analysis are discussed in the first section.

Assuming that such evidence is found, it would further be possible to formulate a definition of a "bomb" that is consistent with this evidence, and is therefore somewhat more meaningful than the current definition. Most importantly, however, it would provide incentive to investigate the possible physical mechanisms responsible for explosive cyclogenesis, such as the role of convective latent heat release. Related to these questions is the continuing effort to adequately forecast explosive deepening via computer or graphical methods. It has been hoped that such a method could be realized based on

parameters of the large scale flow (e.g., 1000-500 mb thickness); however, it would seem that if bombs are indeed a manifestation of some physical process other than or in addition to ordinary baroclinic instability, such efforts are doomed to mixed success, since presumably the mystery deepening process would be related in some fundamental way to smaller scale flow parameters.

The bulk effects of cumulus convection, which investigators such as Gyakum (1981), Sanders and Gyakum (1980), and Bosart (1981) have suggested are of possibly critical importance to the development of such storms, can be represented in terms of the large scale flow through the wave-CISK hypothesis discussed by Lindzen (1974) and Mak (1981) among others. Building on the results of the statistical analysis, the second section deals with an analytic model of wave-CISK as applied to cases of explosive cyclogenesis, and tests the feasibility of the formulation as a means for the forecasting of explosive cyclogenesis.

2.0 Statistical Analysis and Climatology of Cyclones

In order to carry out a statistical analysis of deepening rates, it was first necessary to acquire an adequate data base. All surface lows of a predominantly baroclinic nature (i.e., thermal lows and tropical storms were excluded) that were analyzed on at least two successive NMC 12 hourly hemispheric surface charts were tracked for the extent of their existence, beginning February 1980 and continuing through January 1981. The skewed one year sample was chosen as a result of missing data (February 1981) from the M.I.T. archives. The resultant break in continuity for the 1980-81 cold season is not believed to be serious, since the data set still represents an unbiased sample of one full year; in any case, we do not know a priori which particular season (if any) will show statistically significant deviations in deepening, since the cold season is more baroclinic, but not necessarily more or less Gaussian than the warm season.

The latitude/longitude coordinates and central pressure as analyzed on the NMC charts were recorded at 12 hour intervals for as long as each storm was maintained as a distinct entity. In some cases, the surface low moved off the map or else maps were missing; in other instances, a surface system of a tropical nature was transformed into

a middle latitude baroclinic disturbance. These situations were noted as they occurred, as they affected the subsequent treatment of the raw data. Once the data was recorded, it was condensed in the following manner: the formation position, position of maximum deepening, and dissipation position were recorded for each system, along with the date, time, and, magnitude of the maximum 12 and 24 hour pressure falls. The formation position was taken to be the first analyzed position of the storm, provided it had not simply moved into view from a previous location off of the map. The maximum deepening position was taken to be the position of the storm centered over the interval of most rapid deepening; thus, the position of maximum 24 hour deepening was the position of the storm at 00Z, if the most rapid deepening occurred from 12Z to 12Z, and the position at 12Z, if the most rapid deepening occurred from 00Z to 00Z. The position of dissipation was taken to be the last analyzed position of a storm before it lost its identity, either through absorption by another storm or final decay, so that the low center was no longer analyzed on successive maps. The duration (in days) of each storm was also recorded. All pressure falls were subsequently adjusted geostrophically, based on the principle that two storms of identical pressure gradient would not produce the same maximum geostrophic wind at different latitudes. Thus, the pressure falls can be adjusted according to the

formula:

$$dP(adj) = [\sin a / \sin b]\, dP$$

where "a" is some reference latitude, and "b" is the latitude of the storm. Traditionally, a bomb has been defined as a total 24 hour pressure drop equivalent to 24 mb at 60N, so that for the above definition, with "a" set equal to 42.5N, dP(adj)=-19 mb corresponds to one bergeron, the lower limit of deepening to qualify as a bomb, adjusted to middle latitudes. This altered version of the Bergeron definition is used in this study, since the majority of explosive cyclones occur about the axis of 42.5N. In either case, these are arbitrary definitions, presumably formulated so as to include only the most rapid deepeners in the bomb class. The statistical analysis of deepening rates will make it possible to formulate a new definition consistent with the analysis, and therefore less arbitrary than the current definition.

2.1 Statistical Analysis

The basis of this analysis is the Central Limit Theorem of Statistics, which states that under certain conditions probability distributions will tend to approach the normal curve. If we let Xn, n= 1,2,...,N be a set of N

stochastic variables (e.g., the stochastic variable X1 is the random outcome of process number 1), and we let $_J$ denote the number of independent realizations of that process, then we can define a variable Y_J such that:

$$Y_J = X1,_J + X2,_J + \ldots + XN,_J$$

Thus, the summation is over processes, and the stochastic variables Y_J are the sums of additive effects. If we restrict the $Xn,_J$ such that all have an identical probability density with mean u and standard deviation s, the limiting distribution of the Y_J as N approaches infinity is the normal distribution. This is the simplest (and most restrictive) form of the Central Limit Theorem. The Liapounov Central Limit Theorem requires only that the random variables $Xn,_J$ be independent, and not necessarily identically distributed for the distribution of the Y_J to be normally distributed. In terms of this analysis, one would expect the distribution of the deepening rates to be normal provided the N underlying processes (the nature of which have not been specified, but for baroclinic processes, correspond to warm advection, differential vorticity advection, etc.) are the same in all cases (realizations). This does not require that each of these processes be identically distributed, but only that these processes and no others are operative in all realizations.

The restriction of independence should be approximately correct, although some storms in close proximity may interact. We can say little about the interactions between cyclones, and the effect of cyclones on the upper level flow and subsequent systems, but it seems reasonable to assume that such effects would be statistically negligible.

Analyses of 12 and 24 hour deepening distributions for warm season, cold season, and full year data samples show statistically significant deviations from the normal curve, the largest deviations associated with the tail of the deepening curve (fig. 2.01-08). The analysis was accomplished using a chi-square goodness of fit test at the 5% level of significance; thus there is a 5% probability of erroneously rejecting the null hypothesis that the distributions are Gaussian and concluding the distributions are not normal. An attempt was made to iteratively fit two normal curves with different means and variances to each of the cold season and full year 24 hour deepening distributions; it was discovered that the sum of the two normal curves provided a good fit to the data, that is, there were no longer significant deviations from the observed distributions. The statistics of the distribution associated with most rapid deepening with mean -22.3 mb and standard deviation 6.9 mb indicate that the Bergeron definition of a bomb is quite adequate; 68% of explosive

cases (as defined by the deepening distribution with mean -22.3 mb) are included by the definition, while only 2% of non-explosive cases are included, at least in this sample.

These results provide strong evidence that explosive cyclogenesis is a process distinct in some meaningful way from ordinary baroclinic instability. The fact that such an analysis, based on the oft-times underestimated NMC pressure analyses over data sparse oceans, was able to demonstrate this feature further emphasizes this conclusion. Unfortunately, such a procedure can give no information on the physical process or processes responsible for the explosive deepening mechanism. For such an investigation, one must turn to other methods; this was attempted, and will be dealt with in the next chapter.

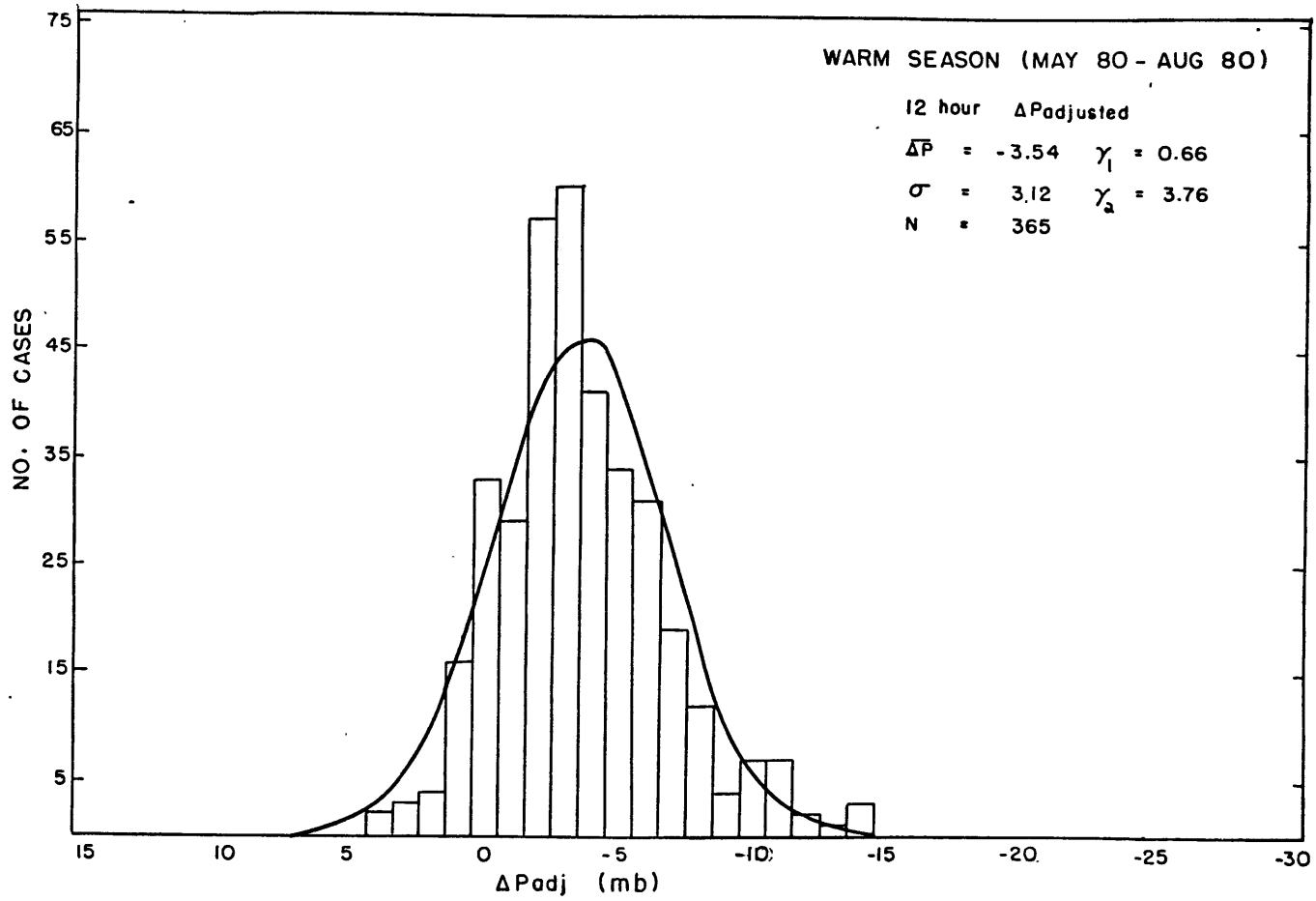

FIGURE 2.01

Deepening distributions with computed sample statistics, Figures 2.01-08. $\overline{\Delta P}$ and σ are the sample mean and standard deviation, N is the total number of cases, $\gamma 1$ and $\gamma 2$ are the coefficients of skewness and kurtosis, respectively, measures of the relative centeredness and peakness of the distributions. The dashed lines represent the two normal distributions of different means and variances; the solid line in those figures represents the sum of the two distributions.

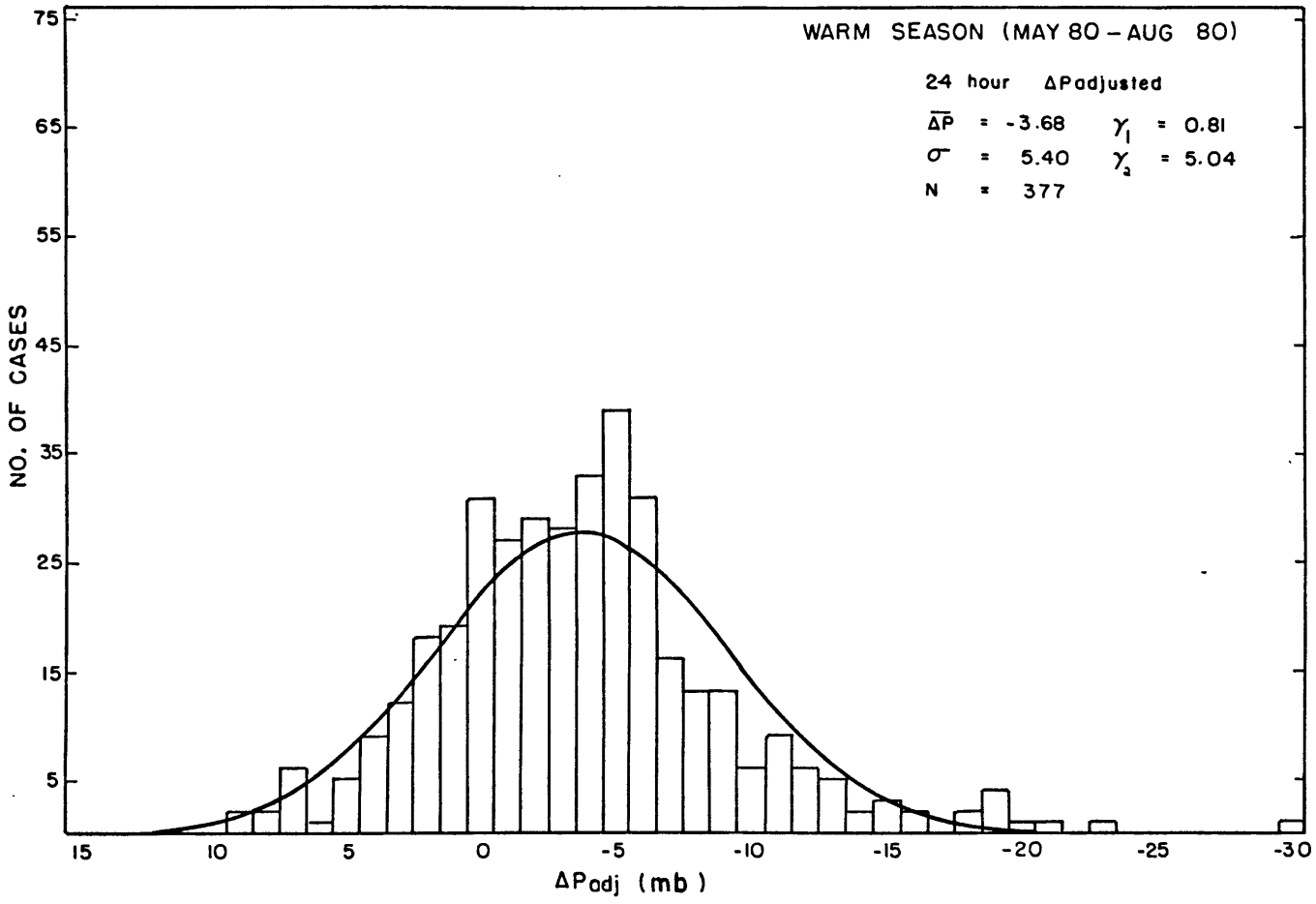
WARM SEASON (MAY 80 – AUG 80)
24 hour ΔPadjusted
$\overline{\Delta P}$ = -3.68
σ = 5.40
N = 377
γ_1 = 0.81
γ_2 = 5.04
NO. OF CASES
75
65
55
45
35
25
15
5
15
10
5
0
-5
-10
-15
-20
-25
-30
ΔPadj (mb)

FIGURE 2.02

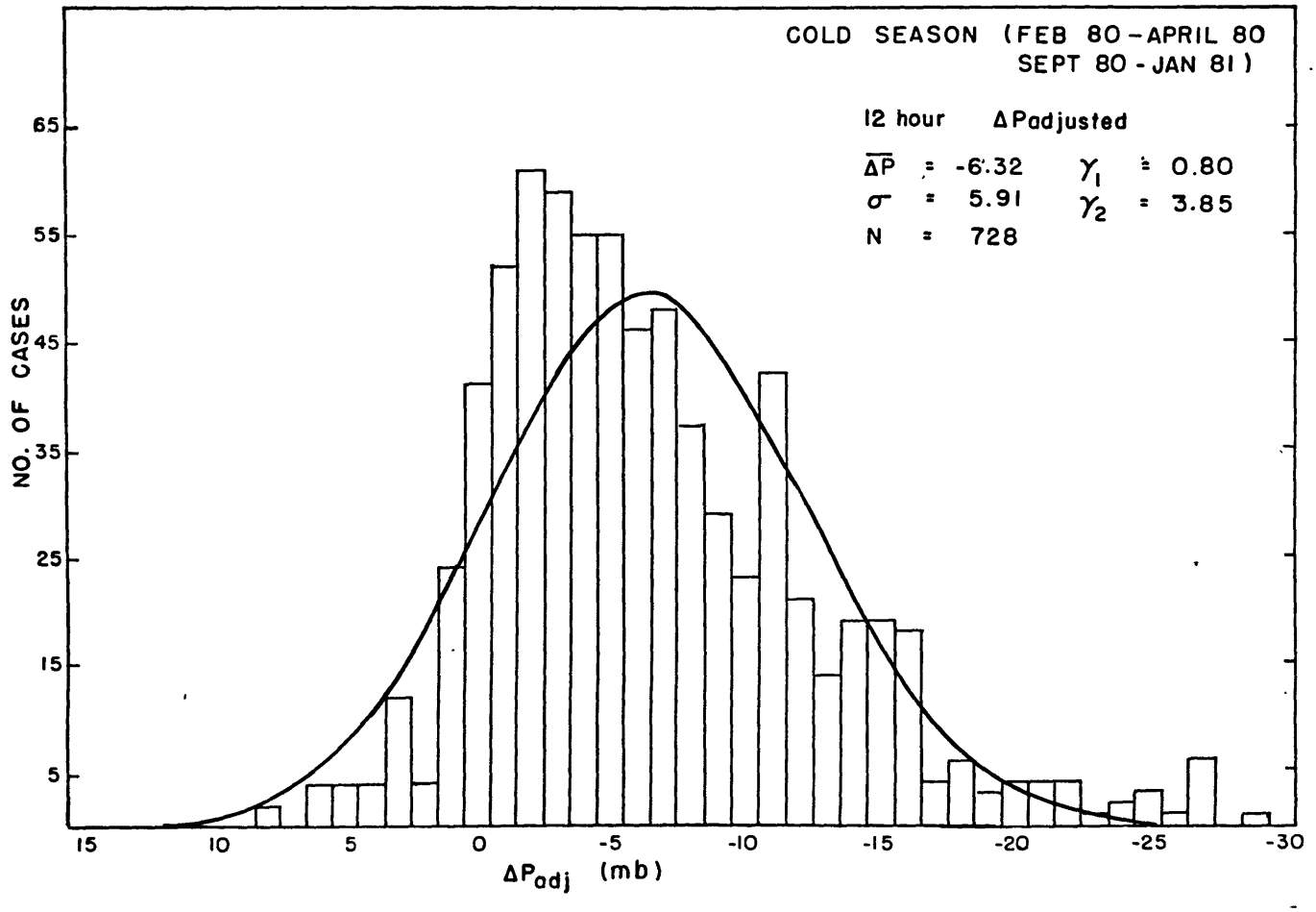
COLD SEASON (FEB 80 - APRIL 80
SEPT 80 - JAN 81)
12 hour ΔPadjusted
$\overline{\Delta P}$ = -6.32
σ = 5.91
N = 728
γ_1 = 0.80
γ_2 = 3.85
NO. OF CASES
65
55
45
35
25
15
5
15
10
5
0
-5
-10
-15
-20
-25
-30
ΔP_{adj} (mb)

FIGURE 2.03

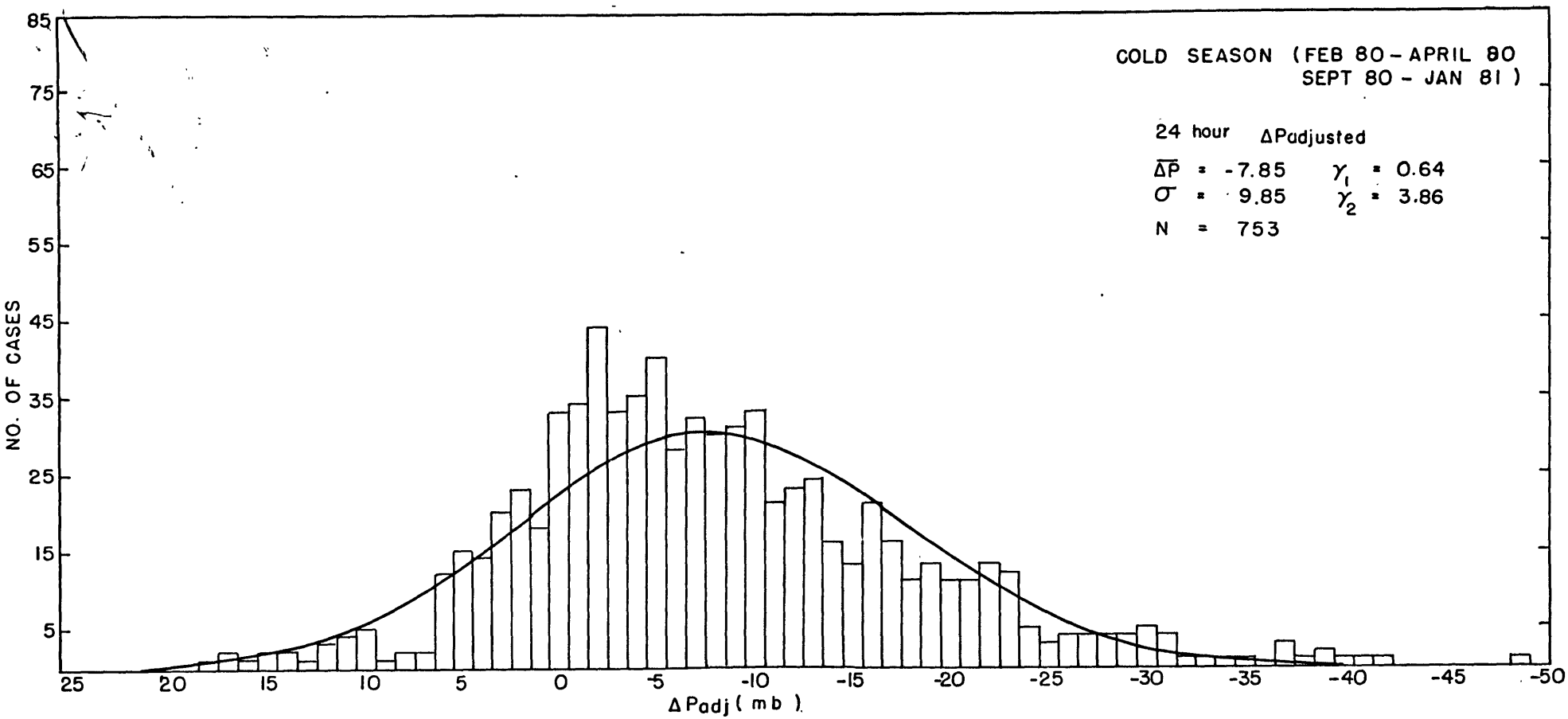
COLD SEASON (FEB 80 - APRIL 80
SEPT 80 - JAN 81)
24 hour ΔPadjusted
$\overline{\Delta P}$ = -7.85
σ = 9.85
N = 753
γ_1 = 0.64
γ_2 = 3.86
NO. OF CASES
85
75
65
55
45
35
25
15
5
25 20 15 10 5 0 -5 -10 -15 -20 -25 -30 -35 -40 -45 -50
ΔPadj (mb)

FIGURE 2.04

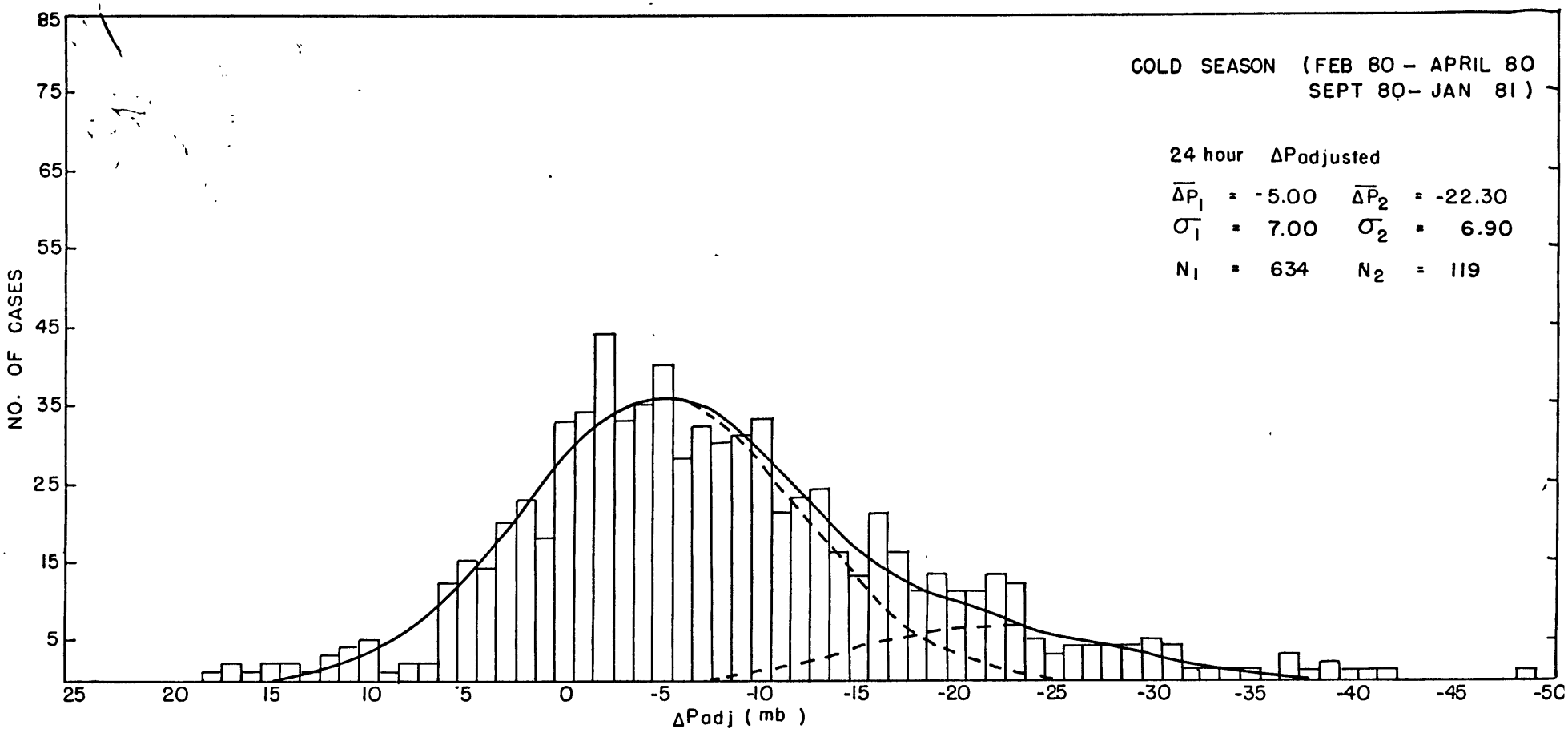
COLD SEASON (FEB 80 – APRIL 80
SEPT 80– JAN 81)
24 hour ΔPadjusted
$\overline{\Delta P_1}$ = -5.00 $\overline{\Delta P_2}$ = -22.30
σ_1 = 7.00 σ_2 = 6.90
N_1 = 634 N_2 = 119
NO. OF CASES
85
75
65
55
45
35
25
15
5
25 20 15 10 5 0 -5 -10 -15 -20 -25 -30 -35 -40 -45 -50
ΔPadj (mb)

FIGURE 2.05

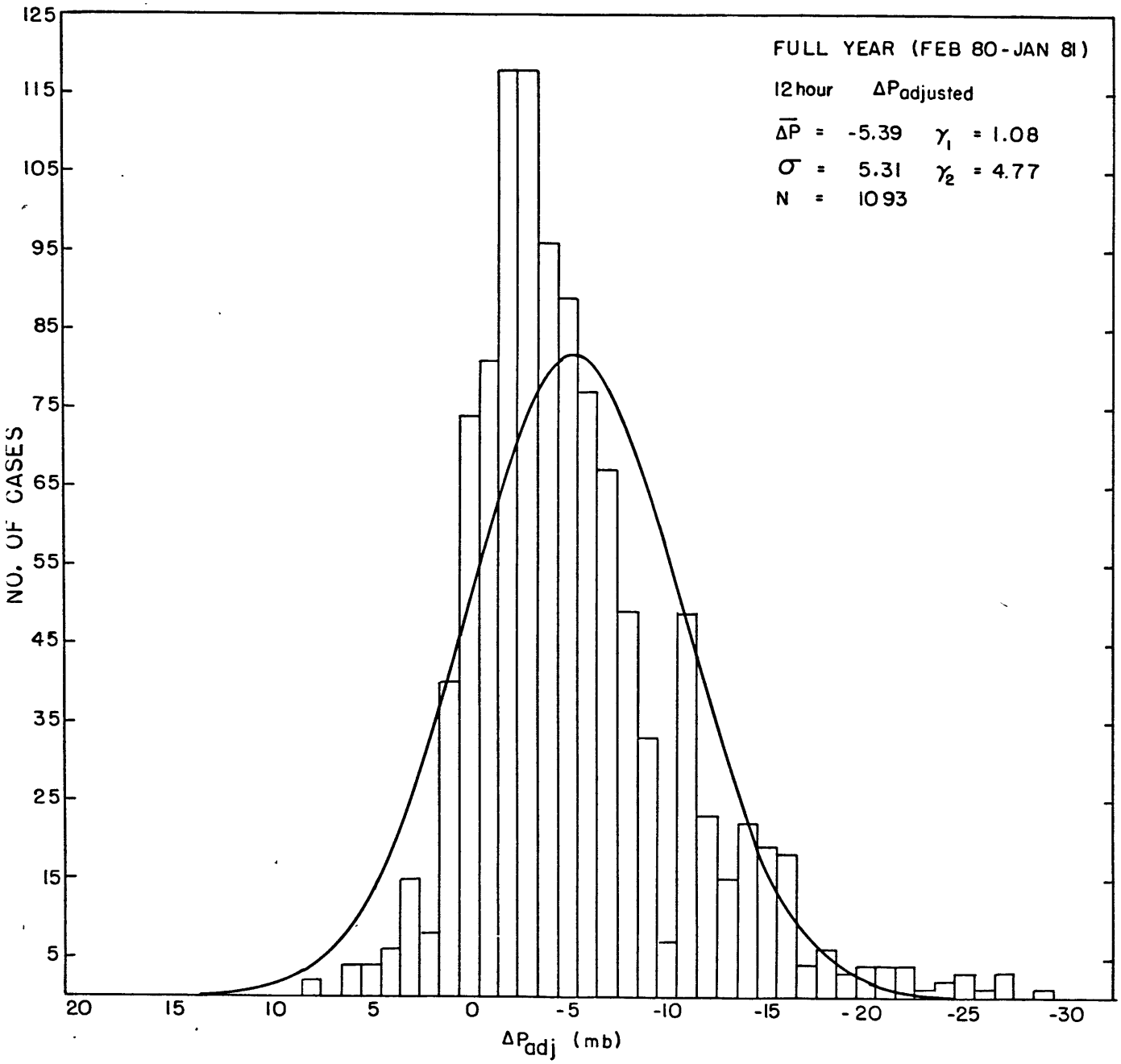
FULL YEAR (FEB 80-JAN 81)
12 hour ΔP adjusted
ΔP̄ = -5.39 γ1 = 1.08
σ = 5.31 γ2 = 4.77
N = 1093
NO. OF CASES
125
115
105
95
85
75
65
55
45
35
25
15
5
20
15
10
5
0
-5
-10
-15
-20
-25
-30
ΔPadj (mb)

FIGURE 2.06

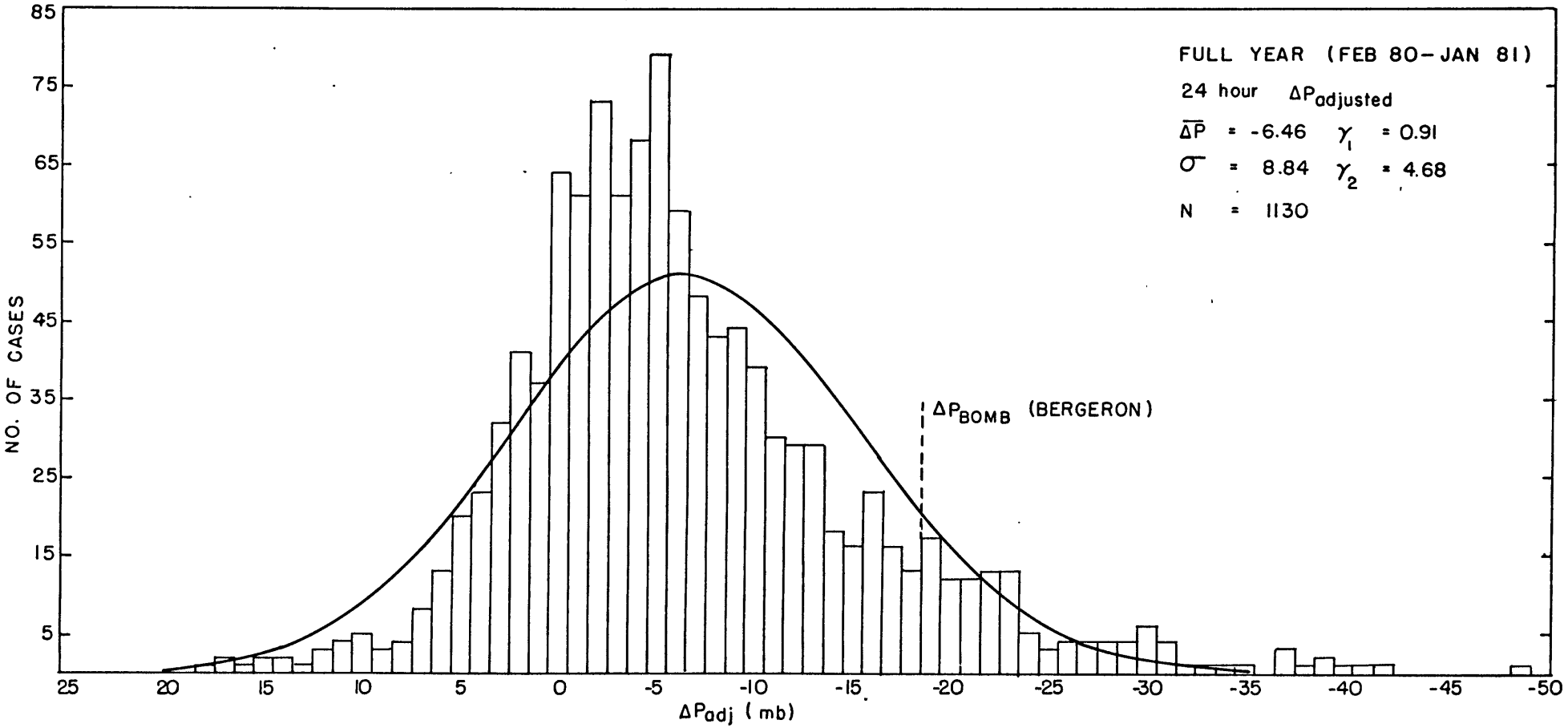
FULL YEAR (FEB 80–JAN 81)
24 hour ΔP adjusted
ΔP̄ = -6.46 γ1 = 0.91
σ = 8.84 γ2 = 4.68
N = 1130
ΔP BOMB (BERGERON)
NO. OF CASES
ΔP adj (mb)
85
75
65
55
45
35
25
15
5
25 20 15 10 5 0 -5 -10 -15 -20 -25 -30 -35 -40 -45 -50

FIGURE 2.07

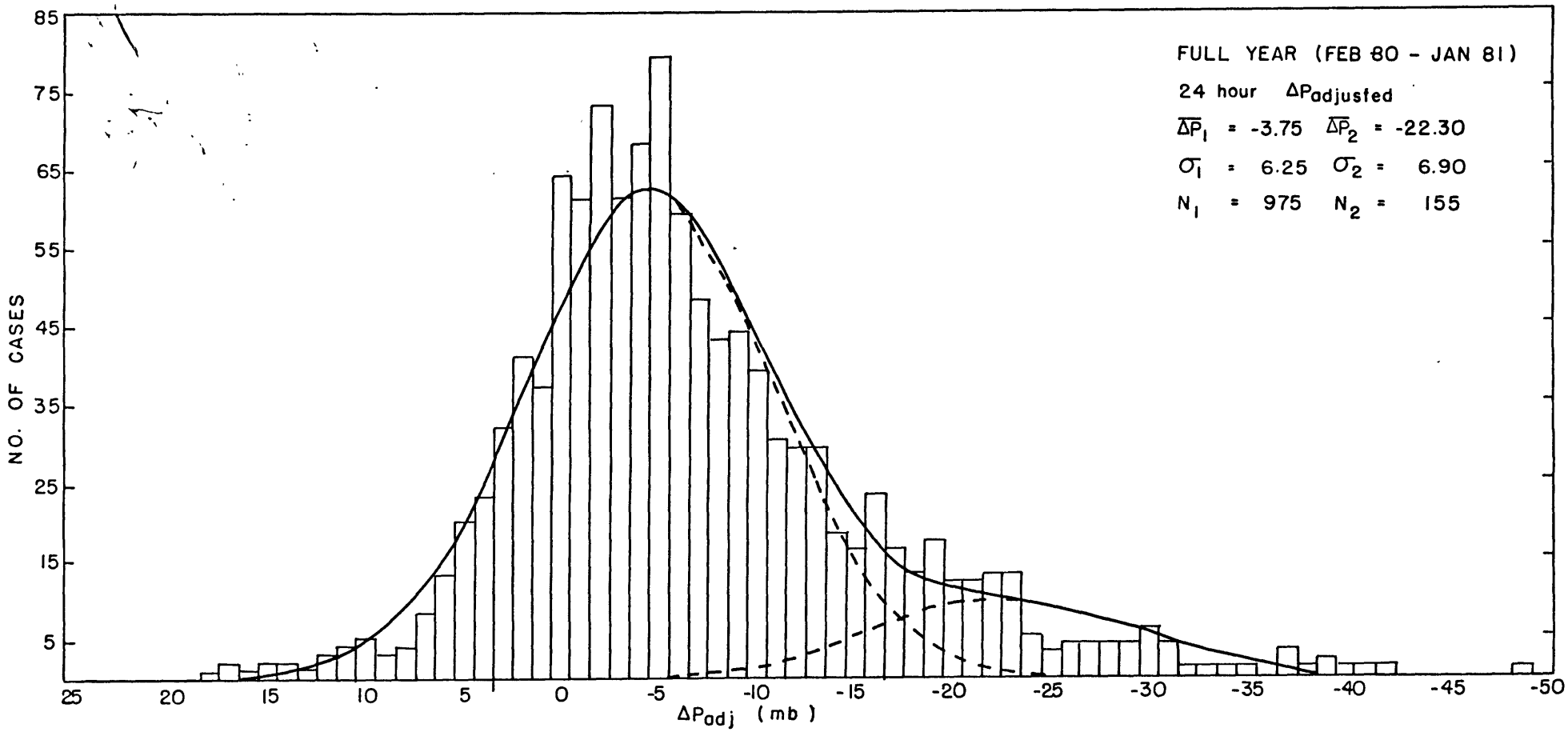
FULL YEAR (FEB 80 - JAN 81)
24 hour ΔPadjusted
$\overline{\Delta P}_1$ = -3.75 $\overline{\Delta P}_2$ = -22.30
σ_1 = 6.25 σ_2 = 6.90
N_1 = 975 N_2 = 155
NO. OF CASES
85
75
65
55
45
35
25
15
5
25 20 15 10 5 0 -5 -10 -15 -20 -25 -30 -35 -40 -45 -50
ΔPadj (mb)

FIGURE 2.08

2.2 Climatology

2.2.1 Statistics of Deepening Cyclones -

A wealth of climatological data can be gleaned from the one year cyclone sample, and in the process, one can learn some additional information about explosive cyclones. Consulting the data in figures 2.06-07, it is evident that the average pressure fall is only one to two millibars greater in the 24 hour sample than in the 12 hour sample. This suggests that, on average, most of the deepening is accomplished in a time period less than 24 hours. The main increase is in the dispersion (broadening) of the 24 hour distribution, confirming that some cases do continue deepening throughout the period. This result has important implications for any attempt to model the evolution of the cyclogenesis.

Since it has been shown that the bimodal distributions of the 24 hour cold season and full year sample deepening rates can be approximated by the sum of two normal curves, it is possible to say something about the true means and variances of the distributions. The results are shown in table 2.09. One can say with 95% confidence that the mean deepening of the 24 hour cold season baroclinic lows is between 4.5 and 5.5 mb, and that the mean deepening of

explosive cyclones in that period is between 21.0 and 23.5 mb. The results for the full year data are similar. The mean deepening of the baroclinic lows is between 3.4 and 4.1 mb, and the mean deepening of the explosive cyclones is between 21.2 and 23.4 mb. The question of possible time bias in the sample was examined. The results of table 2.09 seem to indicate no discernible bias in the 12 and 24 hour deepening samples. No attempt was made to stratify the cases according to ocean basin, where the greatest potential for bias might have been expected; this was done in the study of Sanders and Gyakum (1980), and no bias was found in their sample of bombs.

Within the limits of a 12 hour resolution, the question of the length of the deepening period of all storms and of bombs can be examined. The deepening period is the time interval over which successive 12 hour analyses indicate a continued fall in storm central pressure. The results are plotted in figure 2.10. By 36 hours, more than 75% of all the lows in the sample had ceased deepening, as compared to less than half of the explosive cyclones. The average deepening period of all lows was 24 hours, while that of explosive cyclones was about 45 hours. One should bear in mind when interpreting these results that, for example, a 45 hour deepening period is really 39h+/-6h, and that this analysis can reveal nothing about new sources of

energy introduced into a system after the initial energy source has been dissipated. Thus, a system that is interpreted as deepening 30h+/-6h may really have deepened for 18 hours, remained steady, or filled for 12 hours, and deepened again for the last 6 hours when a new pulse of

DISTRIBUTION	N	95% CONFIDENCE INTERVALS μ	σ
24h Cold Season(baroclinic)	634	$4.5 < \mu < 5.5$	$6.6 < \sigma < 7.4$
24h Cold Season(bombs)	119	$21.1 < \mu < 23.5$	$6.1 < \sigma < 7.9$
24h Full Year(baroclinic)	975	$3.4 < \mu < 4.1$	$6.0 < \sigma < 6.5$
24h Full Year(bombs)	155	$21.2 < \mu < 23.4$	$6.2 < \sigma < 7.8$

Confidence intervals for the true mean, μ, and standard deviation, σ, of particular deepening distributions of sample size N.

DISTRIBUTION	N	TIME DISTRIBUTIONS 12Z	%	00Z	%
12h (12Z-00Z, 00Z-12Z)	1157	619	53.5	538	46.5
24h (12Z-12Z, 00Z-00Z)	1178	579	49.2	599	50.8
Bombs(12Z-12Z, 00Z-00Z)	115	58	50.4	57	49.6

FIGURE 2.09

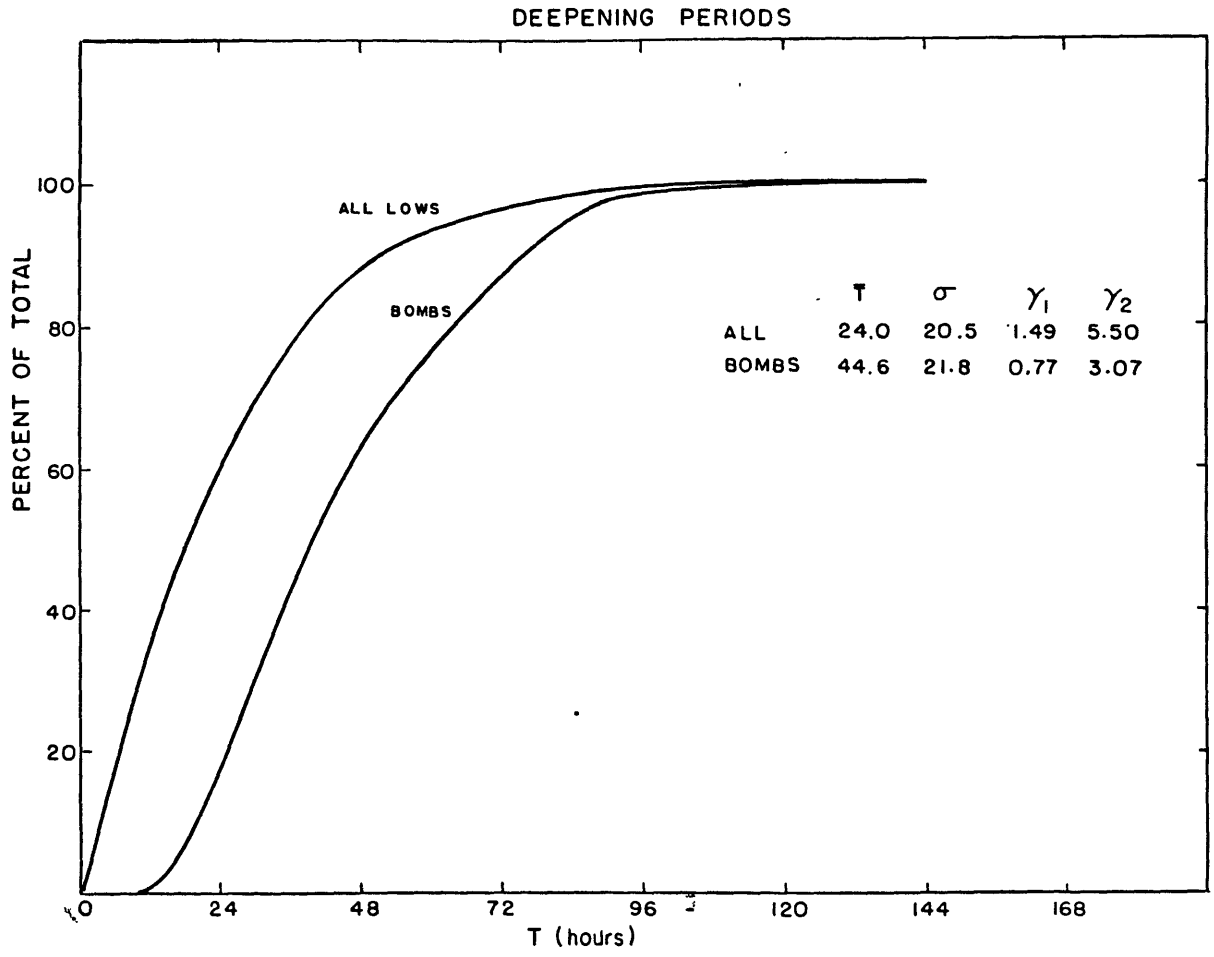

Cumulative distributions of deepening periods for all storms and for bombs. The statistics of the deepening period distributions are also given; $\bar{T}$ is the mean deepening period, σ is the standard deviation, and γ_1 and γ_2 are the coefficients of skewness and kurtosis, respectively.

FIGURE 2.10

energy was introduced. This is an artifact of the 12 hour resolution, and there is little that can be done about it, except to urge caution when interpreting the results. This point is stressed, as the length of the deepening period is crucial to the model analysis of the next chapter.

2.2.2 Geographic Distribution of Cyclones -

A series of maps were drawn up, utilizing the climatological data concerning positions of formation, maximum deepening, and dissipation. The raw frequency data was plotted on a 5 by 5 degree latitude/longitude tessera grid, and smoothed by taking 4 times the central value plus the 4 adjacent values and dividing by 8.

The warm season and full year distributions of formation positions (fig. 2.11-13) both show marked maxima east of the Rocky Mountains. Mean 700 mb height patterns (fig. 2.23-26, obtained from Monthly Weather Review) for May-August 1980 show that in the first 2 months of the warm season there was substantial flow across the mountain barrier, but, by July, the flow had all but ceased over the southern portion of the mountains. August 1980 saw the return of the flow southward, though it could not penetrate as far south as in the first two months of the warm season. Thus, the warm season maximum can probably be attributed to

the same cause as that of the cold season, the process of lee cyclogenesis, though it is not clear why this maximum is comparable to the cold season value unless some of the warm season events represent thermal lows as well. Minor maxima are also located over Japan, and to a lesser extent, over the southeastern United States, the Atlantic Ocean (45N,45W), and the lee side of the Canadian Rockies along the Alaskan border. These appear to reflect lee cyclogenesis and the baroclinic zones associated with the warm ocean currents off the coasts of Japan and the eastern United States. The areas off of Japan and the U.S. may actually reflect a combination of orography and ocean currents. The maximum out over the Atlantic is likely an area of redevelopment, with old lows cutting off in the cold air and new lows forming alongside the baroclinic zone associated with the Gulf Stream.

In the full year data, these maxima are intensified, with the greatest increases occurring along the eastern seaboard of the United States. The maxima forced by vortex stretching on the lee side of mountain barriers are increased proportionately; it is the coastal areas that are most strongly activated in the winter months, reflecting the enhanced baroclinicity of these areas. There is a noticeable maximum in the eastern Pacific Ocean (42N,155W) not apparent in the warm season climatology

which becomes established in the winter months. This is probably associated with the breakdown of the warm season Pacific high aloft (figure 2.24), and the establishment of the wintertime regime. The full year bomb distribution shows maxima associated with all the major cyclogenetic areas discussed previously, with the exception of those induced by orographic effects alone. It is noteworthy that the Pacific maximum does not appear on the bomb distribution, suggesting that this area is not a birthplace of explosive cyclones.

The positions of maximum deepening (fig. 2.14-16) are well correlated with the positions of initial cyclogenesis, located slightly upstream. The Pacific Ocean region where the maximum in formation position was found also displays a maximum in deepening; this maximum is not downwind of the initial formation position, and the magnitude is greater, suggesting that other cyclones moving through this region are intensifying. This area has no warm ocean currents akin to the Kuroshio or the Gulf Stream, but it can still be quite baroclinic, owing to outbreaks of Arctic air moving through the Bering Straits and across the warmer ocean water. The climatology suggests that storms that do form in the area are redevelopments of existing storms that subsequently move into the Gulf of Alaska and decay. Storms moving through the area deepen in response to the

enhanced baroclinicity.

The maximum deepening positions of the bombs in the year sample are well correlated with the positions of the warm ocean currents, primarily the Kuroshio and the Gulf Stream. These areas are general baroclinic zones, however, so the climatology does not suggest that any process other than baroclinicity is necessarily operative in explosive cyclones.

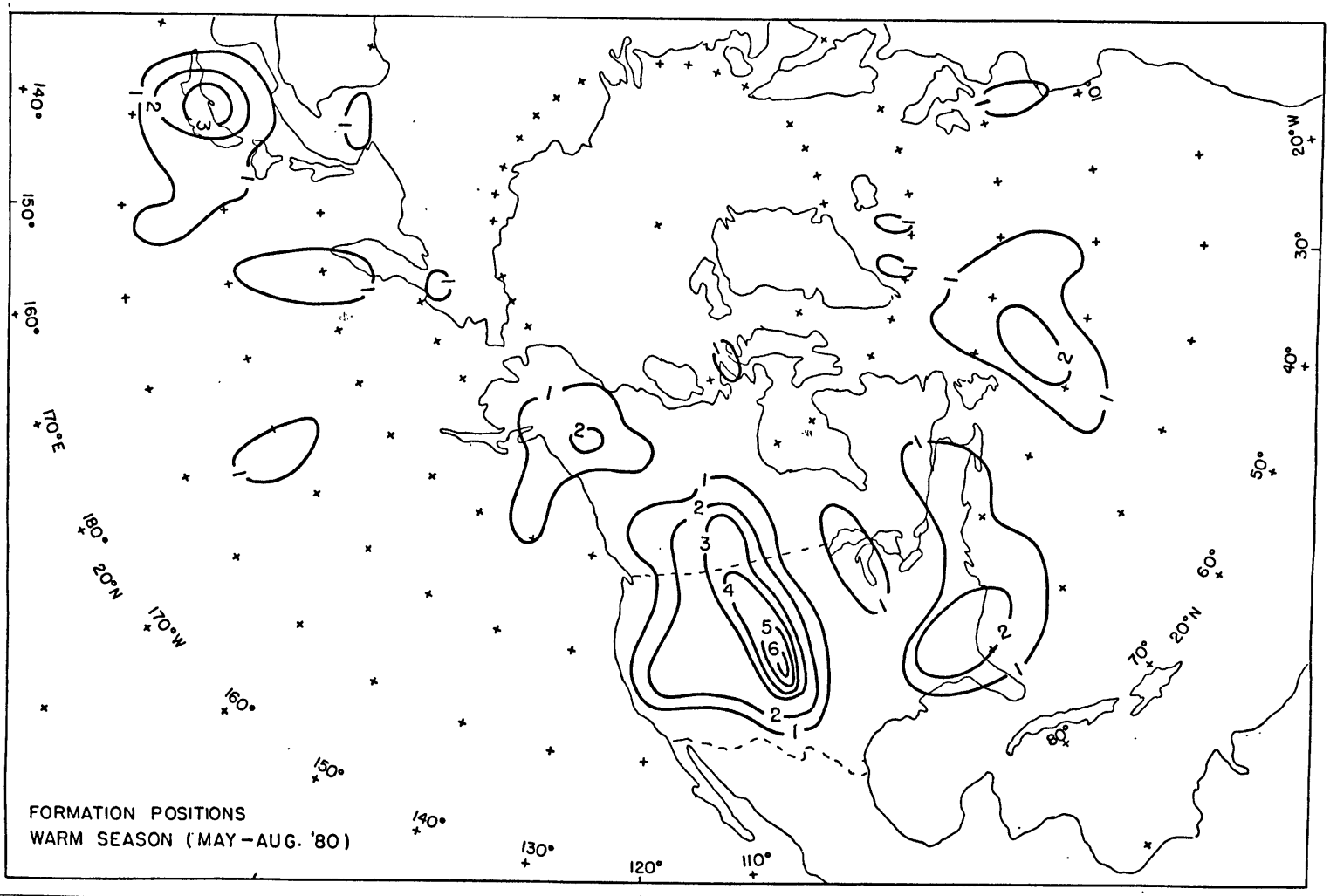

Geographic distribution of formation position, maximum deepening position, and dissipation position, Figures 2.11-22. Frequencies are smoothed from the 5 degree latitude by 5 degree longitude tessera grid of raw data, according to the formula of 4 times the central frequency plus each of the 4 adjacent frequencies, all divided by 8.

FIGURE 2.11

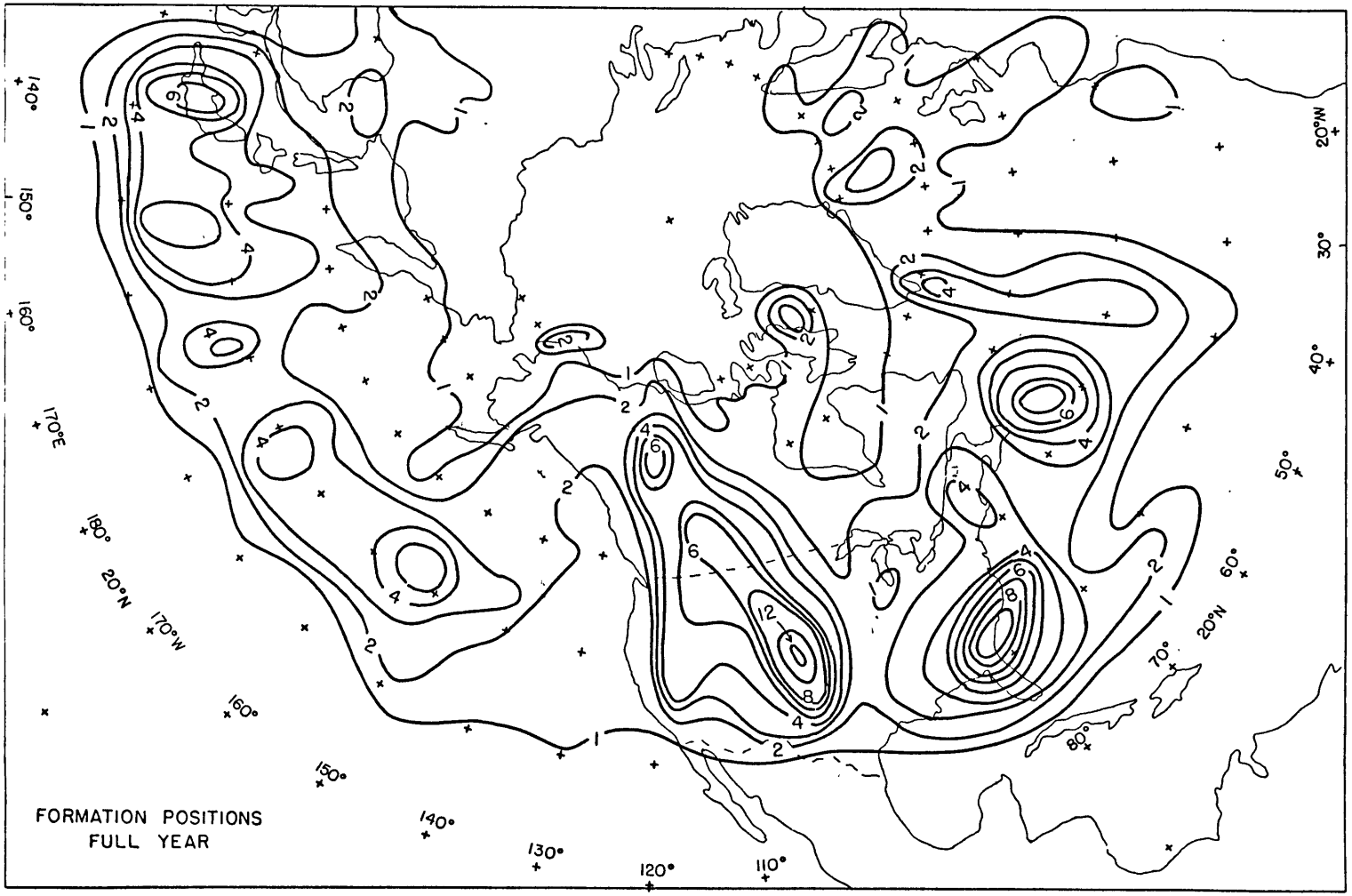
FORMATION POSITIONS
FULL YEAR
140°
150°
160°
170°E
180°
170°W
160°
150°
140°
130°
120°
110°
20°N
20°W
30°
40°
50°
60°
70°
80°

FIGURE 2.12

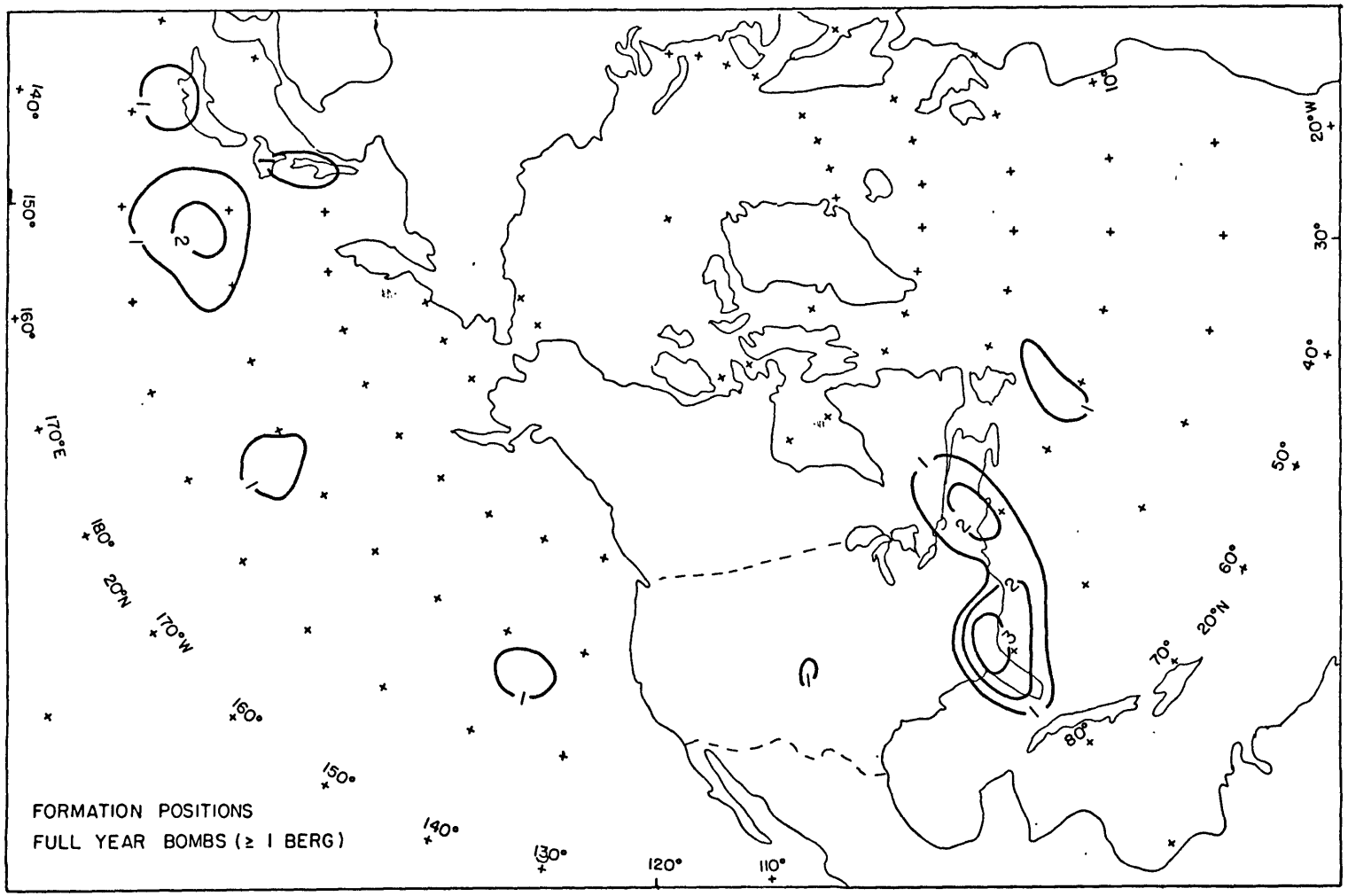
FORMATION POSITIONS
FULL YEAR BOMBS (≥ 1 BERG)
140°
150°
160°
170°E
180°
170°W
160°
150°
140°
130°
120°
110°
10°
20°W
30°
40°
50°
60°
70°
80°
20°N
20°N

FIGURE 2.13

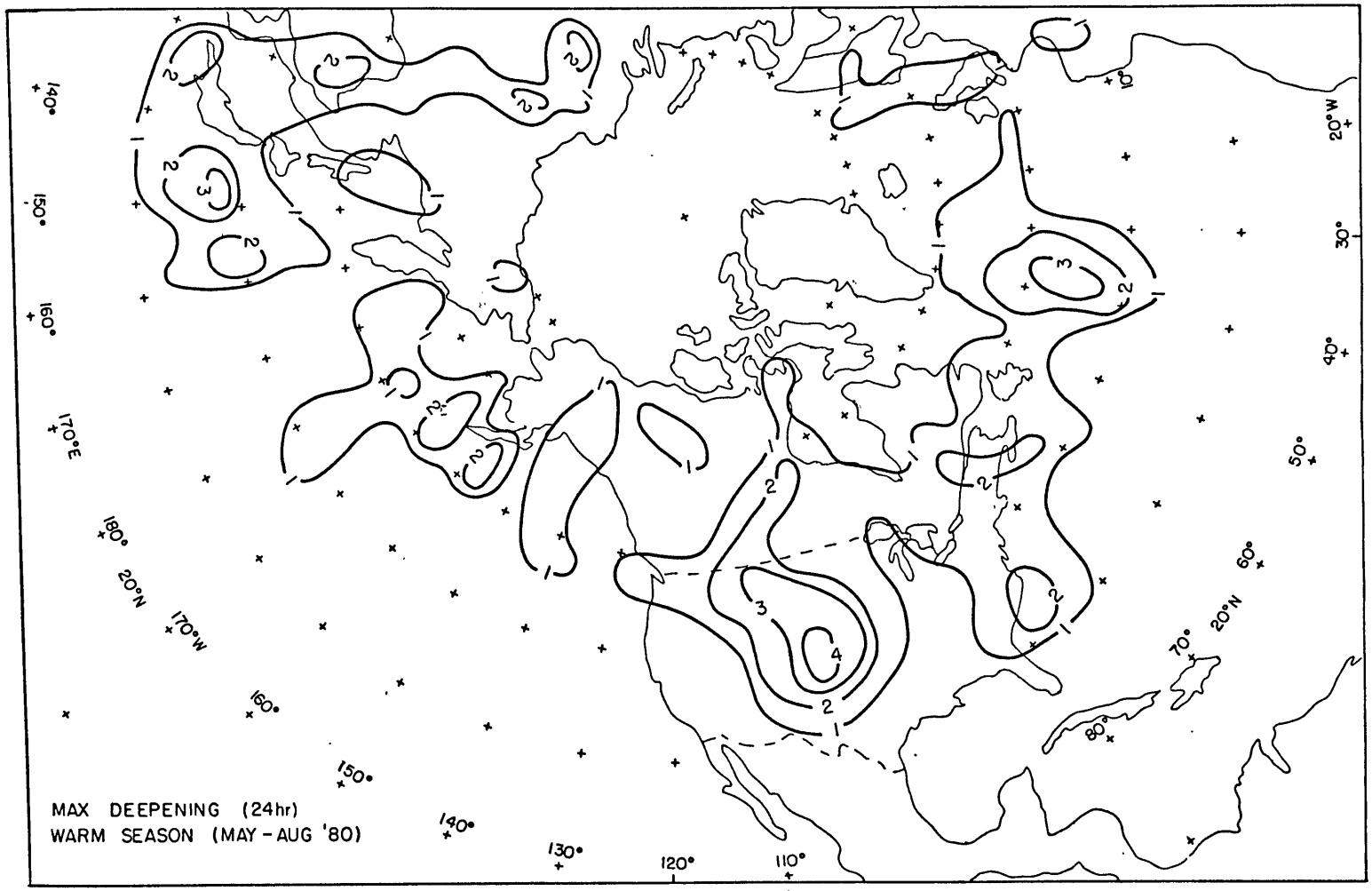
MAX DEEPENING (24hr)
WARM SEASON (MAY - AUG '80)
140°
150°
160°
170°E
180°
170°W
160°
150°
140°
130°
120°
110°
100°
90°
80°
70°
60°
50°
40°
30°
20°W
20°N
20°N

FIGURE 2.14

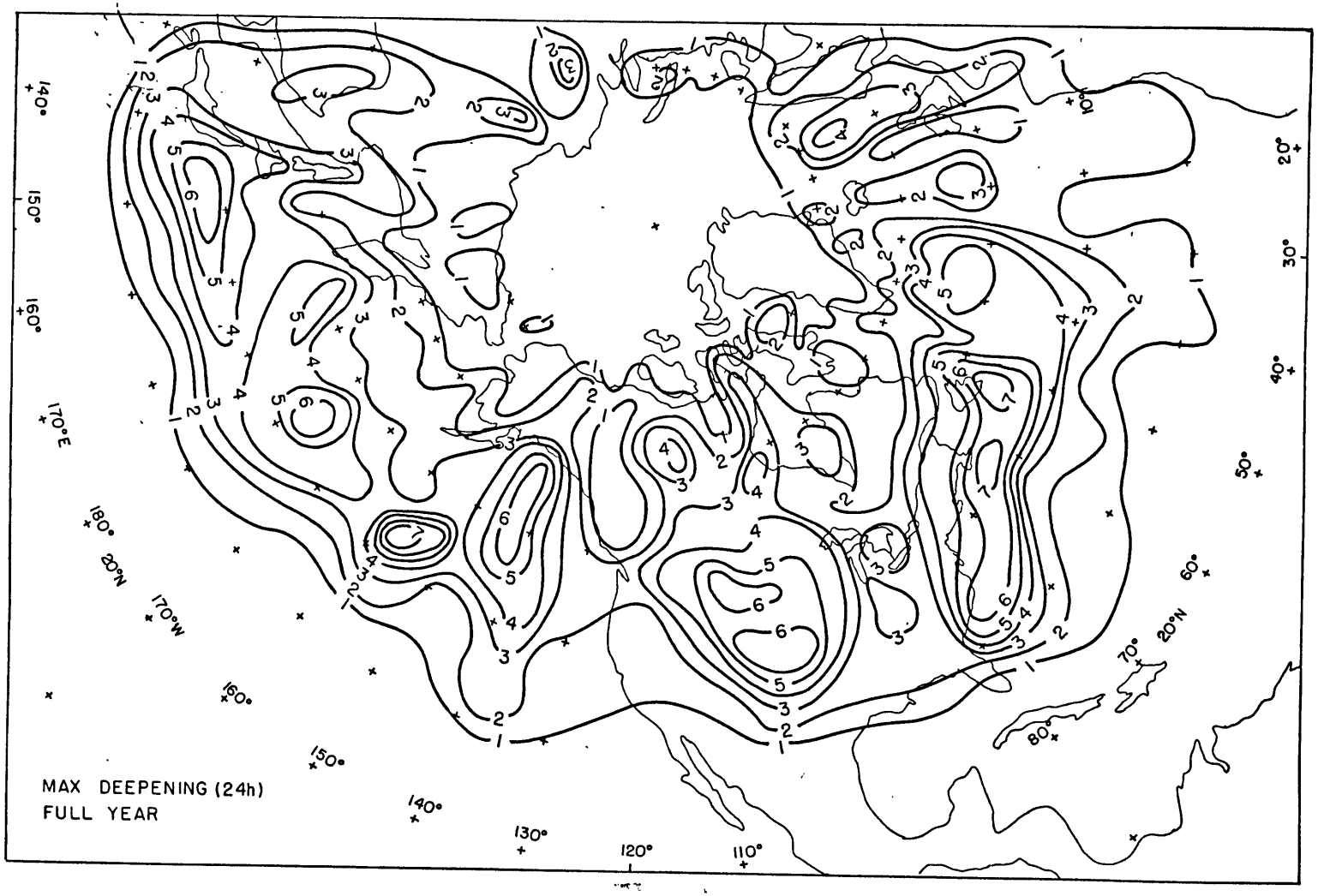
MAX DEEPENING (24h)
FULL YEAR
140°
150°
160°
170°E
180°
170°W
160°
150°
140°
130°
120°
110°
100°
90°
80°
70°
60°
50°
40°
30°
20°
20°N

FIGURE 2.15

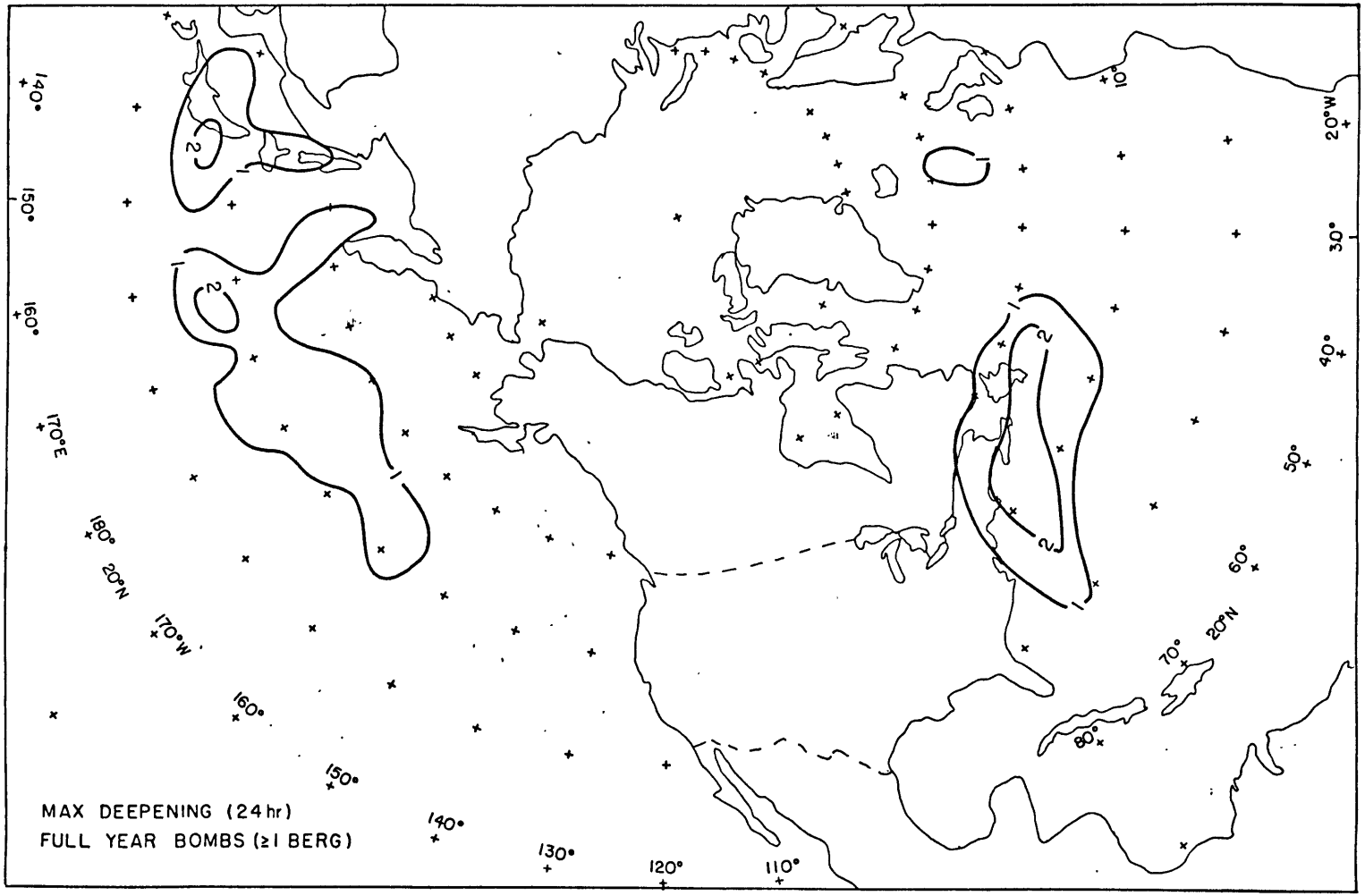
MAX DEEPENING (24 hr)
FULL YEAR BOMBS (≥1 BERG)
140°
150°
160°
170°E
180°
20°N
170°W
160°
150°
140°
130°
120°
110°
10°
20°W
30°
40°
50°
60°
70°
80°
2
1

FIGURE 2.16

The maximum deepening positions of all the 24 hour bombs (12Z-12Z) for the periods 1976-79, 1979-82, and 1976-82 are plotted (fig. 2.17-19). There are some small but non-negligible differences in the samples. The maximum off the eastern coast of the United States strengthened and moved closer to land in the later three year period. The Pacific Ocean maximum around 145W was also greater in the latter period, but the maximum off the Japanese coast was somewhat less. There appears to be little correlation between mean flow fields at upper levels (e.g. 700 mb), and the day to day occurrence of of explosive cyclogenesis in these areas. A better method of judging the relationship between the upper level and intense surface features would be to perform an analysis as in Sanders and Gyakum (1980), where each explosive event was examined individually with respect to the flow at 500 mb. In that study, the authors found the relationship between the explosive cyclones and the upper trough to be qualitatively typical of deepening baroclinic lows, with most of the storms intensifying within or just poleward of the region of maximum 500 mb wind and baroclinicity. It is not likely that such a study could explain the small variations in distributions of explosive cyclones found in the two 3 year samples, however, and was not attempted here.

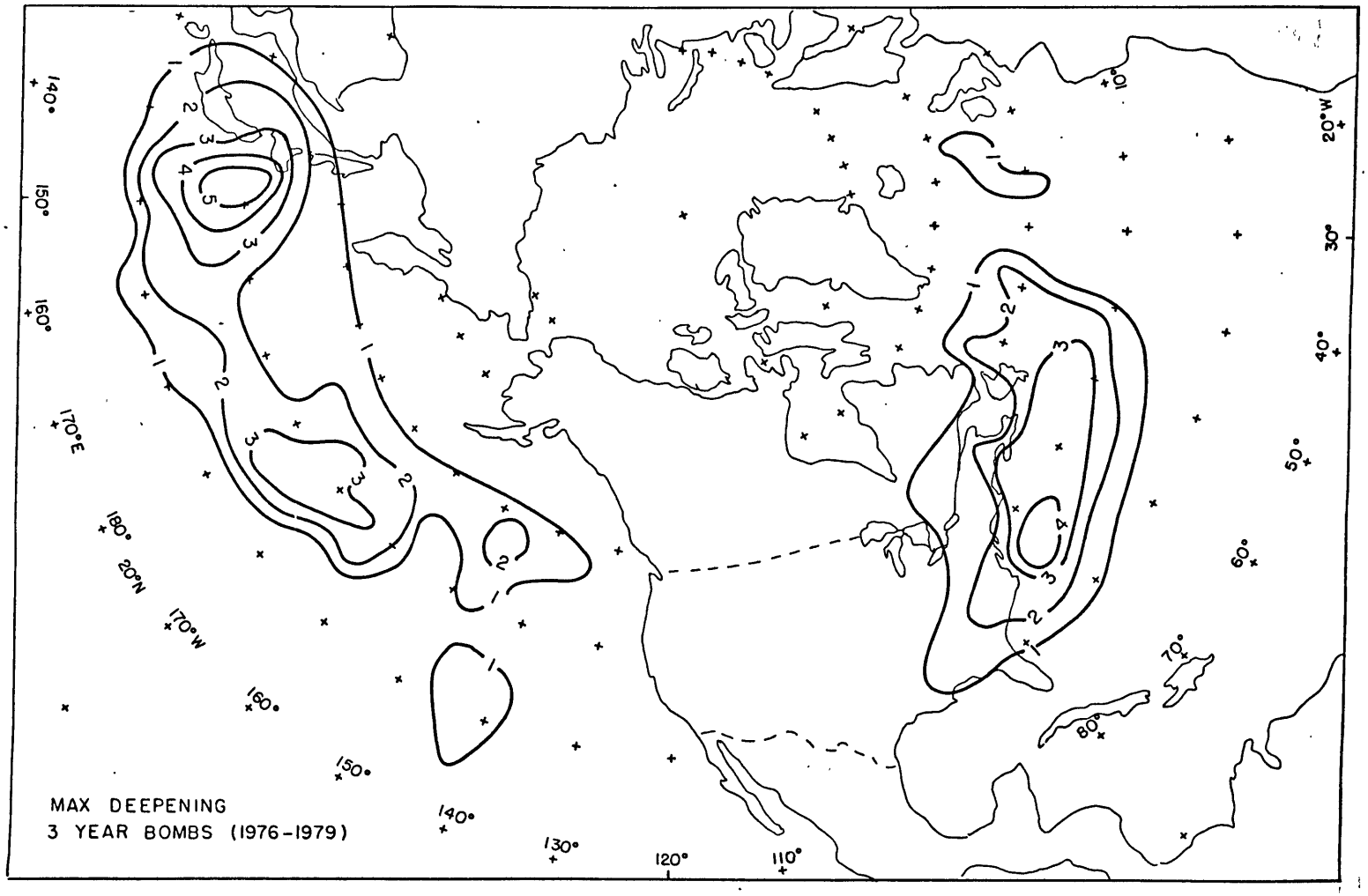
MAX DEEPENING
3 YEAR BOMBS (1976-1979)
140°
150°
160°
170°E
180°
170°W
160°
150°
140°
130°
120°
110°
10°
20°W
30°
40°
50°
60°
70°
80°
20°N

FIGURE 2.17

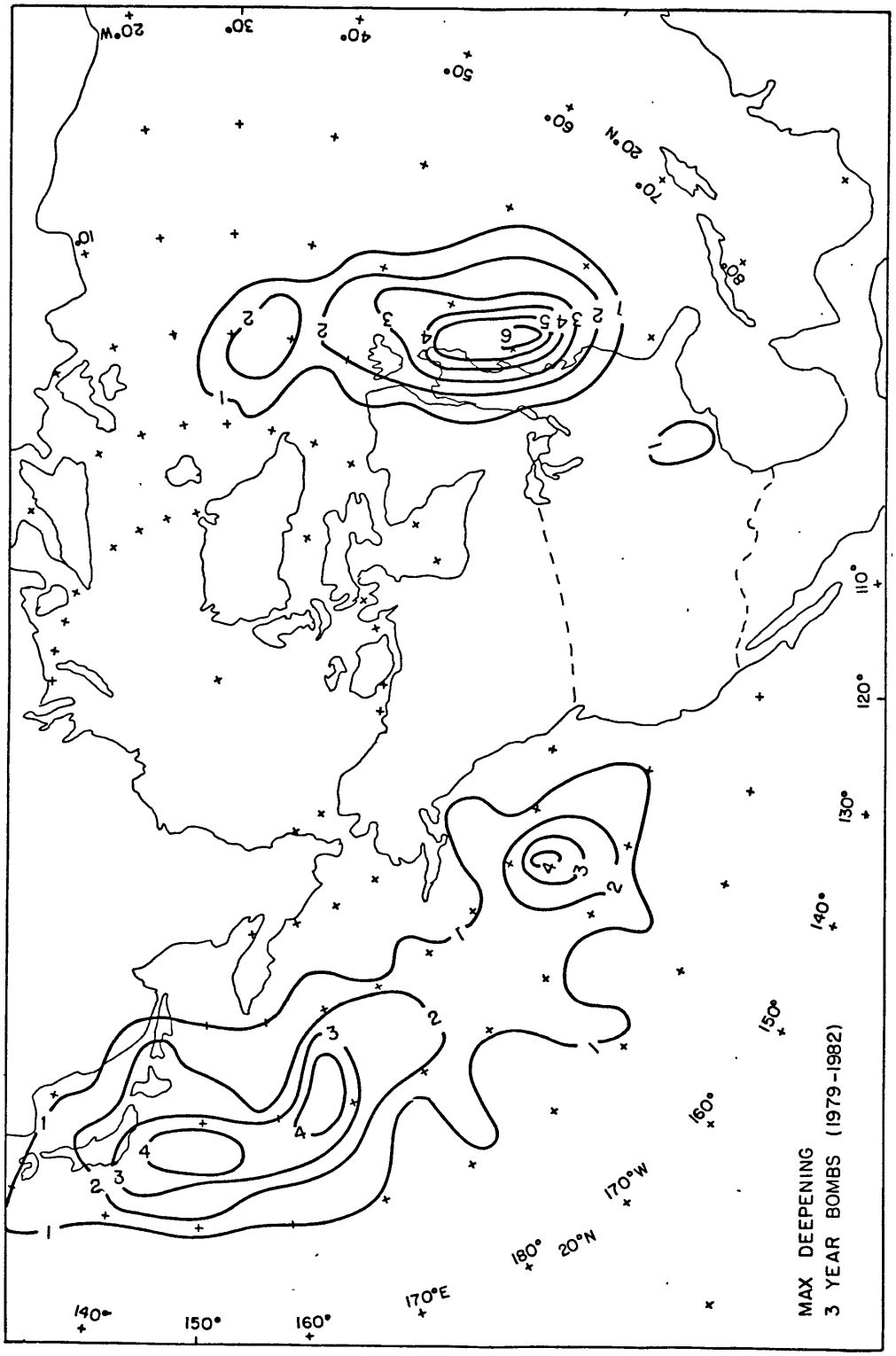
MAX DEEPENING
3 YEAR BOMBS (1979-1982)
20°W
30°
40°
50°
60°
70°
80°
20°N
10°
110°
120°
130°
140°
150°
160°
170°W
180°
170°E
140°
150°
160°
20°N

FIGURE 2.18

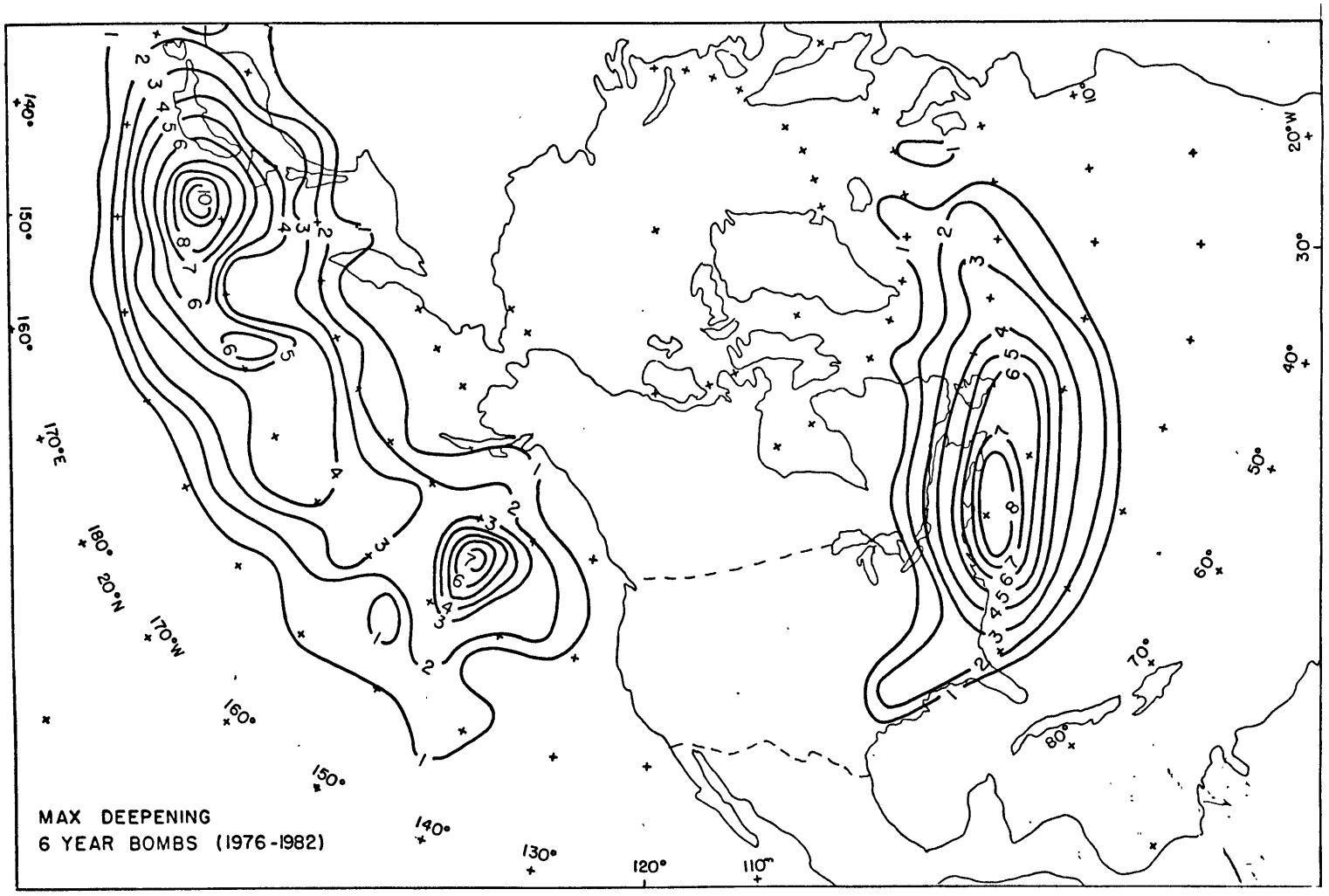
MAX DEEPENING
6 YEAR BOMBS (1976-1982)
140°
150°
160°
170°E
180°
170°W
160°
150°
140°
130°
120°
110°
20°N
10°
20°W
30°
40°
50°
60°
70°
80°

FIGURE 2.19

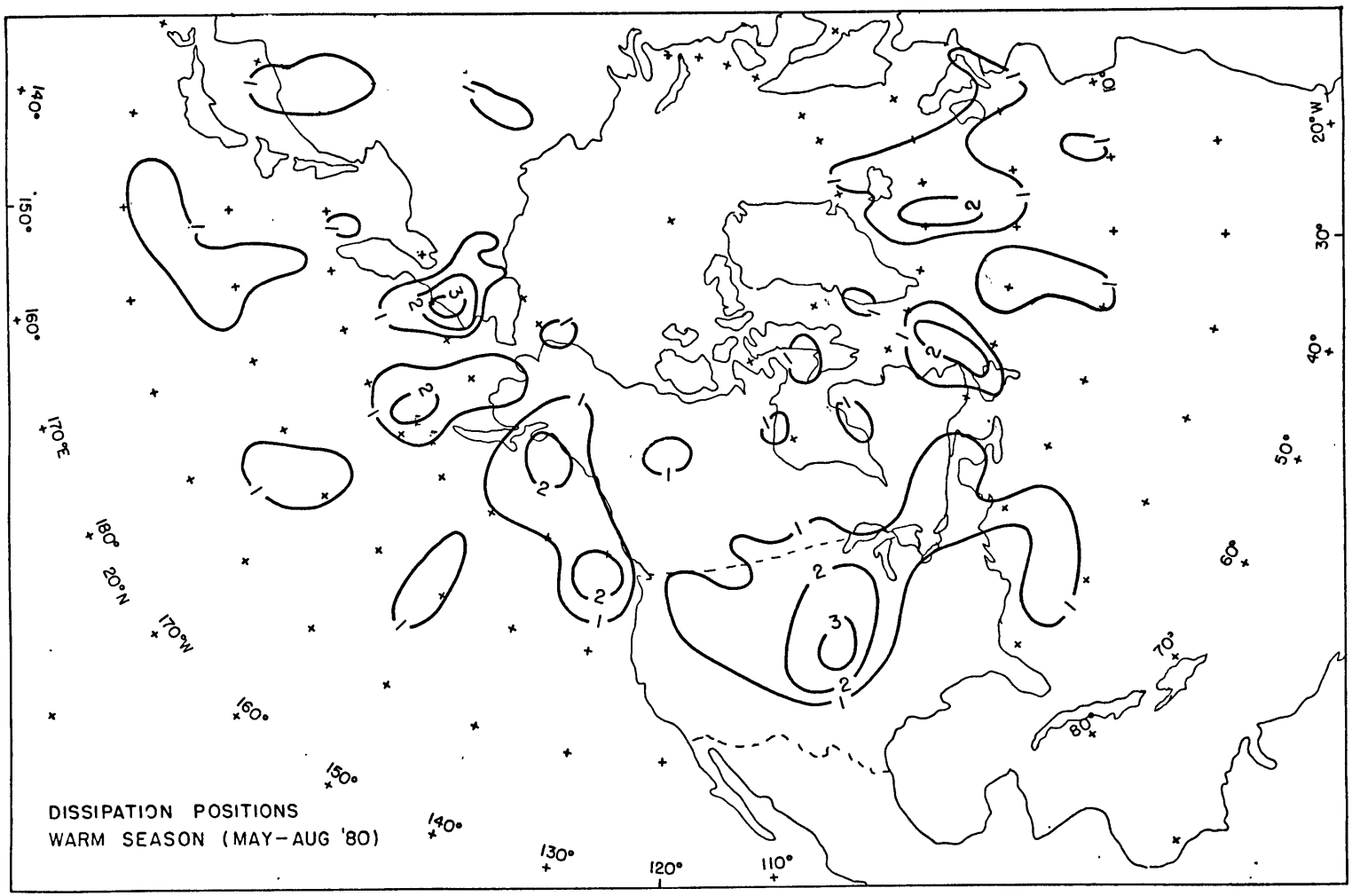
DISSIPATION POSITIONS
WARM SEASON (MAY–AUG '80)
140°
150°
160°
170°E
180°
170°W
160°
150°
140°
130°
120°
110°
10°
20°W
30°
40°
50°
60°
70°
80°
20°N

FIGURE 2.20

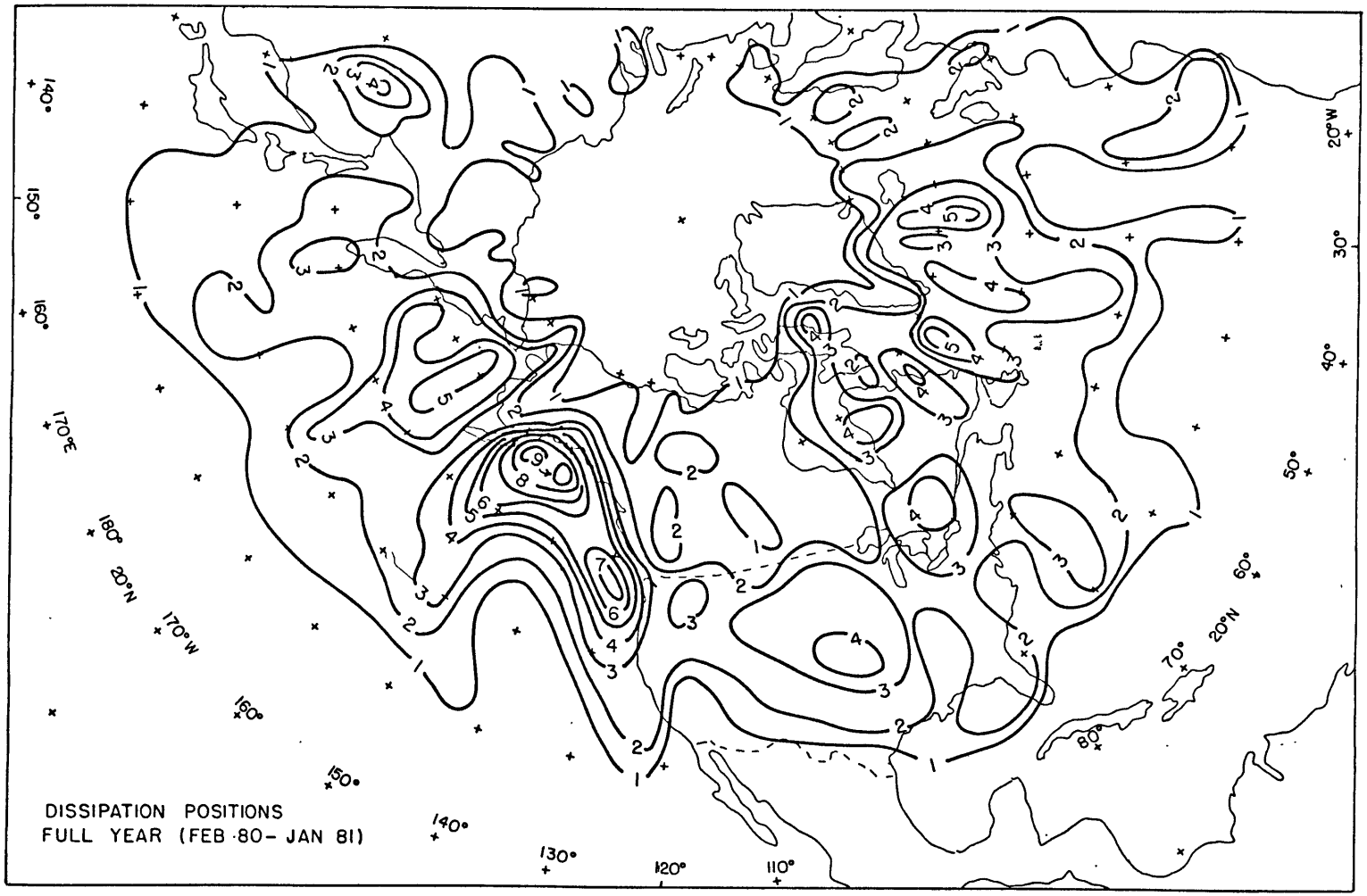
DISSIPATION POSITIONS
FULL YEAR (FEB 80 - JAN 81)
140°
150°
160°
170°E
180°
170°W
160°
150°
140°
130°
120°
110°
20°N
20°W
30°
40°
50°
60°
70°
80°

FIGURE 2.21

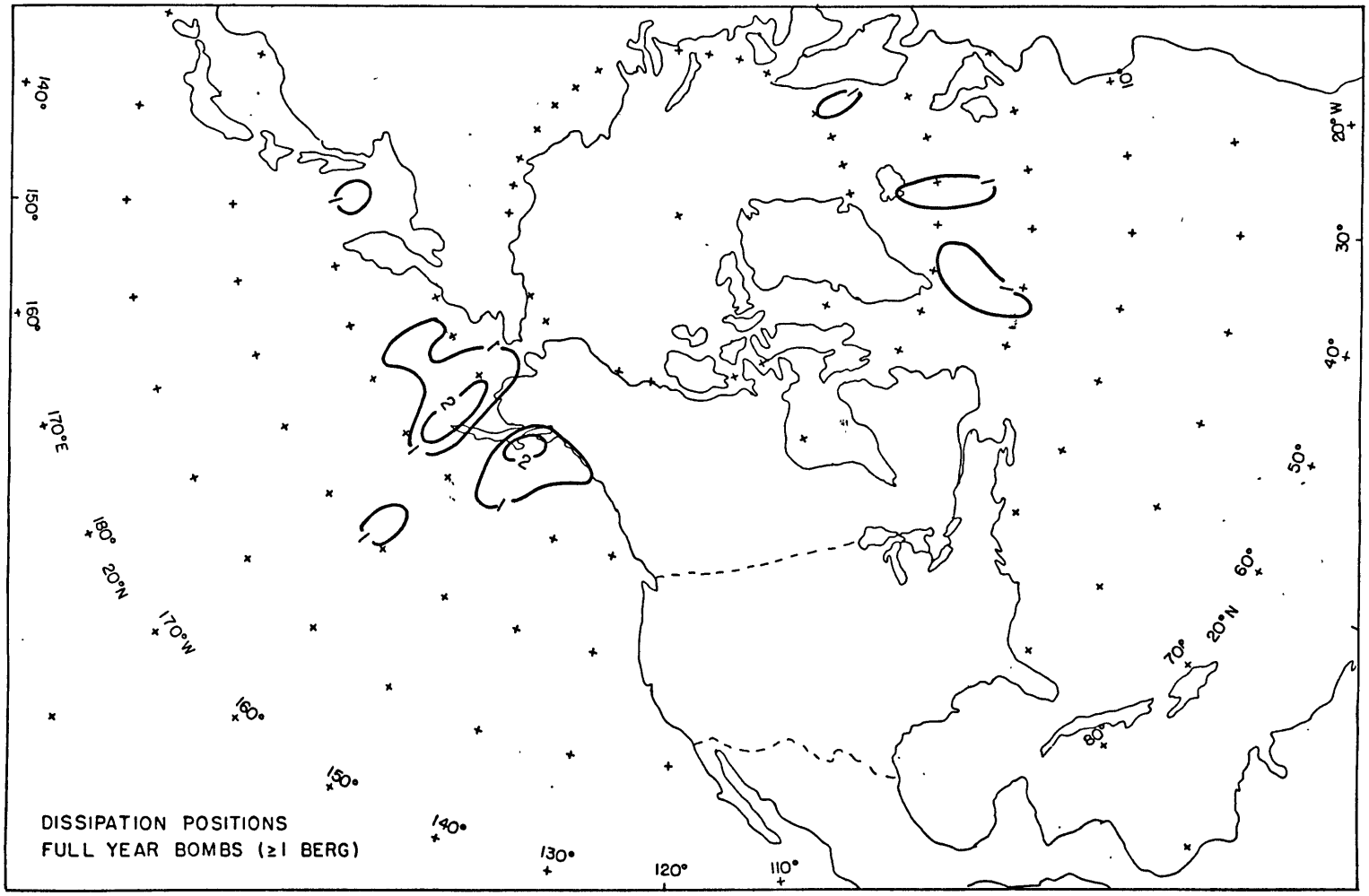
DISSIPATION POSITIONS
FULL YEAR BOMBS (≥1 BERG)
140°
150°
160°
170°E
180°
20°N
170°W
160°
150°
140°
130°
120°
110°
10
20°W
30°
40°
50°
60°
70°
20°N
80°

FIGURE 2.22

The 6 year pattern of bomb distribution clearly shows the eastern Pacific maximum. Apparently, the blasts of cold, Arctic air were sufficient to compensate for the lack of exceptionally warm ocean currents, since this feature is almost of the same magnitude as the maxima associated with the Kuroshio current and the Gulf Stream. Another possible explanation is an increase in available data, but it seems unlikely that this location is frequented by ships more than some other areas of the Pacific Ocean which do not show any such maximum.

The distribution of dissipation positions are shown in figures 2.20-22. The warm season pattern is somewhat diffuse, though maxima are discernible. There is the suggestion of a preference for the Gulf of Alaska region, as well as the area between Newfoundland and Greenland, and to the south of Iceland. There are slightly greater maxima in the midwest of the U.S. and the easternmost tip of the Soviet Union. These surface features appear to be reflected in the 700 mb pattern for June, which show mean low centers in the Alaskan coastal region and the Kamchatka peninsula. The full year distribution greatly accentuates the Gulf of Alaska as a region of cyclolysis, unparalleled anywhere else in the Northern Hemisphere. The regions about the southern tip of Greenland again show relative maxima, and there is a maximum over the Aleutian chain,

with no evidence of a maximum over Kamchatka. A minor maximum over Manchuria suggests this area as the likely final resting place of lows migrating over the Asian continent. The dissipation positions of bombs appear to be primarily located in the Gulf of Alaska for Pacific cyclones, and the Greenland/Iceland area for Atlantic cyclones. It is clear that the observed mean low centers in these areas are indications of the final resting place of lows rather than regions of active cyclogenesis. Cyclones move into the region, and remain in a more or less fixed position until another storm moves into the area and absorbs them, or else simply decay until they can no longer be identified as cyclones.

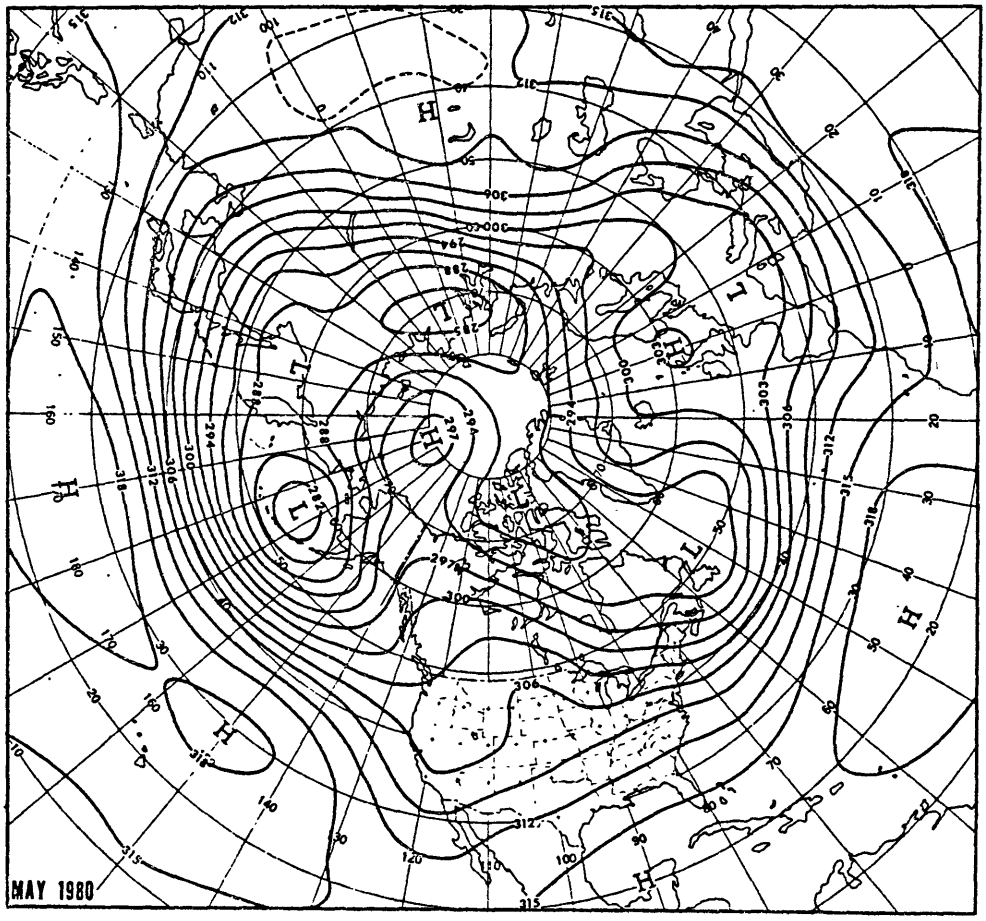

Mean 700 mb height contours (dam) for May 1980.

Mean 700 mb height contours for selected months, as published by Monthly Weather Review, Figures 2.23-26.

FIGURE 2.23

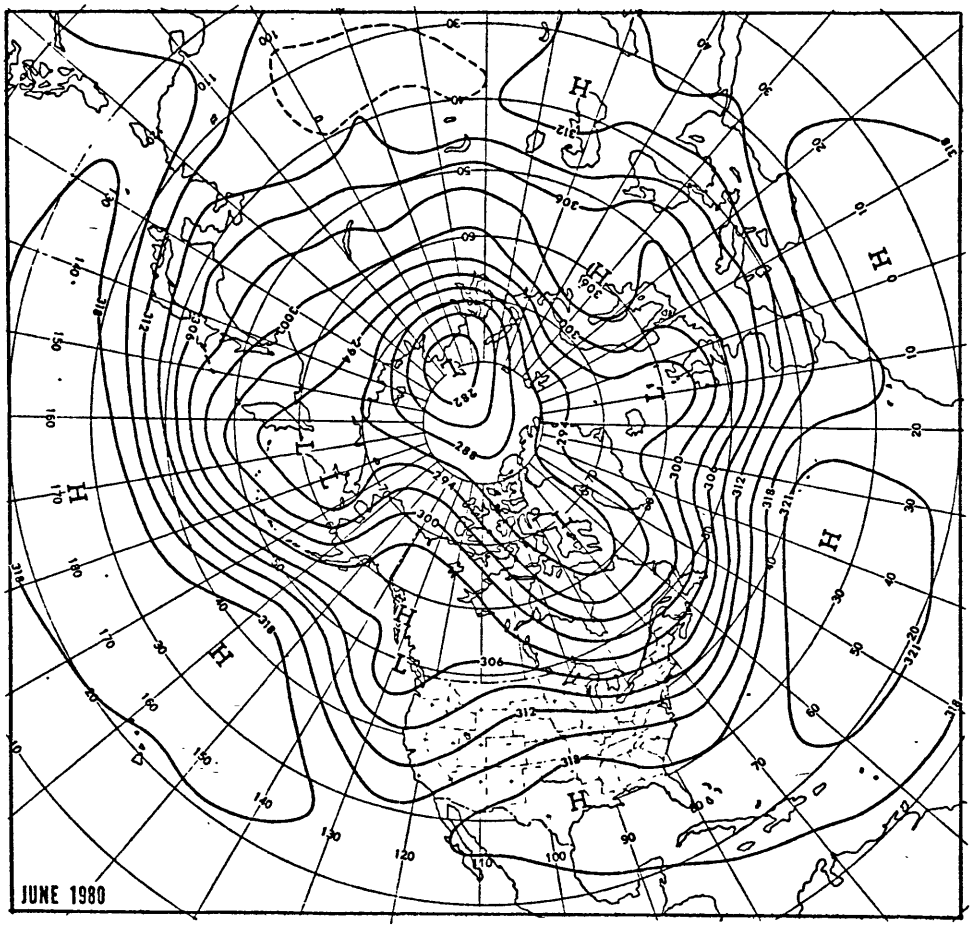

Mean 700 mb height contours (dam) for June 1980.

FIGURE 2.24

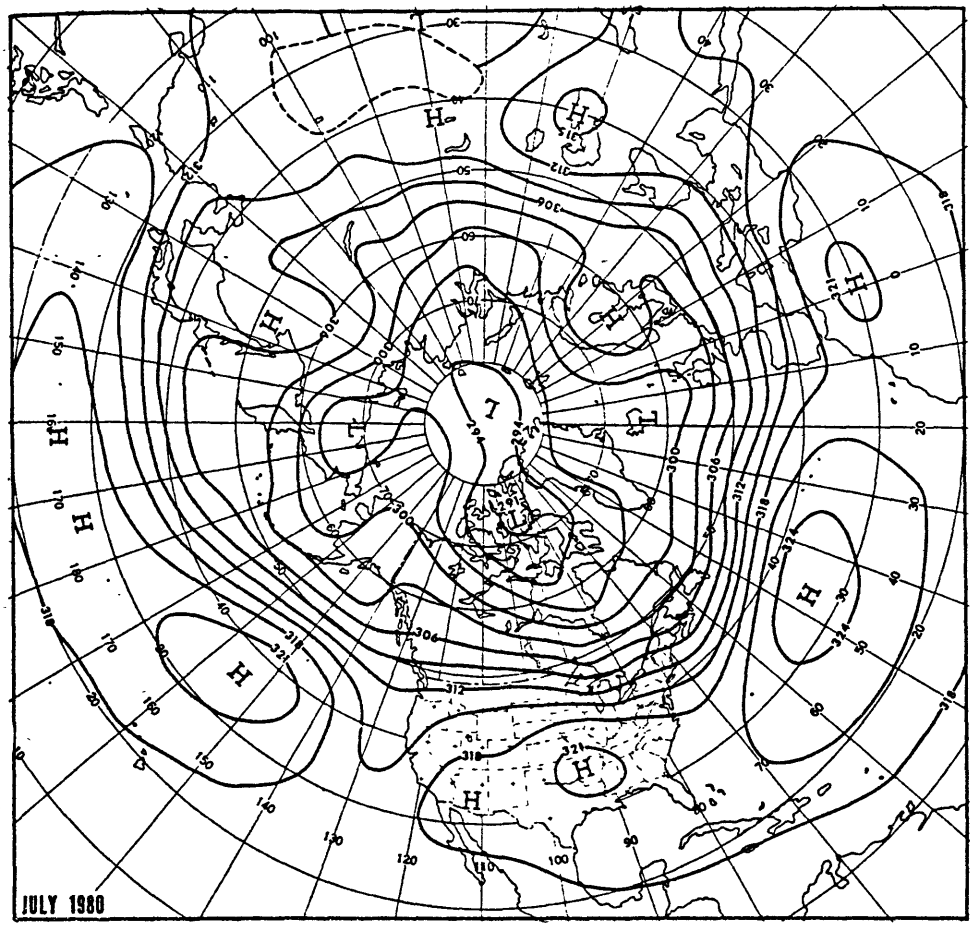

Mean 700 mb height contours (dam) for July 1980.

FIGURE 2.25

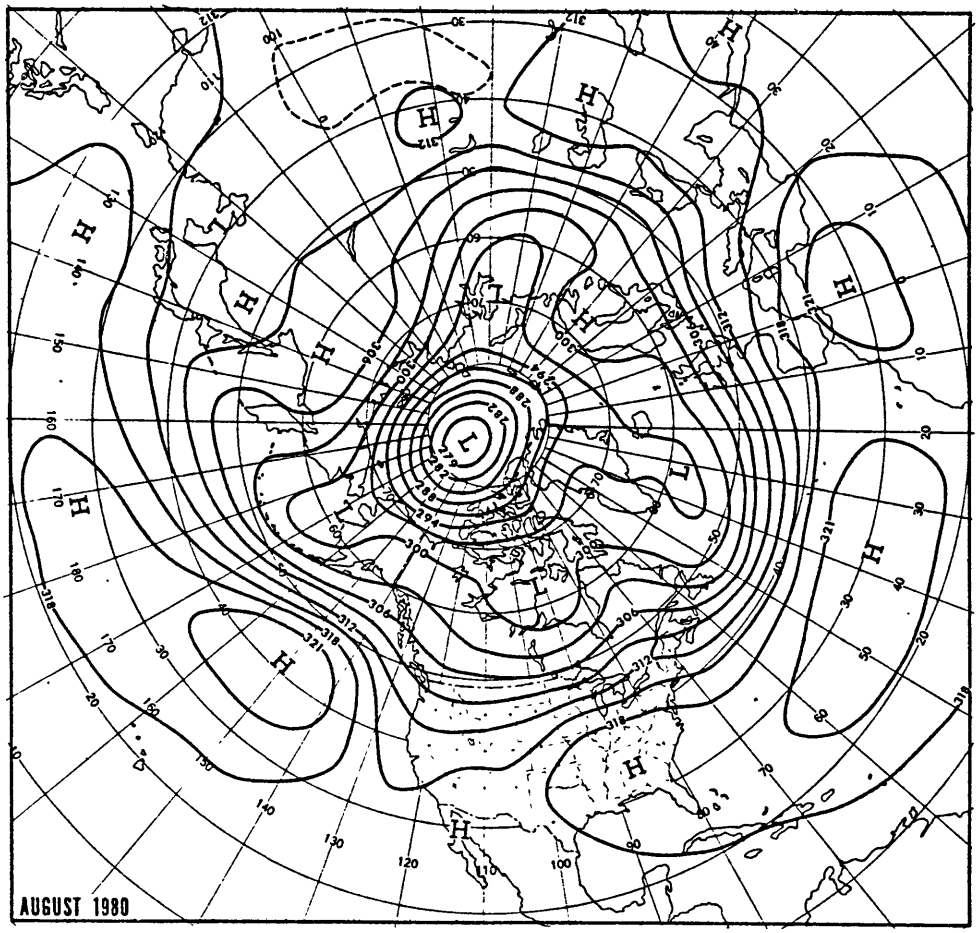

Mean 700 mb height contours (dam) for August 1980.

FIGURE 2.26

2.3 Summary

This section has dealt with the climatology of cyclones, and, particularly, of explosive cyclones. The question of explosive cyclogenesis as a phenomenon distinct from ordinary baroclinicity has been examined, and statistical evidence was found that supported this hypothesis. The climatology of cyclones indicated that the preferred regions of explosive cyclogenesis are primarily baroclinic zones, areas which support the development and continued existence of ordinary low pressure systems; this finding is consistent with that of Sanders and Gyakum (1980), that explosive cyclones exhibit a relationship to the upper level flow that is qualitatively similar to less intense storms. The evidence thus suggests that the mechanism operative in cases of explosive cyclogenesis is some combination of the baroclinic process with some other mechanism. This is entirely consistent with the results of Gyakum (1981) and Bosart (1981), who studied particular cases of explosive cyclogenesis in detail, and suggested that the bulk effects of cumulus convection in combination with the baroclinic process was the explosive forcing mechanism. An investigation of this process was conducted; the results will be detailed in the next section.

3.0 Application of an Analytic Model of Wave-CISK

3.1 Objectives

The results of the previous section provide strong statistical evidence that there is a distinct physical process operative in most cases of explosive cyclogenesis that is in some fundamental way different from ordinary baroclinicity. Unfortunately, a statistical analysis cannot tell us anything more about the mechanism itself; other methods must be utilized to continue the investigation.

Gyakum (1981) has provided substantial evidence that in the QE II case, the storm was driven by the combined effects of convective condensational heating and the baroclinic process. Bosart (1981), in his analysis of the Presidents' Day storm of 1979, suggested that this mechanism was operative in that case as well. Rather than perform additional case studies, where the data sets would likely be less complete, it might be helpful to analyze the convective condensational heating process in a sample of explosive cases. This approach may make it possible to ascertain whether or not this combination of baroclinicity and convective latent heat release is a likely explanation for the incidence of explosive cyclogenesis.

A sample of 21 cases of east coast explosive cyclogenesis was analyzed, within the context of an analytic, quasi-geostrophic model modified to include a wave-CISK (conditional instability of the second kind) parameterization suggested by Mak (1982) in order to incorporate the diabatic effects of convection. It was hoped that the evolution of these storms could be accounted for within the limits of this simple model, and that subsequently, a simple forecast scheme for explosive cyclogenesis could be developed.

3.2 Review of wave-CISK

In wave-CISK, cumulus convection cooperatively interacts with the large scale pattern of convergence and divergence to amplify the synoptic disturbance. In a conditionally unstable environment, forced ascent through low-level convergence associated with the propagating large scale disturbance produces convective towers, which act to produce a solenoidal field of vertical motion through the release of latent heat. Thus, the large scale disturbance is amplified, and a positive feedback loop is established. There is an important distinction between CISK and wave-CISK; the CISK mechanism operates through Ekman pumping in the boundary layer, whereas the wave-CISK process provides moisture convergence through the inviscid

wave itself; modifications (i.e. increased convergence) are made possible through the inclusion of viscous effects.

The theoretical advantage of both the CISK and wave-CISK mechanisms is in the ability to relate the magnitude of the convective heating to parameters of the large scale flow field, specifically to the vertical velocity at some low level. Without such a formulation, one would have to model the convective elements themselves, and calculate the heating directly, at substantial increases in difficulty and cost.

In CISK parameterizations, the latent heating is taken to be distributed in the vertical according to some specified profile. Unfortunately, it has been shown that the CISK mechanism is sensitive to the vertical profile of heating, with maximum large scale instability associated with a heating maximum at low levels (Davies, 1979). Such a profile would presumably correspond to either severe entrainment or shallow convection. Stark (1976) used a version of the Arakawa-Schubert (1974) cumulus parameterization in a CISK model; this avoided the problem of specifying the vertical heating profile, since it results as a by-product of the calculations. His results suggested that the CISK mechanism was not effective in amplifying a disturbance, but the study has been criticized

(Lindzen and Stevens, 1978) as an inappropriate usage of a sophisticated cloud model. In the usual formulations, the heating is implicitly assumed to occur instantaneously, that is, the time it takes the entire cloud ensemble to process the low level moisture supply and convert it to heat that is noticeable on the large scale is infinitesimal. There is little data on the true time scale of such a process, but estimates have ranged up to 12 hours.

Probably the most serious defect of wave-CISK is the lack of a short wave cutoff. The fastest growing scale is the smallest one, that of an individual convective element. Even when a closed parameterization scheme is used (Stark, 1976), this feature prevails. The usual method for dealing with this problem has been to introduce an additional frequency dependent heating parameter to suppress the short wave modes. This prescribes a scale, and thus represents a quick-fix rather than a solution to the problem. Davies (1979) included a time lag in the heating response to the forcing, and found that for a lag of 12 hours, the most unstable mode is of finite wavenumber. The time scale of 12 hours seems long, and Davies himself noted that the lag effect was not a viable means of scale selection based on this consideration. Thus, it is clear that there are still some significant theoretical problems in current wave-CISK

formulations that remain to be solved.

3.3 Model formulation

In this work, the wave-CISK formulation suggested by Mak (1982), which follows from his earlier theoretical findings (Mak, 1981), will be used. In the earlier work, Mak suggested that the short wave cutoff problem is intimately related to the phenomenon known as Type B CISK (Bates, 1973). In Type B CISK, the growth rate becomes infinite for a particular length scale when the heating intensity reaches a critical value. Some investigators have argued that since the critical heating intensity is somewhat larger than that found in the atmosphere, one can ignore the result; that argument seems unsatisfactory from a theoretical point of view, and Mak demonstrates that the phenomenon arises from the same mathematics as the shortwave cutoff problem, namely, the relation of the heating to the divergent (secondary) component of the flow. If the forcing of the heating is related to the rotational (primary) component of the flow alone at some level, both problems are eliminated. The divergent component of the velocity field still appears in the non-zero divergence term of the vorticity equation, and is expressed in terms of the vertical derivative of the vertical p-velocity. While this avoids the necessity of introducing a new

parameter and allows the flow to determine the scale of the cutoff, it is not clear how the atmosphere distinguishes between the two vertical velocity components. This formulation introduces an intrinsic time lag in the parameterization (on the order of the inverse of the Coriolis parameter, approximately 2-4 hours for middle latitudes), since the rotational component of the flow is strongly influenced by the rotation of the earth. Thus, the internally determined time scale of the large scale (rotational) flow dictates the time scale of the conversion of the low level moisture to heating that is noticeable on the large scale.

The problem can be easily formulated through the quasi-geostrophic omega equation in p-coordinates, generalized to include diabatic effects (Haltiner, 1971). Thus,

$$\left(\sigma\nabla^2 + f_0\eta_0\frac{\partial^2}{\partial p^2}\right)\omega = f_0\frac{\partial}{\partial p}(V_g\cdot\nabla\eta) - \nabla^2\left(V_g\cdot\nabla\frac{\partial\Phi}{\partial p}\right) - \frac{R}{c_p p}\nabla^2 q$$

LF(dynamic/adiabatic) LF(diabatic)

The vertical velocity can then be written as the sum of two components, directly related to the two forcing terms above:

$$W = Wa + Wd$$

where Wa is the vertical p-velocity induced by the dynamic/adiabatic forcing

Wd is the vertical p-velocity induced by the diabatic forcing (convective latent heat)

The parameterization problem is in relating $\dot{q}$ to the dynamic vertical p-velocity at some low level; this was done in the following way:

$$\dot{q} = -Cp\ E\ h(p)\ Wa*$$

where Cp is the heat capacity at constant pressure

E is a heating intensity parameter (K/mb)

h(p) is the vertical heating profile

Wa* is the vertical p-velocity at p=PL induced by dynamic and adiabatic effects

A continuous, moist (but not necessarily saturated) layer from p=PO to p=PL is postulated; the moisture supply to the condensational process is assumed to be proportional to -Wa*, and to the specific humidity of the layer. This moisture flux is entirely precipitated out, giving a certain total heating related to the vertical integral of the heating profile, h(p). The heating intensity

parameter, E, crudely represents the moisture content of the layer. One can therefore relate the heating intensity to the mixing ratio of the layer, as will be discussed later. One can, of course, relate the moisture flux to the entire vertical p-velocity (rotational plus divergent) at some low level (p=PL), but the resultant flow would exhibit the unwanted feature of Type B CISK. An example of this will be provided later, within the context of the model.

For the vertical profile of heating, two idealized but reasonable profiles have been chosen. They are of the form:

$$h1(p) = \{ H(p)\ p\ /\ PO \}$$

$$h2(p) = \{ K\ H(p)\ /\ p \}$$

where $H(p) = 0$ for $p > PL,\ p < PU$

$= 1$ for $PL > p > PU$

$K = (PU^2 - PL^2)\ /\ 2\ PO\ \ln(PU/PL)$

These are essentially top-hat profiles, one with a low level maximum at p=PL, the other with an upper level maximum at p=PU. These profiles are pictured in figure 3.01, with PL= 850 mb and PU= 400 mb. One can associate the PL level with the lifting condensation level, and the PU level with the cloud top. Although 850 mb is probably

slightly too high for the LCL in the maritime atmosphere, sample calculations showed this level yields the maximum large scale instability. 850 mb may represent the level of optimum moisture convergence, since the vertical motion field is stronger than at lower levels, while the air itself is still relatively moist. Since the heating profile represents diabatic effects alone (and not adiabatic warming through compensating subsidence), the h1(p) profile is probably the more realistic of the two. Some sample calculations were performed with the two profiles; the results indicated that the low level maximum was slightly more effective (15%) in producing deepening than the high level maximum; this result is consistent with that of Davies, although he found the discrepancy between the two profiles to be greater, with heating profiles with maxima at low levels to be about twice as effective as those at high levels.

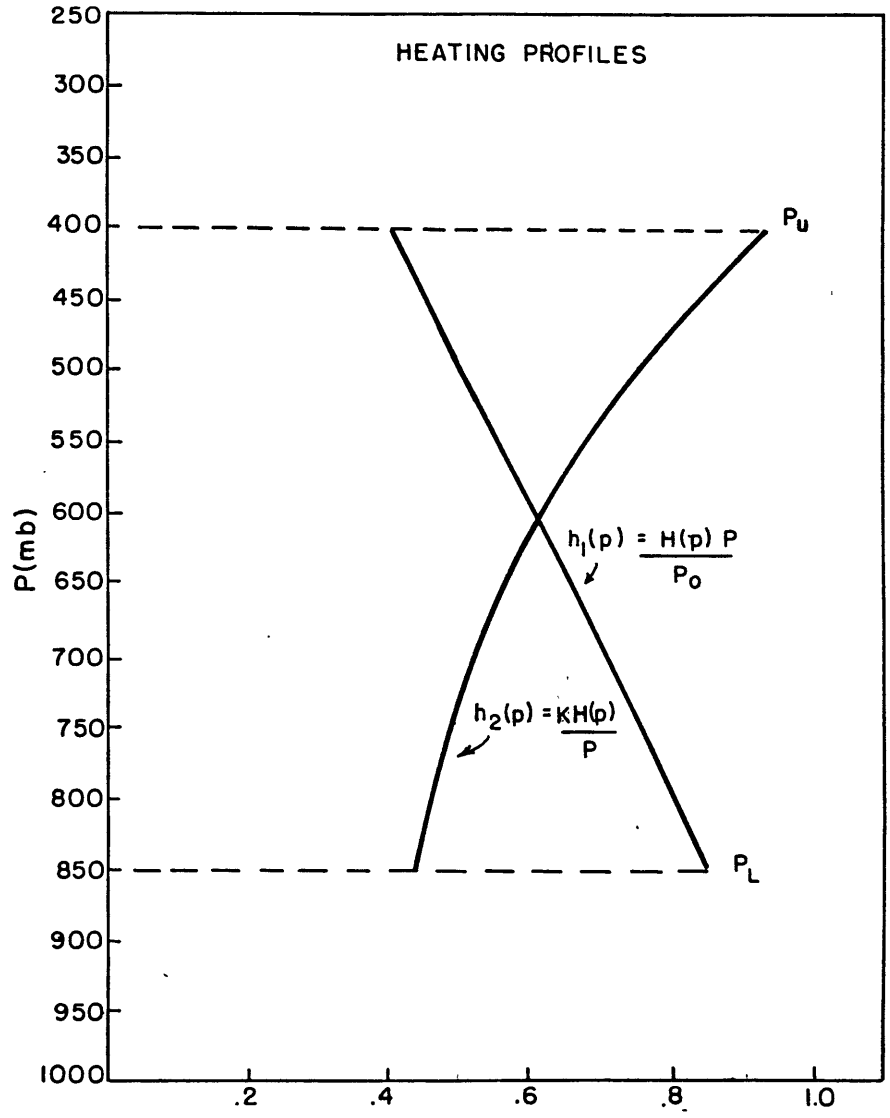
HEATING PROFILES
P(mb)
250
300
350
400
450
500
550
600
650
700
750
800
850
900
950
1000
.2
.4
.6
.8
1.0
P_u
P_L
$h_1(p) = \frac{H(p)\,P}{P_o}$
$h_2(p) = \frac{KH(p)}{P}$

FIGURE 3.01

This parameterization allows negative (unconditional) heating; this is done primarily for convenience, as it is clearly unphysical. In the tropical atmosphere, it has been suggested that the total convective heating can be looked upon as the sum of mean and perturbation quantities; the mean heating is taken to be of the same magnitude as the perturbation, so that there is never any negative heating. It is not clear that this interpretation remains valid in the middle latitudes, however; there, the convective activity in a sense propagates along with the large scale pattern of convergence and divergence, and is therefore more akin to a nondispersive wave packet than a single mode. The main effect of unconditional heating appears to be an enhancement of the effective amplitude of the CISK heating, and thus, of consequent growth rates (Davies, 1979).

The CISK parameterization was inserted into an analytic, baroclinic model after Sanders (1971) and Sanders and Gyakum (1980). In this way, one can examine the relationships between the model parameters and the CISK mechanism, and hopefully learn something about the process, rather than accept the black box approach of a numerical model. The main disadvantage of such an approach is that the results, strictly speaking, are diagnostic rather than prognostic; the instantaneous results must be extrapolated

in some meaningful way if one wishes to make a forecast. Instead of starting with an exact system, and obtaining approximate results, as with a numerical model, one begins with an approximate system, and obtains exact results.

The following thermal structure was assumed:

$$T(x,y,p) = Tm(p) - (ay + \hat{T} \, Cos \, kx \, Cos \, ly)$$

$$Tm(p) = Tm(PO)\{ p/PO \}^{b}$$

The term in parantheses represents the horizontal variation of the temperature field, the first term representing a constant meridional temperature gradient with intensity a, and the second representing a two dimensional harmonic variation with amplitude $\hat{T}$. The horizontal variation is taken as constant in the vertical, representing fairly well the small change in intensity of horizontal temperature contrasts through the maritime troposphere. The term Tm(p) represents the average over a wavelength in X and Y on a constant pressure surface, and essentially provides a label for the isotherms at each level. The expression for Tm(p) reveals that the temperature drops off monotonically with height, that is, there is no isothermal region above the tropopause. It appears to represent the atmosphere quite well in the

troposphere, the region of primary interest for this study, as shown in figure 3.02 for the Presidents' Day case.

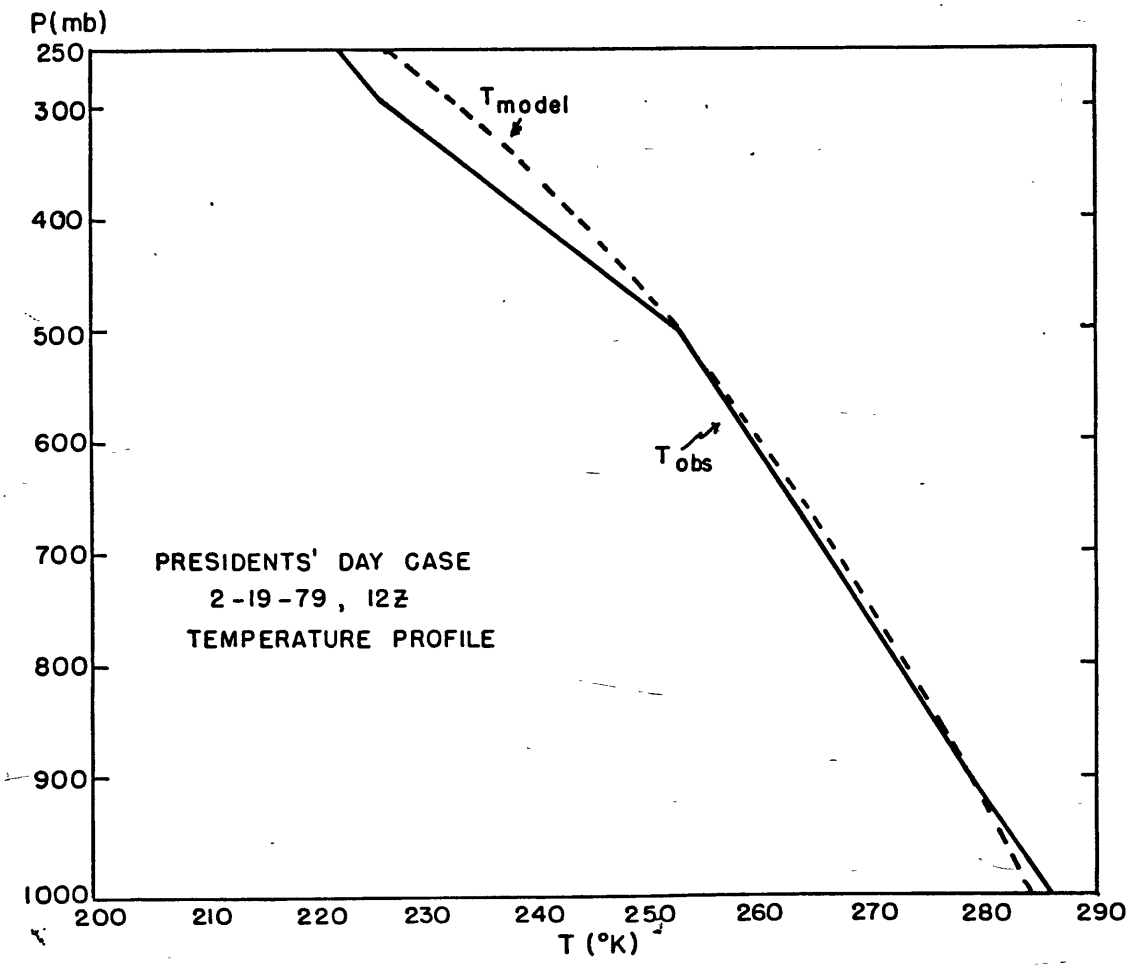

FIGURE 3.02

In this study, the expression for the stability factor, σ, is derived as in Sanders (1971); the constant value of temperature adopted is the vertical average of Tm(p). The adoption of the constant value of temperature in the expression for the stability factor appears to make little difference, except in the upper reaches of the troposphere, where it is too large. The discrepancies are small, however, as shown in figure 3.03, again for the Presidents' Day case.

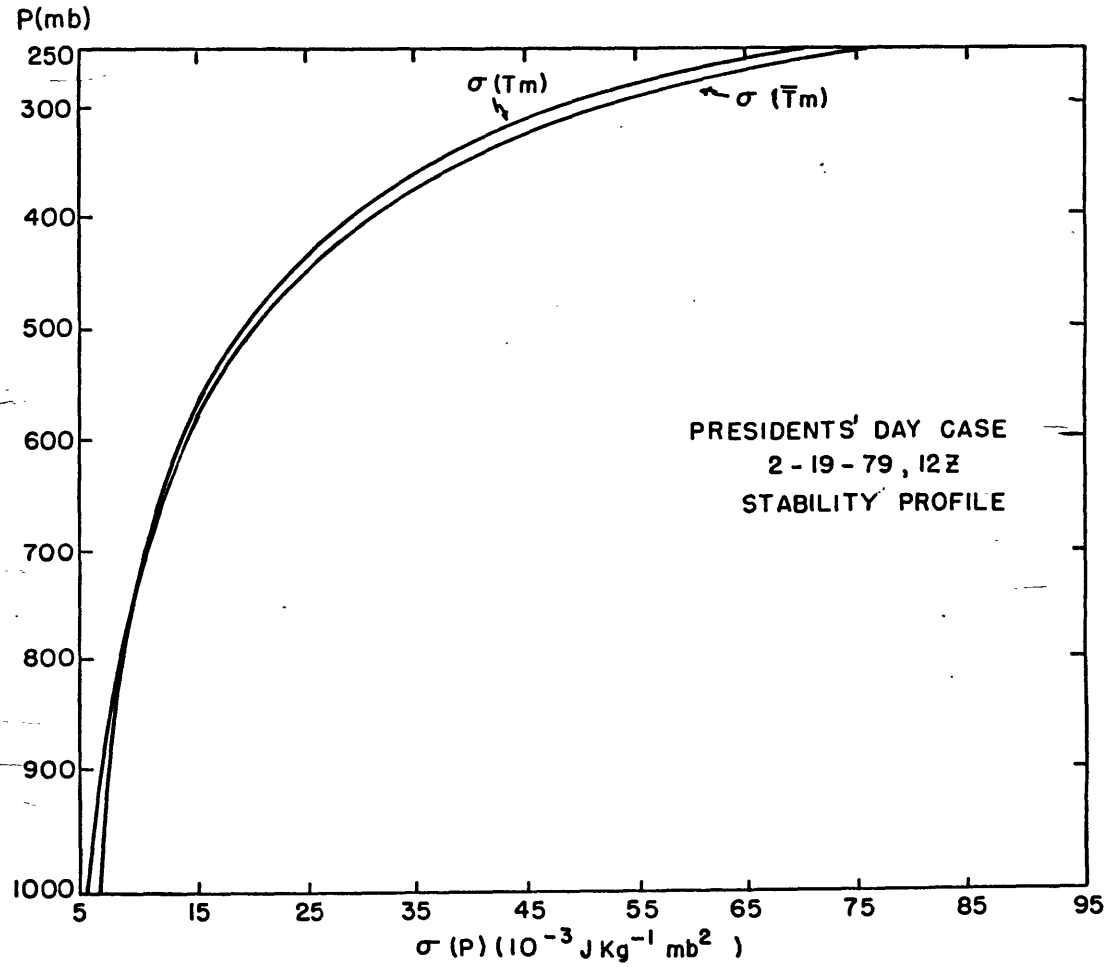

FIGURE 3.03

The geopotential field is determined at the base of the atmosphere, as in Sanders (1971); thus, from hydrostatics, the geopotential is known at all levels. From the relations for temperature and geopotential, one can easily obtain relations for the geostrophic wind and geostrophic relative vorticity at any point in the three dimensional model atmosphere.

The procedure for solving the omega equation is identical to that in Sanders; the boundary conditions are that W go to zero at the top and bottom of the troposphere, p=PO and p=PT. The forms of the solutions are listed in the appendix. The forcing of the vertical motion terms are identified as in Sanders (1971), to wit:

W11; the advection of the component of thermal vorticity due to the gradient of the perturbed temperature field by the component of the thermal wind due to the meridional temperature gradient.

W12; the advection of planetary vorticity by the component of the thermal wind due to the gradient of the perturbed temperature field.

W2 ; the advection of surface relative vorticity by the component of the thermal wind due to the meridional temperature gradient plus the advection of the meridional temperature gradient by the surface wind.

W3 ; the advection of the perturbation temperature by the surface wind.

Profiles for the maximum values of these parameters appear in figure 3.04 for the Presidents' Day storm.

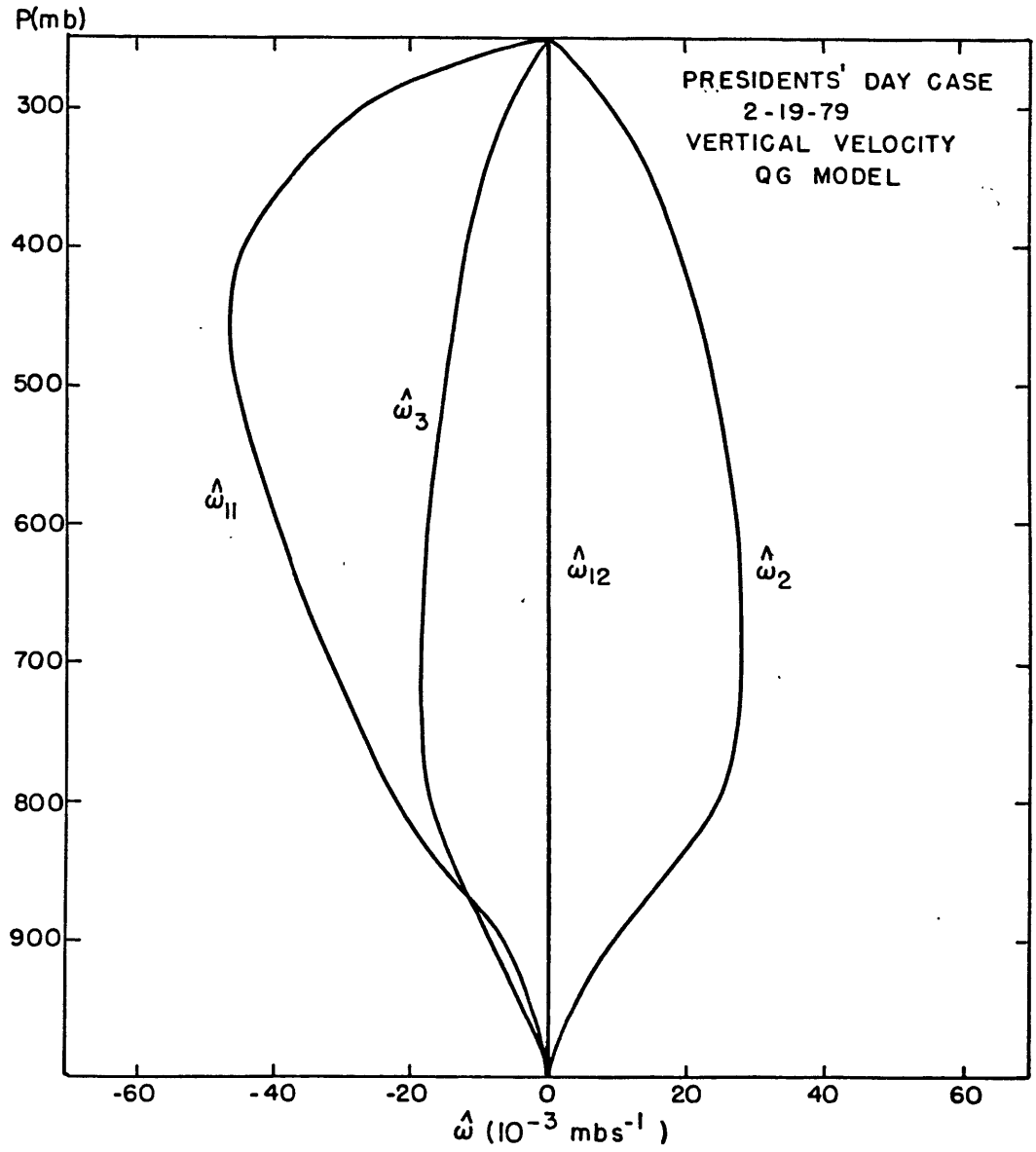
P(mb)
300
400
500
600
700
800
900
PRESIDENTS' DAY CASE
2-19-79
VERTICAL VELOCITY
QG MODEL
$\hat{\omega}_3$
$\hat{\omega}_{11}$
$\hat{\omega}_{12}$
$\hat{\omega}_2$
-60
-40
-20
0
20
40
60
$\hat{\omega}$ (10^{-3} mbs^{-1})

FIGURE 3.04

Although in a wave-CISK formulation it is not necessary to include viscous effects, common sense suggests that friction likely plays an important role in the evolution of an intense storm, particularly one that intensifies rapidly. The inclusion of such effects would also make it possible to examine, within the limitations of the model, the supposition that frictional balance is attained prior to occlusion in explosive cases. The derivation begins by postulating a balance between the pressure gradient force, the Coriolis force, and friction in the planetary boundary layer:

$$f \vec{K} \times (\vec{V} - \vec{V}g) = (d\vec{\tau}/dz) / \rho = \vec{F}$$

Applying the operator $\vec{K} \cdot (\nabla \times \ )$ to the above yields, in pressure coordinates:

$$\vec{K} \cdot (\nabla \times \vec{F}) = -g \vec{K} \cdot (\nabla \times d\vec{\tau}/dp)$$

neglecting the variation of the Coriolis parameter. The form of the stress is specified according to:

$$\vec{\tau} = \vec{\tau}O (p/PO)^{n} ; \quad \vec{\tau}O = \rho \, Cd \, |\vec{V}|^{a} \vec{v}$$

where $\vec{v}$ is the unit vector in the direction of $\vec{V}$. In evaluating the parameter $|\vec{V}|$ in the equation for the

stress, it seems reasonable to choose the maximum geostrophic surface velocity; thus:

$$|\vec{V}| = Vg(max) = (b_i^{n/2} \hat{\Phi}_i) / 8 f0$$

For n sufficiently large, $\vec{\tau}(p)$ goes to zero above the PBL. The expression for the surface stress, $\vec{\tau}0$, is a well established form in fairly good agreement with the available data. The vertical profile is an ad-hoc formulation, designed to maximize analytic convenience while still capturing the exponential decrease of the stress through the PBL. Figure 3.05 displays the vertical profile of the frictional force through the PBL for the Presidents' Day case, with the value of n equal to 9. The profile of the frictional force is quite close to that produced by the formulation used in Gyakum (1983b).

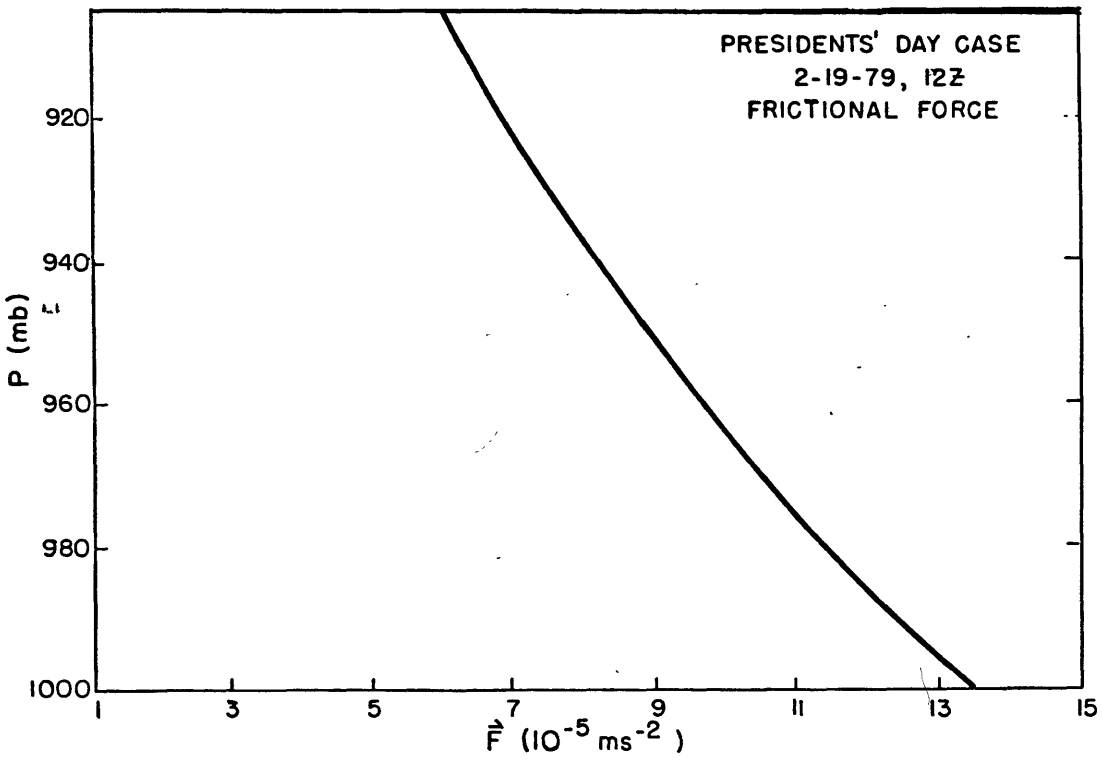

FIGURE 3.05

To determine the vertical motion field induced by frictional convergence the following equation must be solved:

$$\left(\sigma\nabla^2 + f_0\eta_0\frac{\partial^2}{\partial p^2}\right)\omega_4 = -f_0\frac{\partial}{\partial p}\left(\vec{K}\cdot\nabla\times\vec{F}\right)$$

Assuming the horizontal distribution of the vertical velocity field is the same as that of the forcing:

$$W4(p) = \hat{W}4(p)\ \mathrm{Cos}\ k(x+\lambda)\ \mathrm{Cos}\ ly$$

In the same manner as before, one can then solve for W4(p),

subject to the boundary conditions that the vertical velocity vanishes at the surface and at the tropopause. The expression for W4(p) is detailed in the appendix.

This is the complete set of equations for diagnosing the vertical motion field for the case without the effects of latent heating. To solve for the heating induced vertical motion, one must find the solution of:

$$\left(\sigma \nabla^2 + f_0 \eta_0 \frac{\partial^2}{\partial p^2}\right) \omega_d = \frac{-R}{c_p p} \nabla^2 \dot{q}$$

Using the parameterization for $\dot{q}$ discussed earlier, the equation can be written:

$$\left(p^2 \frac{\partial^2}{\partial p^2} - \frac{\gamma R \bar{T}_m}{f_0 \eta_0} b_i\right) \hat{\omega}_{di} = r_i H(p) p^2$$

where bi = b_1 for i = 1, 2, 4

= b_2 for i = 3

where ri = (-R E bi / f0 η0 P0) $\hat{W}a*i$ for h = h1(p)

= (ri P0 PT / p) for h = h2(p)

Thus, it is necessary to solve Euler equations of the form:

$$P^2 \hat{W}di'' + B \hat{W}di = ri\ p^2 \quad \text{for } PU < p < PL$$
$$= 0 \quad \text{for } p > PL,\ p < PU$$

Once again, the boundary conditions are that the vertical motion vanish at p=PO and p=PT. The details of the solutions can be found in the appendix. The convective condensational heating induced vertical motion field of the Presidents' Day case is shown in fig. 3.06-07. The magnitude of the maximum values are increased from three to four times the dry model values, and the profiles show a maximum at low levels, where the maximum heating occurs (these profiles are for the h1(p) heating distribution, PL=850 mb, PU=400 mb).

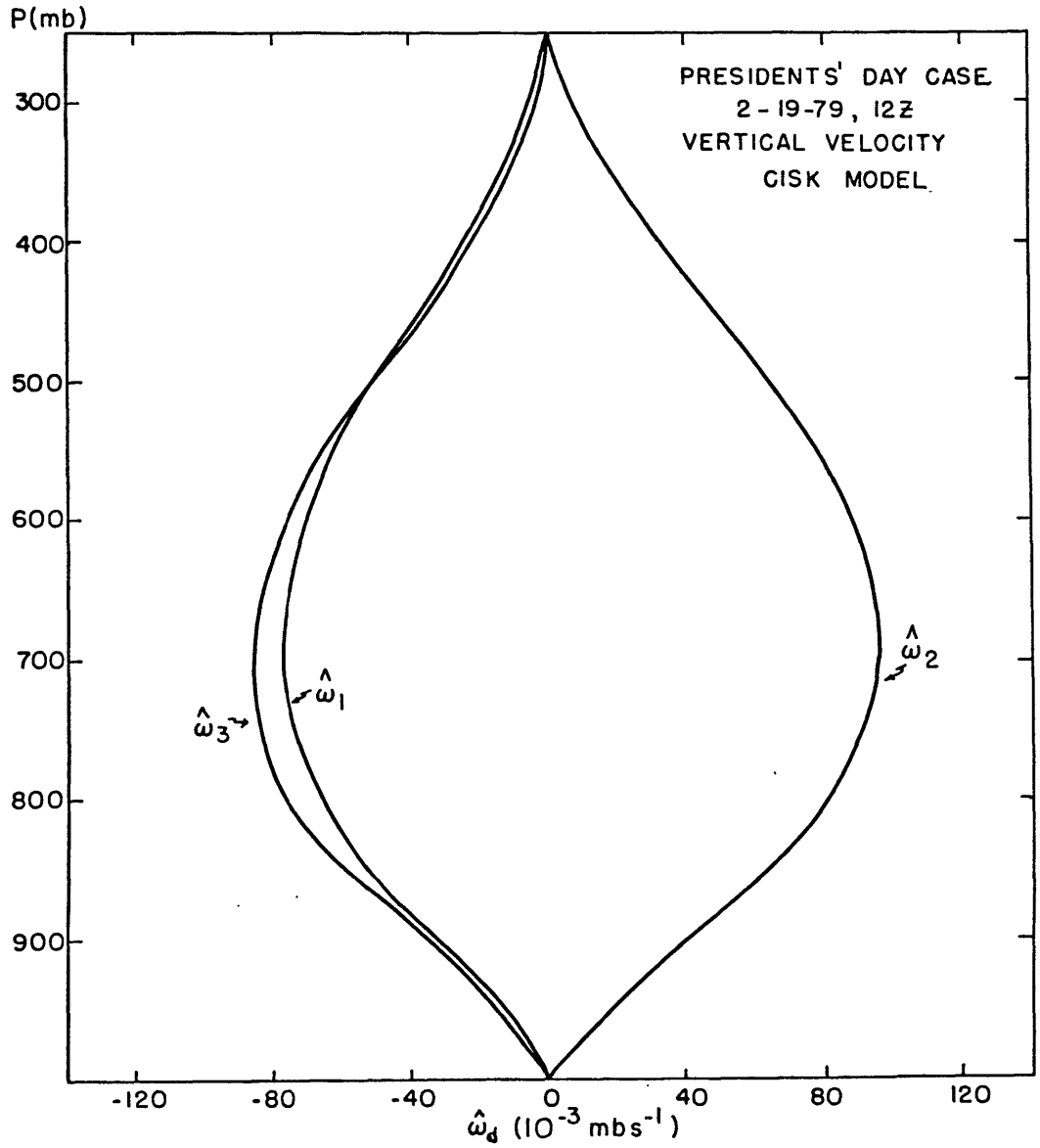
P(mb)
300
400
500
600
700
800
900
PRESIDENTS' DAY CASE
2-19-79, 12Z
VERTICAL VELOCITY
CISK MODEL
$\hat{\omega}_1$
$\hat{\omega}_2$
$\hat{\omega}_3$
-120
-80
-40
0
40
80
120
$\hat{\omega}_d$ (10^{-3} mbs^{-1})

FIGURE 3.06

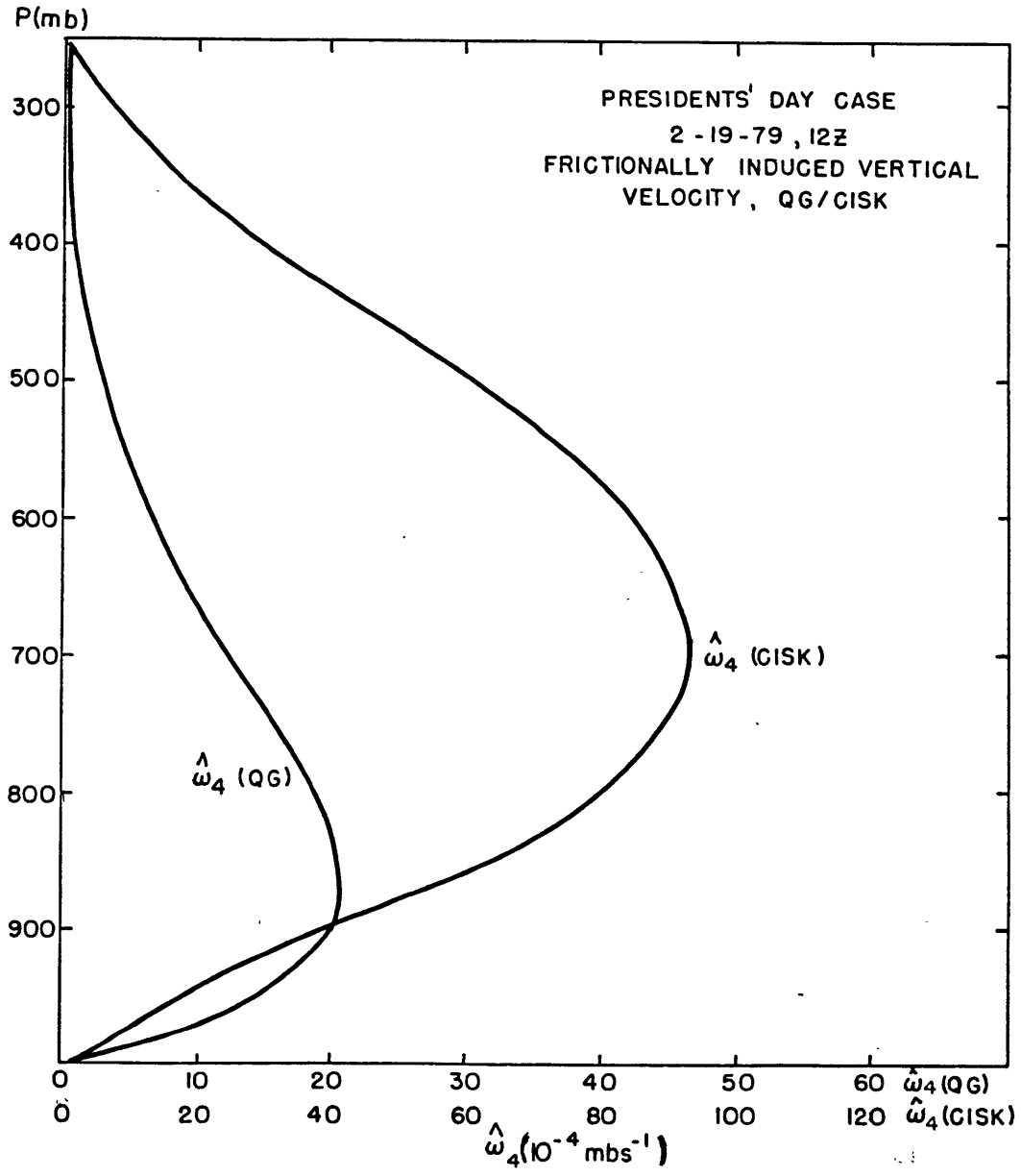
P(mb)
300
400
500
600
700
800
900
PRESIDENTS' DAY CASE
2-19-79, 12Z
FRICTIONALLY INDUCED VERTICAL
VELOCITY, QG/CISK
$\hat{\omega}_4$ (CISK)
$\hat{\omega}_4$ (QG)
0 10 20 30 40 50 60 $\hat{\omega}_4$(QG)
0 20 40 60 80 100 120 $\hat{\omega}_4$(CISK)
$\hat{\omega}_4(10^{-4}\,mbs^{-1})$

FIGURE 3.07

Once the vertical motion field is determined, the field of geopotential tendency can be derived from the vorticity equation. The solution for the geopotential tendency at the surface low center can be written:

$$X(\text{center}) = X(\text{dyn/adiabatic}) + X(\text{diabatic}) + X(\text{friction})$$

The details of the functions are shown in the appendix. The effect of heating is to increase the instantaneous deepening rate through the addition of two new terms, one augmenting the effect of the dynamic/adiabatic forcing, the other opposing frictional dissipation through increased low level convergence. The scenario is as follows: the vertical motion induced by low level temperature advection and vorticity advection aloft results in the release of latent heat through the lifting of conditionally unstable air past the level of free convection. This results in a heating induced vertical motion field in addition to the vertical motion induced by dynamic/adiabatic effects; the increased low level convergence and upper level divergence associated with the vertical motion field leads to greater intensification. The additional effect of frictional convergence and associated lifting of conditionally unstable air (and resulting convection/latent heat release) helps to oppose the damping effects of friction. The heating contribution to intensification is through W11, the

advection of the component of thermal vorticity due to the gradient of the perturbation temperature field.

One can derive the relations for the phase speeds of the surface features, and their relationship to the upper level flow (e.g., 500 mb), in a manner identical to that of Sanders (1971). Thus,

$$Cx(PO) = Cx_1 \cos k\lambda + Cx_0$$

$$Cy(PO) = Cy(dyn/adiab) + Cy(diab)$$

where $Cx_i = Cx_i(dyn/adiab) + Cx_i(diab)$

The specific forms of the terms are shown in the appendix. Two new terms appear in the relation for Cx, the effect of X(diabatic) in Cx_1 and the effect of latent heat release ahead of the storm associated with W2 in Cx_0. Whereas in the dry model, Cx_1 was usually quite small, the effect of X(diabatic) is to greatly increase the retarding (enhancing) effect of the term for warm (cold) lows. The effect on Cx_0, on the other hand, is an almost negligible increase in eastward propagation speed; the end result of heating is then to decrease the eastward propagation speed of the disturbance. There is one additional heating term in the expression for Cy, related to the latent heat release associated with W3. The increase in Cy can be quite substantial, and there are no retarding effects to

compensate. The result is an increase in the northward component of phase velocity with heating. The overall effect of heating is usually to increase the phase speed of the disturbance, most particularly in the northward direction. Since the instantaneous 500 mb flow in a developing system is generally west-southwest over the surface center, this effect is a possible explanation of the observed "left-movers," cyclones that move to the left of the instantaneous upper level flow over the center, in contradiction of the usual baroclinic result. An analysis of 67 explosive cyclones in the period September 1981 through April 1982 showed 51% of those storms moved to the left of the instantaneous 500 mb flow. The left movers showed a slight bias towards less rapid deepening, with twice as many of the strongest deepeners moving to the right. A possible explanation of this observation is that in the weaker deepeners, the CISK mechanism is able to overcome the right moving tendency of the baroclinic process.

It is now possible to provide an example of Type B CISK. One can show that in the case where the heating is parameterized in terms of the total vertical motion field (dynamic/adiabatic plus diabatic):

$$W(PL) = Wa^* / (1 - E B)$$

where B is some constant that depends on all the parameters

of the model. Thus, for certain values of E, W(PL) goes to infinity. Some tests were run, using the scheme; as an example, a plot of phase speeds and geopotential tendency as a function of heating intensity for the Presidents' Day case are presented in figure 3.08. As can easily be seen from the plot, both the geopotential tendency and the phase speed become unbounded for certain values of E, in contrast to the parameterization relating the heating to only the dynamically and adiabatically induced vertical velocity. It is clear that such a scheme is highly unstable relative to small changes in heating intensity, so for the remainder of this work, the Mak scheme is used.

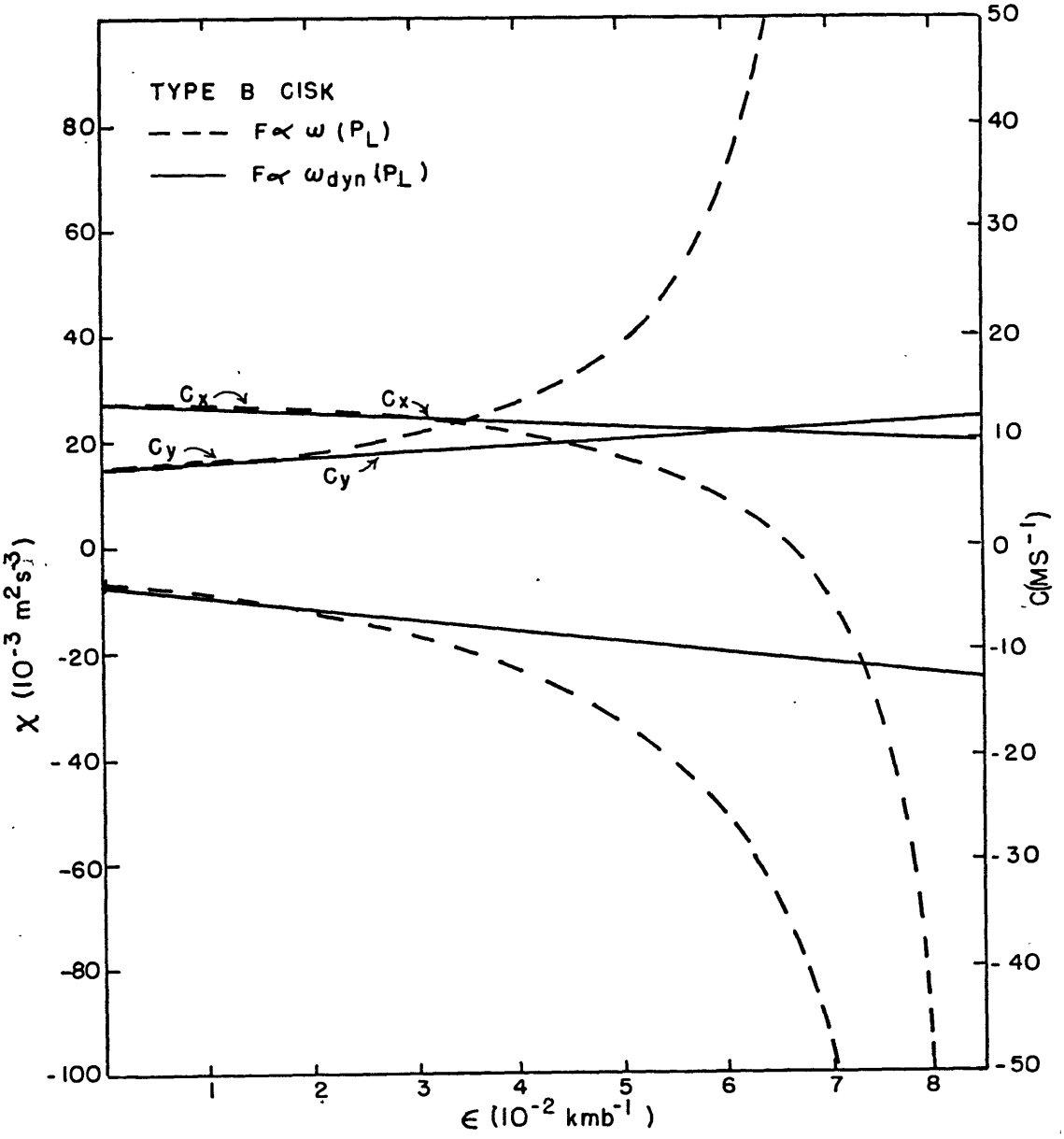
TYPE B CISK
F∝ ω (P_L)
F∝ ω_dyn (P_L)
Cx
Cx
Cy
Cy
χ (10^-3 m^2 s^-3)
C(MS^-1)
∈ (10^-2 kmb^-1)
80
60
40
20
0
-20
-40
-60
-80
-100
50
40
30
20
10
0
-10
-20
-30
-40
-50
1
2
3
4
5
6
7
8

FIGURE 3.08

It is now possible to determine the vertical motion fields, phase speeds, and instantaneous deepening rates of a disturbance at any instant for which the 1000-500 mb thickness field is available. It is not clear how one determines whether a CISK mechanism is operating, however; in terms of this model, one still must determine a value for the heating intensity. Since this parameter is fundamentally related to the mixing ratio at p=PL (see appendix), one approach would be to choose the value of E which corresponds to the saturation mixing ratio at p=PL. Thus, it would be necessary to know only what the temperature structure was at that pressure level to estimate qs and E. This still does not answer the question of determining the existence of a CISK process; consultation of satellite photos would provide information on the existence of convection (though not whether that convection was cooperating with the large scale).

Once the instantaneous fields have been determined, strictly speaking, it is not possible to say what those fields will look like at any time thereafter. The next step, then, is to determine a logical procedure for extrapolating the instantaneous results in time. Since there is no additional information concerning the continued evolution of the large scale forcing, a reasonable assumption (for short periods) might be that the initial

value holds for the entire period. In some cases, continued development will result in an underestimation of the overall forcing, while in others, the initial forcing will represent the height of the disturbance organization, resulting in an overestimate. Still, one might expect that such an assumption remains reasonably accurate for time periods less than some critical time scale for the synoptic scale, say 12 hours.

The simplest approach is a linear extrapolation. The assumption is that the forcing and the friction remain constant over the interval:

$$DP(t) = 4 \, (XO + XFO) \, t \, / \, 300 \; ; \; XF(t) = XFO$$

$$\text{where } XO = X(dyn/adiab) + X(diab) = const$$

$$XFO = XF(dyn/adiabatic)$$

This will hereafter be referred to as the linear/constant friction extrapolation (LCF). It is possible to develop a scheme that accounts for the increase of friction with time in an intensifying system. One can write:

$$XF(t) = C \, \zeta \, (t)$$

In order for the above relationship to be consistent with the original form of the stress, $|\vec{V}(t)|=|\vec{V}(t0)|$. In

reality, in an intensifying system, one would expect the magnitude of the wind speed to increase with time, so this representation is still an underestimate of the actual frictional drag. The frictional dissipation is linear in the sense that a doubling of vorticity with time results in a doubling of the rate of frictional filling. Using the relation:

$$d\,\zeta/dt = -\nabla^2 X / f0$$

yields a differential equation for ζ (t):

$$d\,\zeta\,(t)/dt + (b, C / f0)\,\zeta\,(t) = -b, X0 / f0$$

It is possible to solve this equation for the relative vorticity as a function of time; once the vorticity is known, it is possible to solve for the geopotential, and thus, the pressure so that:

$$DP(t) = 4\,\hat{\Phi}_c\,[\,1 + X0/XF0\,][\,1-\exp(-XF0\,t/\hat{\Phi})\,] / 300$$

$$XF(t) = XF0\,\exp(-XF0\,t/\hat{\Phi}) - X0\,[\,1-\exp(-XF0\,t/\hat{\Phi})\,]$$

It is possible to solve for the maximum total pressure drop, and the time for the pressure to drop to 90% of that maximum:

$$DPmax = 4\,\hat{\Phi}_o\,[\,1 + XO/XFO\,]\,/\,300$$

$$T(90\%) = 2.3\,\hat{\Phi}_o\,/\,XFO$$

This will be referred to as the linear/linear friction (LLF) scheme. In this scheme, the pressure change asymptotically approaches a constant value which is reached when the friction balances the forcing. In the constant friction scheme, the cyclones deepen forever, since there can never be a balance between friction and forcing. As an example of an application of these schemes to an explosive cyclone, consider fig. 3.09-11, pressure traces for the Presidents' Day case. The dry model could not handle the explosive deepening of the first 6 hours at all. Subsequently, it improved, since the real storm had stopped deepening while the model continued to develop the system. The model with the CISK mechanism included performed quite well for the first 6 hours; however, the continued CISK forcing resulted in model deepening after the real disturbance had ceased to develop. In the final figure, the CISK mechanism was cut off after 6 hours, so that any development after that time would be a result of the baroclinic forcing; the forecast trace is quite realistic, suggesting that in this case, the CISK mechanism was operative for the period of explosive development only, the first 6 hours.

Figures 3.12-16 display the initial state of the observed and model surface and 500 mb flow of the Presidents' Day case. The model appears to represent the flow reasonably well, except for the excessive wind speeds and gross overestimate of the vorticity field at 500 mb. Since this results in greater temperature and vorticity advection than would be expected if the actual wind and vorticity fields had been more exactly reproduced, the vertical motion field and consequent pressure falls in the baroclinic model are probably exaggerated. This result shows even more clearly the failure of the dry model to account for the cyclogenesis in the Presidents' Day case.

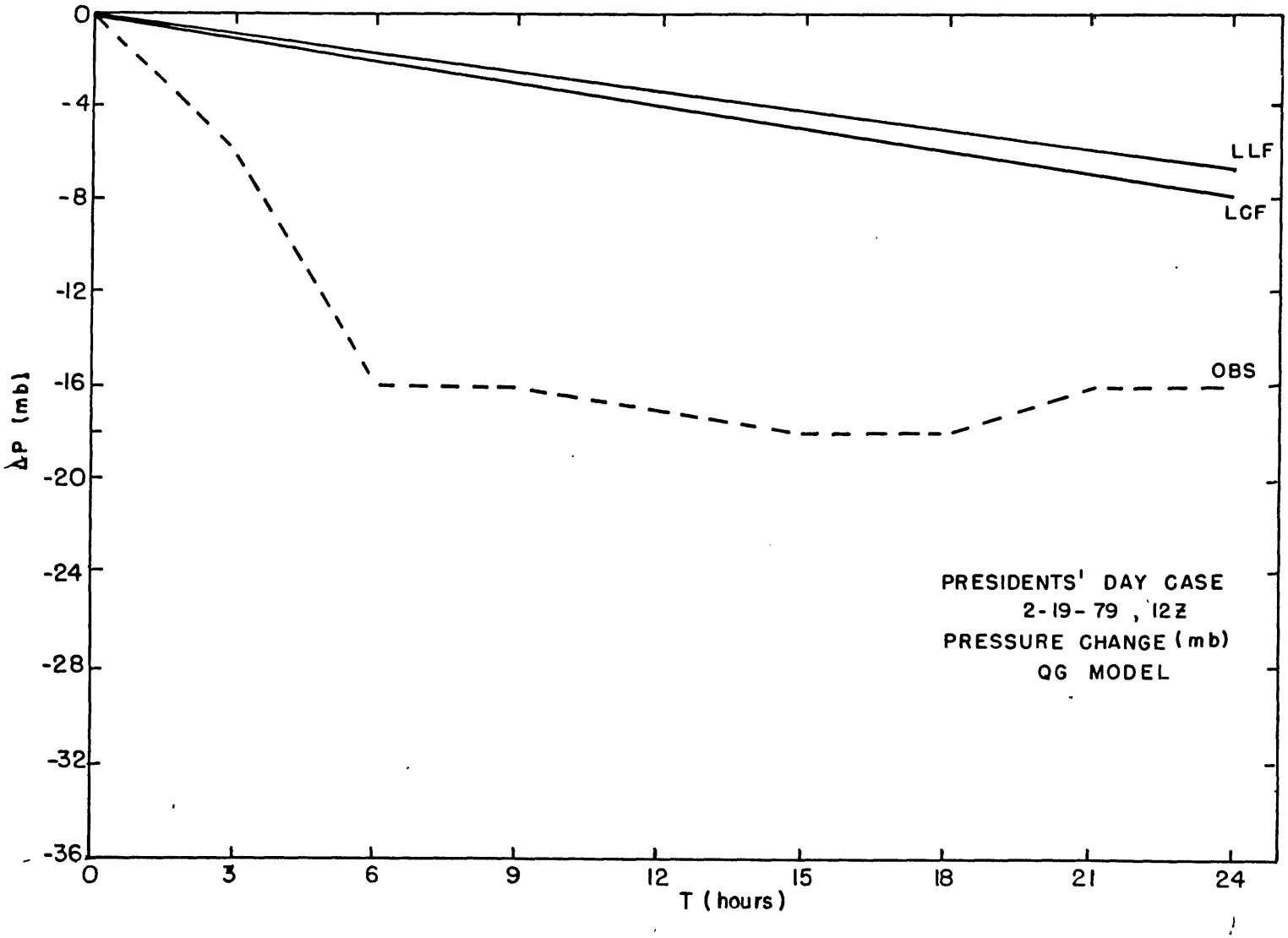
0
-4
-8
-12
-16
-20
-24
-28
-32
-36
ΔP (mb)
0
3
6
9
12
15
18
21
24
T (hours)
LLF
LCF
OBS
PRESIDENTS' DAY CASE
2-19-79 , 12Z
PRESSURE CHANGE (mb)
QG MODEL

FIGURE 3.09

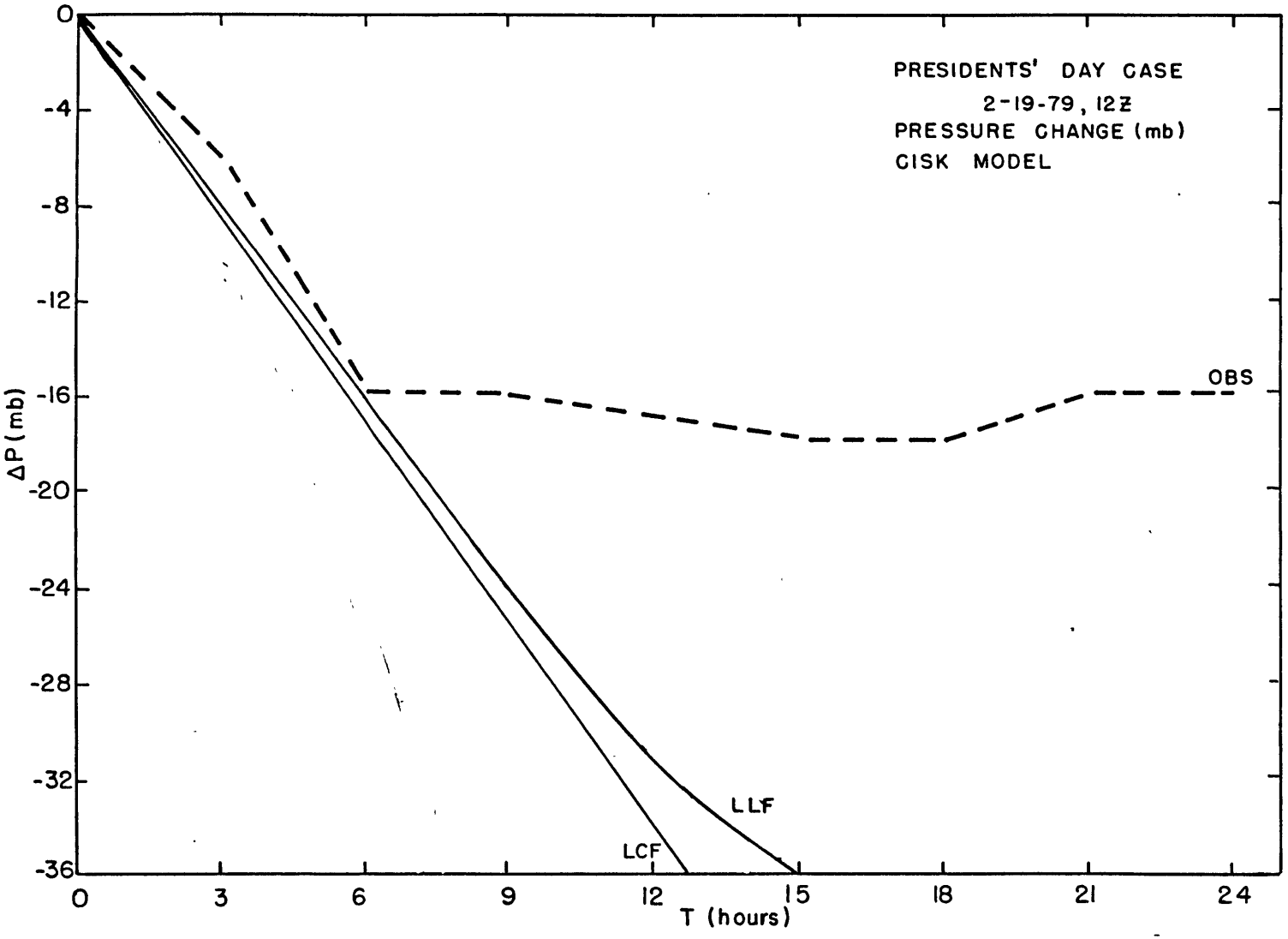
PRESIDENTS' DAY CASE
2-19-79, 12Z
PRESSURE CHANGE (mb)
CISK MODEL
OBS
LLF
LCF
ΔP (mb)
T (hours)
0
-4
-8
-12
-16
-20
-24
-28
-32
-36
0
3
6
9
12
15
18
21
24

FIGURE 3.10

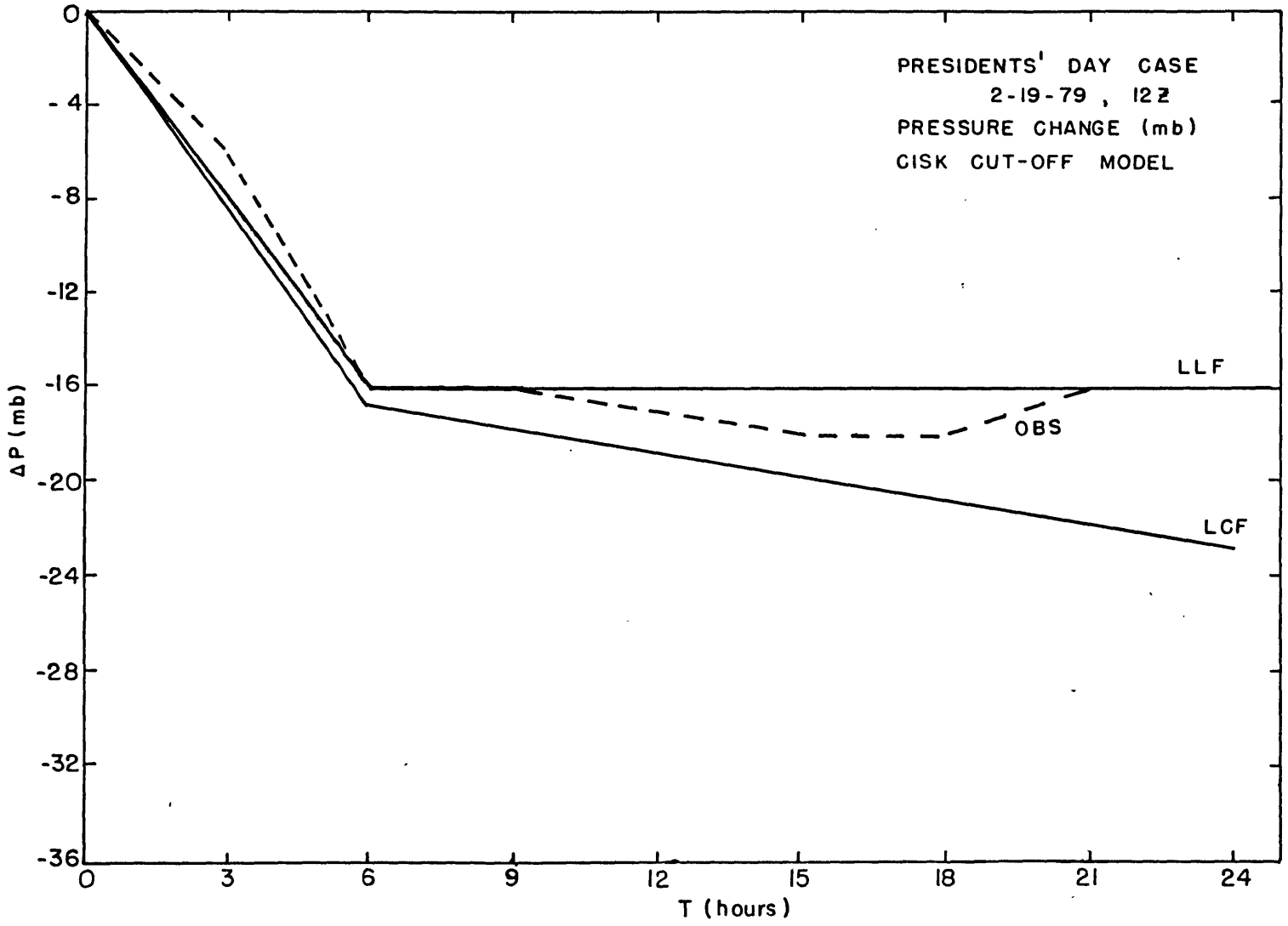
PRESIDENTS' DAY CASE
2-19-79 , 12Z
PRESSURE CHANGE (mb)
CISK CUT-OFF MODEL
LLF
OBS
LCF
ΔP (mb)
0
-4
-8
-12
-16
-20
-24
-28
-32
-36
0
3
6
9
12
15
18
21
24
T (hours)

FIGURE 3.11

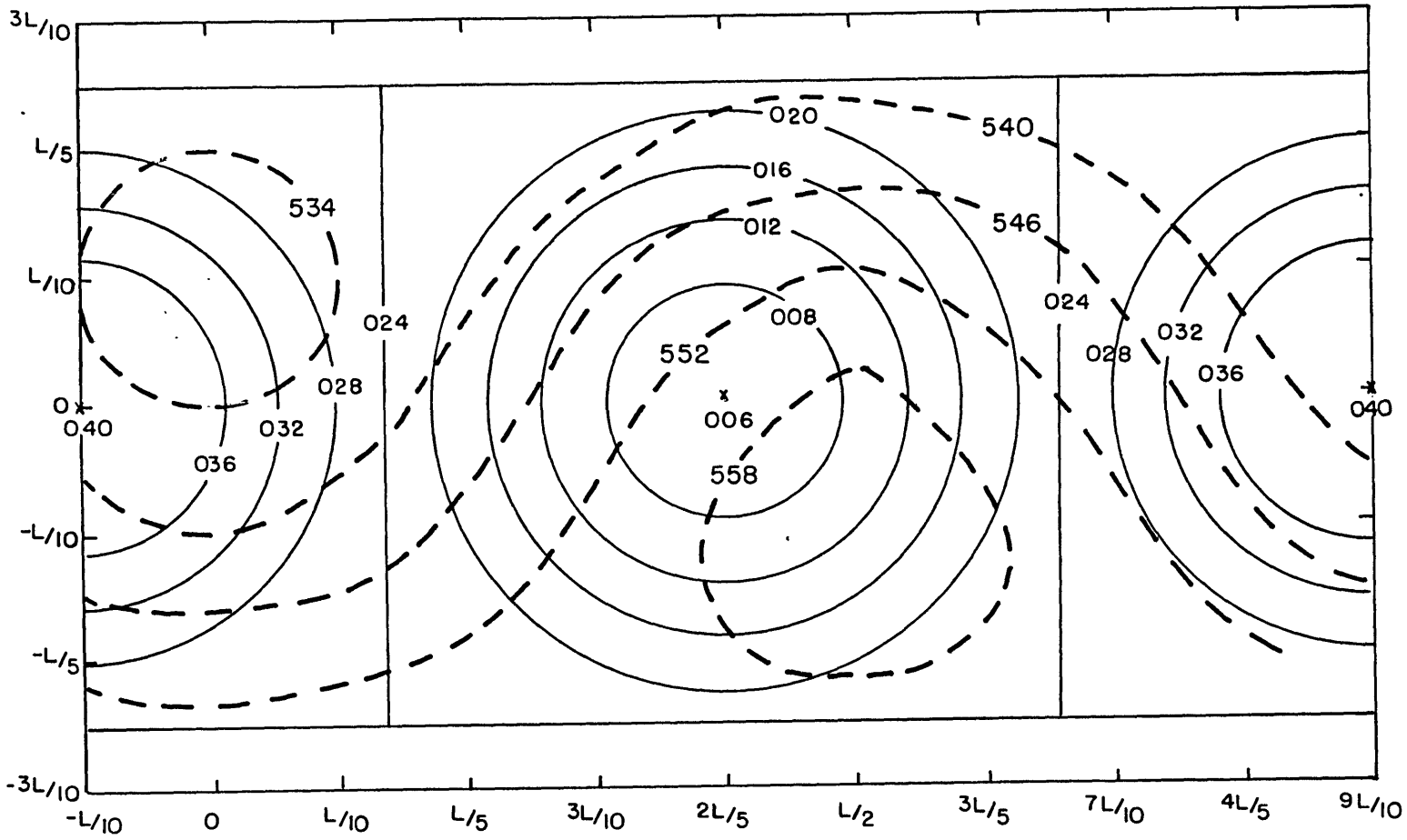

Model surface analysis, Presidents' Day case (2-19-79, 12Z). Solid lines are surface isobars. Dashed lines are isopleths of 1000-500 mb thickness, in dekameters.

FIGURE 3.12

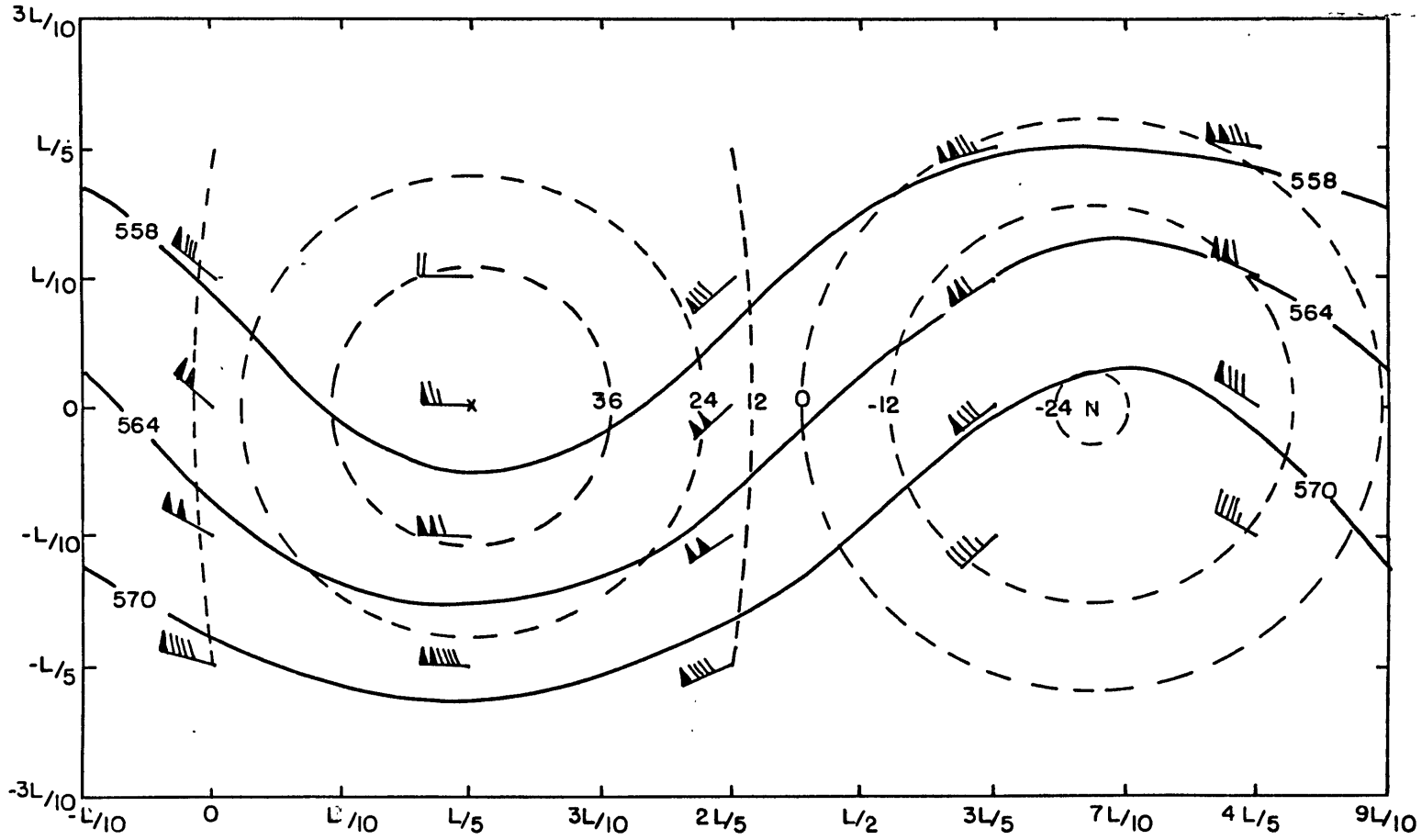

Model 500 mb analysis, Presidents' Day case (2-19-79, 12Z). Solid lines are isopleths of 500 mb height, in dekameters. Dashed lines are isopleths of absolute vorticity, in 10^{-5} s^{-1}.

FIGURE 3.13

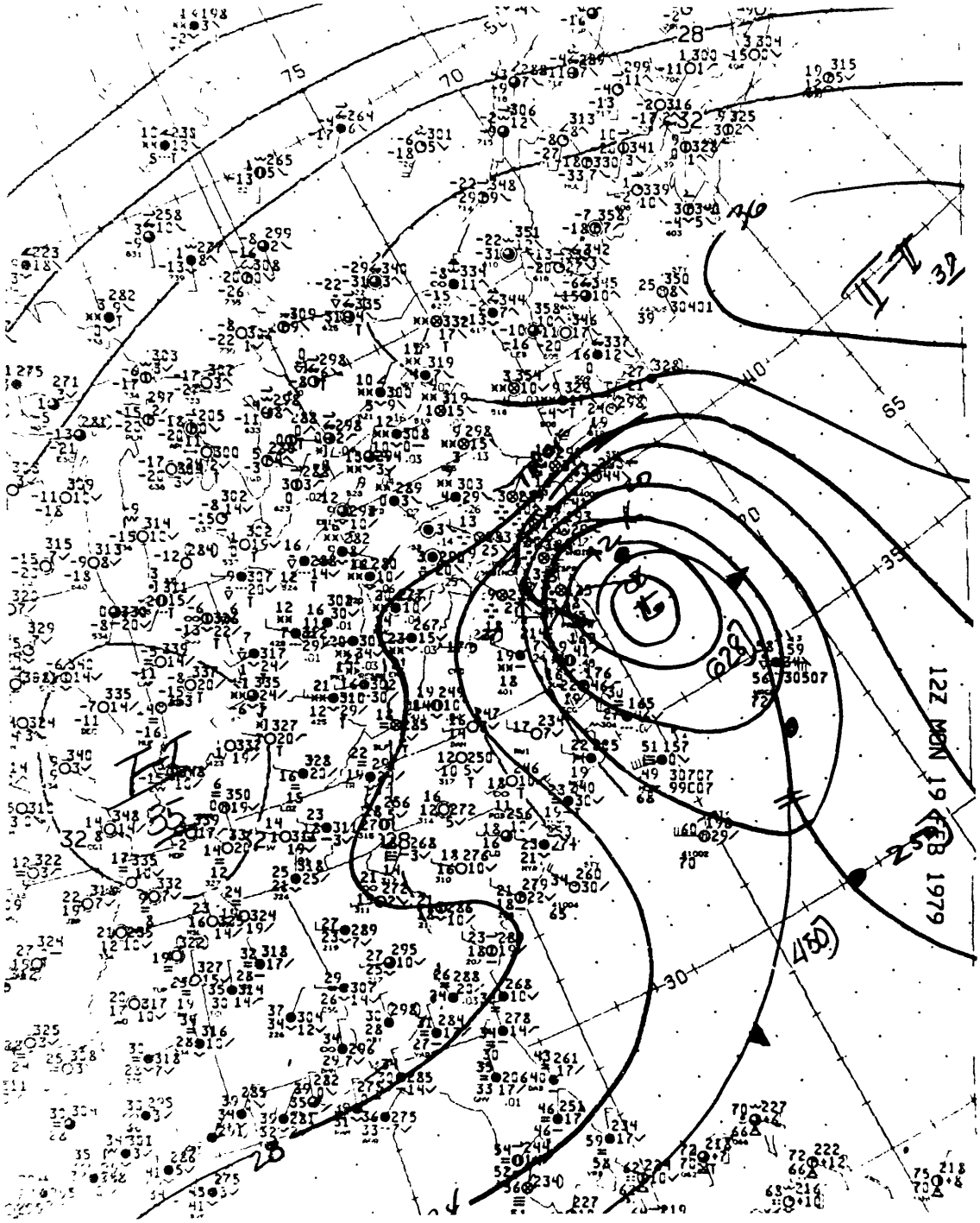

FIGURE 3.14

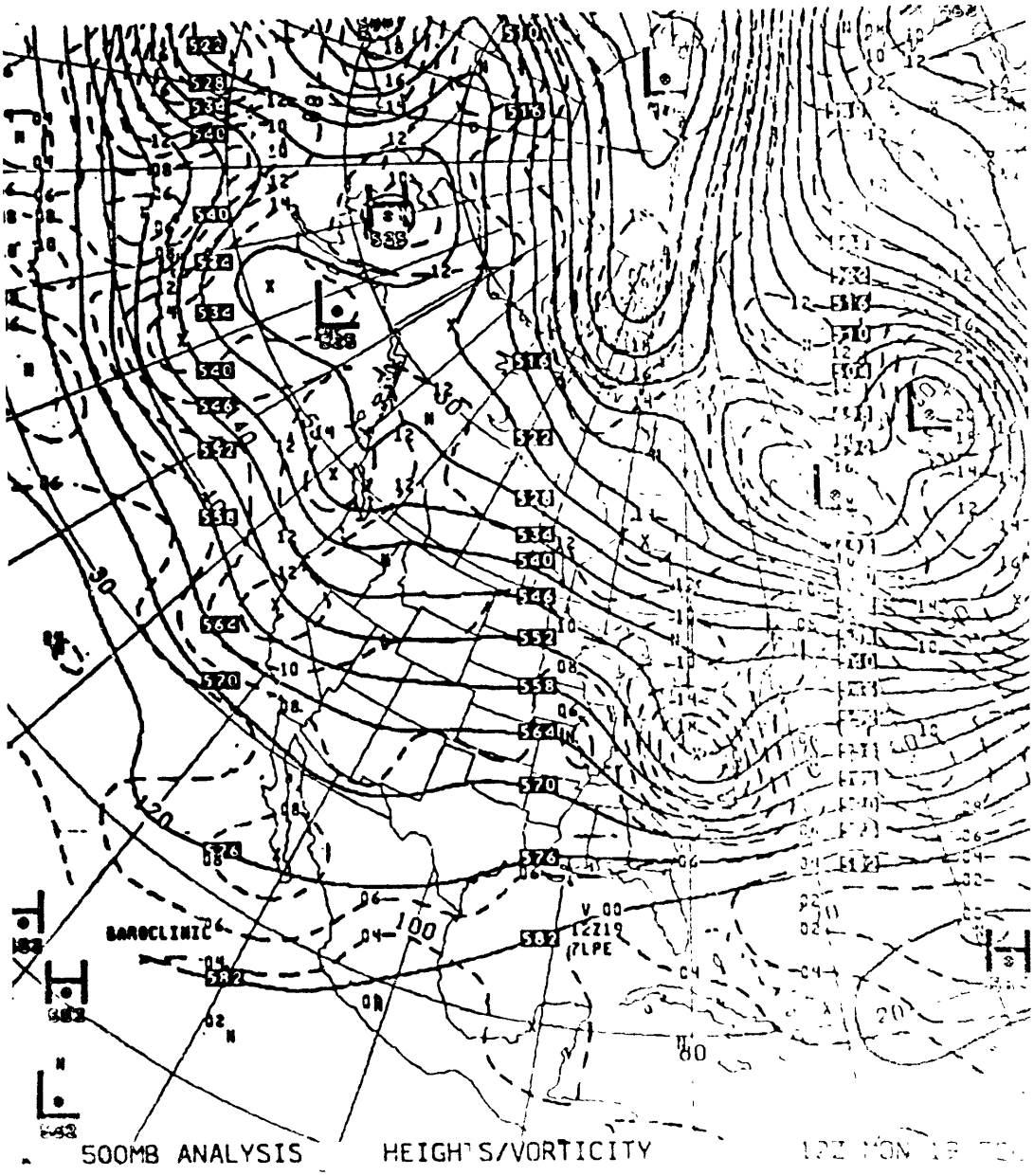

FIGURE 3.15

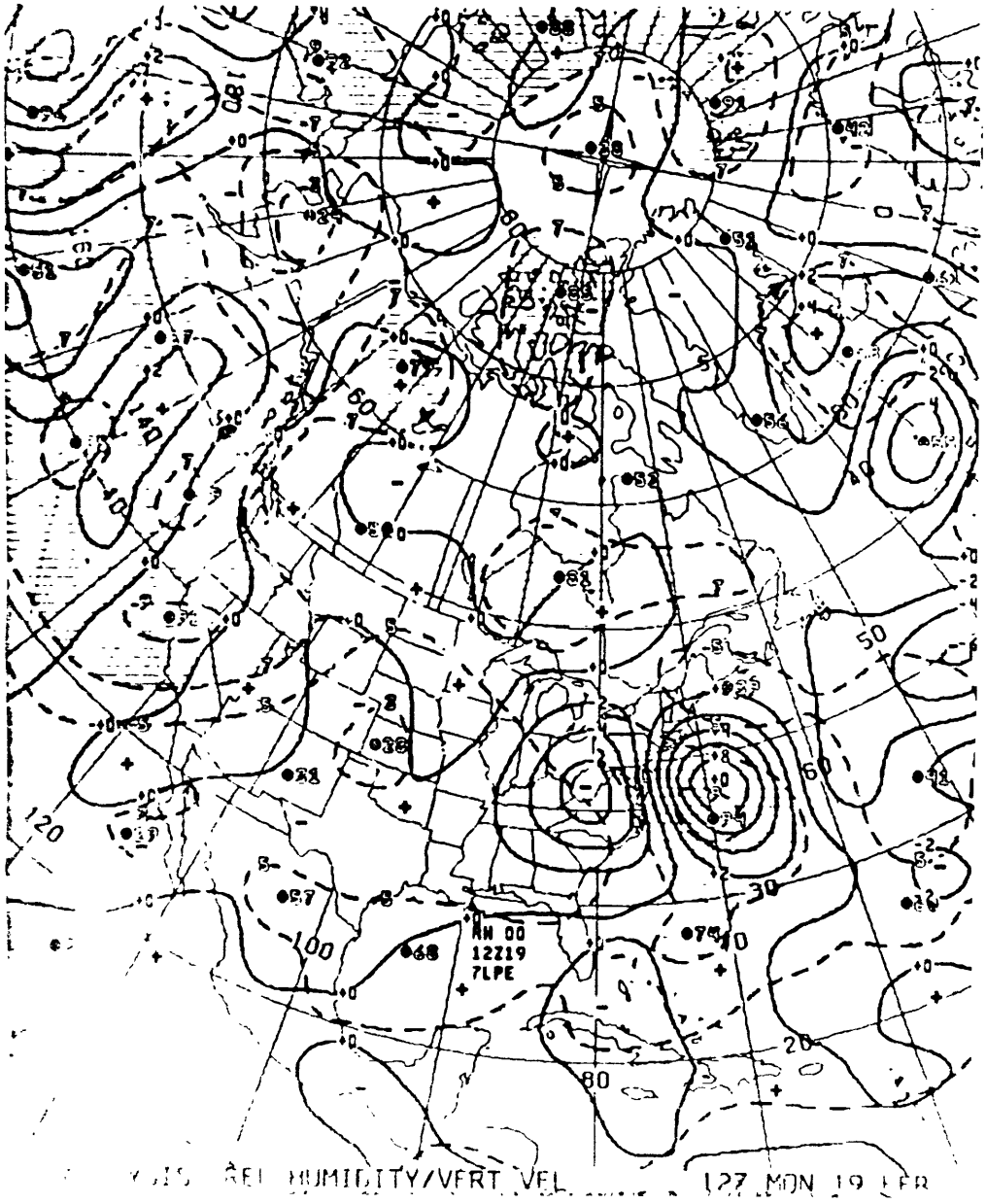

FIGURE 3.16

3.4 Model Climatology of explosive cyclones

The initial test of the model on the Presidents' Day case suggests that it would be fruitful to examine a larger sample of explosive cyclones, to test the general performance of the CISK model in those cases. Thus, it might be possible to evaluate the wave-CISK hypothesis as a generally credible explanation of explosive cyclogenesis. With this in mind, explosive cyclones in the period from January 1978 to March 1981 which occurred in the region covered by the GOES-East satellite were modeled. In the M.I.T. archives for this period, in addition to the usual 00Z and 12Z hemispheric surface pressure/ 1000-500 mb thickness and upper air charts, 3 hourly North American surface analyses and 6 hourly hemispheric surface analyses were available on microfilm. Since the upper air (and consequently, the thickness) charts are available only at 12 hour intervals, the instantaneous model results must be extrapolated from 00Z and 12Z. The additional surface charts make it possible to extrapolate the results for periods less than 12 hours, since it is then possible to verify the deepening rates with observations. In particular, the desire is to model the period of most rapid deepening, so only those cases whose explosive phases were initiated at 00Z or 12Z were modeled, 21 cases in all. The first 6 hours of the rapid deepening phase was modeled, on

the basis that the underlying assumptions concerning the forcing would introduce the least serious error in the calculations for such a time period, while still preserving the important and measurable characteristics of the explosive phase.

Satellite pictures were examined for evidence of convection, using the necessarily qualitative criteria of observable small scale structure on visible and/or high tops on infrared. The value of E was chosen such that the observed 6 hour deepening was approximately accounted for by the diagnostic model extrapolation, provided evidence of convection was found on the satellite pictures. If no evidence was found, the model with no diabatic heating was used. If no satellite images were available, the value of E was chosen to fit the observations. Although the satellite evidence was clear cut in only about 1/3 of the cases (the majority being somewhat ambiguous), the calculations were performed based on the assumption of convection as long as the evidence did not preclude it. The table (fig. 3.17) lists the observed data and the inferences concerning convection for 18 of the 21 total cases. The results of these 18 cases were statistically analyzed rather than the full 21; the 3 cases that were excluded did not exhibit any particular explosive phase, but rather a steady, strong deepening.

MODELED EXPLOSIVE CASES

DATE mm/dd/yy	TIME (GMT)	LAT (N)	LONG (W)	PRESS(mb) NA	PRESS(mb) NH	SATELLITE NOTES
1/03/78	00	44	58.5	988	988	Not Avail.
	03	47.5	57	984	---	
	06	47.5	55	972	---	
2/22/78	12	34	71	1001	1000	Barotropic
	15	34	68	997	---	instability
	18	35.5	66	988	---	Structure.
2/28/78	00	42.5	52.5	994	992	Not Avail.
	03	42.5	51	980	---	Eye struc.
	06	43	50.5	970	---	earlier.
3/04/78	12	42	67.5	984	983	Conv. east
	15	43	65	978	---	center.
	18	43	63	970	---	
11/29/78	00	46	56.5	999	999	Not Avail.
	03	46	55	995	---	No evid.
	06	47	56	988	989	earlier.
12/10/78	00	41	67	995	996	Not Avail.
	03	41	66	991	---	
	06	41.5	65	985	984	
12/25/78	00	36.5	78	992	992	-40C IR
	03	38	76	988	---	center.
	06	40	75	983	983	
1/18/79	12	42	66	1001	998	-45C IR
	15	41.5	64.5	994	---	near center
	18	41	61.5	986	987	
2/01/79	00	35.5	69	993	992	-50C IR
	03	33	69	990	---	center.
	06	34	67	984	980	
2/10/79	12	41	54	990	990	-50C IR.
	15	41	54	990	---	Structure
	18	41.5	50.5	972	960	earlier.
12/17/79	00	34	73	1006	1006	-75C IR.
	03	35	72.5	996	---	-60C IR.
	06	35.5	70	996	996	Ci shield.
1/24/80	00	45	65	983	980	-45C IR.
	03	45	63.5	978	---	-60C early.
	06	46	61	973	972	Noth. vis.

FIGURE 3.17

DATE mm/dd/yy	TIME (GMT)	LAT (N)	LONG (W)	PRESS(mb) NA	PRESS(mb) NH	SATELLITE NOTES
2/29/80	12	40.5	61.5	1001	1001	Cell. struc
	15	42	58.5	994	---	-45C IR.
	18	45.5	56	984	984	
3/02/80	00	32	77	1009	1008	Vis. evid.
	03	34.5	76.5	1000	---	NE.
	06	33.5	75	998	998	
3/03/80	00	35	74.5	997	995	-50C IR.
	03	34.5	73.5	986	---	
	06	35	73	986	986	
11/22/80	00	36	72	1011	1011	Not Avail.
	03	39	68.5	1007	---	
	06	40.5	68	1004	---	
1/17/81	12	41	66.5	1002	1002	-80C IR
	15	42	66	996	---	point. Stri
	18	42	64.5	988	988	ations.
3/03/81	12	44	65	998	996	Not Avail.
	15	42	65	997	---	
	18	38.5	63	980	982	

The question as to whether the moisture convergence necessary to supply the model heating intensity, E, can be supported by the observations was considered. A relationship between the heating intensity and the mixing ratio can be established using the assumption that the rate of precipitation is proportional to the moisture convergence into the column plus the surface evaporation. The precipitation rate, in turn, can be related to the integrated heating by condensation so that:

$$q(PL) > \{E\ Cp\ (\ PL^{\partial} - PU^{\partial}\ )\} \ /\ 2\ Lc\ PO\ \{1 + Wd^*/Wa^*\}$$

where Wd* is the diabatically induced

p-velocity at p=PL.

The details of the derivation are supplied in the appendix. Thus, we can evaluate the right hand side of the above equation, and compare this "implied" mixing ratio to the saturation value as computed from the observed temperature at p=PL, in the model, 850 mb. In 5 of the 18 cases, the required magnitude of E implied a mixing ratio greater than the saturation value in the actual atmosphere, as analyzed by NMC. The discrepancies were small, on the order of 1-2 g/kg; since the actual temperature at 850 mb was not directly observed (the value used was interpolated from the analysis), this finding may not be too serious, but it suggests that caution be used in interpreting the results

of this analysis. In any case, the computed mixing ratios support the idealization of a nearly saturated boundary layer to the pressure level PL.

An attempt was also made to estimate the stability of the atmosphere in the vicinity of the low center for the 18 cases. Interpolated temperatures were obtained from the surface, 850 mb, and 500 mb level NMC analyses, and plotted on a pseudo-adiabatic diagram. This analysis indicated that in 4 out of the 8 cases that showed fairly clear evidence of convection on the satellite photos, the atmosphere was absolutely stable. Even after the layer from the surface to 850 mb was lifted (150 mb), 3 of the 8 cases remained absolutely stable. These inconsistencies graphically demonstrate the rather substantial problem of data availability in the regions of these storms.

The values of E were plotted on a map according to the latitude/ longitude coordinates of the storm center, based on the logical supposition that this parameter would have some recognizeable geographic distribution, at least in a climatological sense. Figure 3.18 reveals a reasonable distribution of heating intensity, with the axis of maximum heating intensity located slightly to the warm side of the mean position of the maximum gradient of sea surface temperature, associated with the Gulf Stream. This is an

area one might expect to be conditionally unstable with a warm, moist boundary layer; furthermore, this differs from the distribution of maximum bomb occurrence detailed in the previous section and discussed by Sanders and Gyakum (1980), which revealed no preference for maximum sea surface temperatures, but was associated instead with the region of maximum SST gradient. This result is consistent with a CISK mechanism, since such a region would tend to maximize baroclinic instability without paying too great a price in terms of warmth and moisture availability. It should be noted, however, that 21 data points do not constitute a very complete data set, and provide a degree of leeway in the analysis.

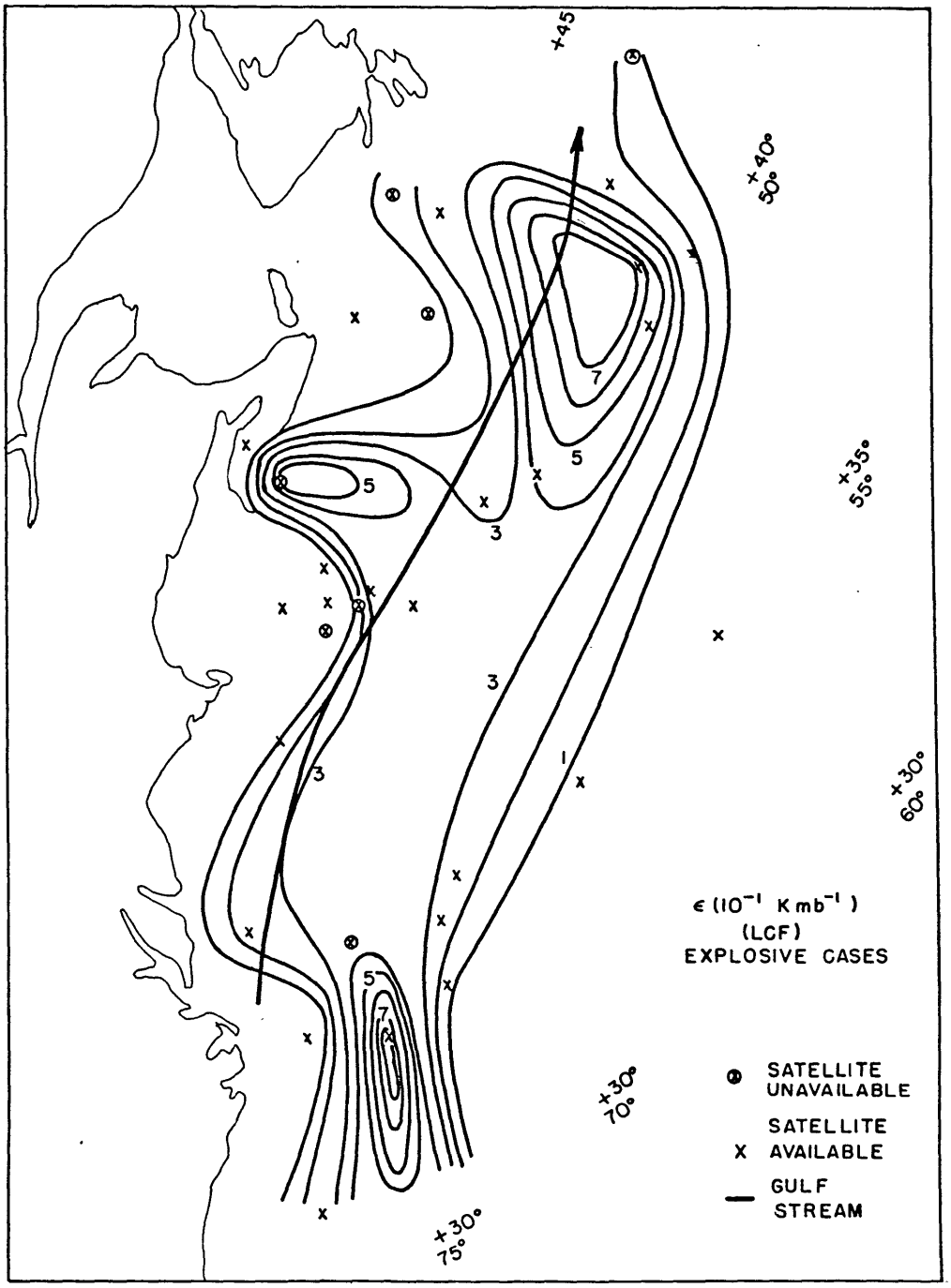
+45
+40°
50°
+35°
55°
+30°
60°
+30°
70°
+30°
75°
ϵ (10⁻¹ K mb⁻¹)
(LCF)
EXPLOSIVE CASES
SATELLITE UNAVAILABLE
SATELLITE AVAILABLE
GULF STREAM

FIGURE 3.18

The results for the 18 cases are presented in the table (fig. 3.20). In particular, the poor performance of the 6 hour baroclinic forecast should be noted, the minimal reduction of variance suggesting a no skill forecast. The baroclinic mechanism was clearly insufficient, as it averaged 6 mb less than the deepening actually observed. The phase speeds were also not well correlated with the observed displacement speeds, averaging about 7 m/s too fast. This is a persistent and puzzling feature of the model. Krishnamurti (1968) found that the amplitude of the vertical motion predicted by quasi-geostrophic theory was too large; the phase speed problem is most likely related to this feature. The phase speeds in the CISK model are somewhat better correlated with the observations, though the net effect of the mechanism is to increase the velocity of the systems; thus, the variance of the speeds is better explained by the CISK mechanism, but not their magnitude. The dramatic improvement in the reduction of variance of the northward component of the phase velocity is due to a large negative correlation with the observations. While this suggests a strong statistical link between the CISK model and the observations, and thus makes a forecast of them feasible, it renders the underlying physical mechanism somewhat questionable. The result implies that when large northward phase speeds are predicted, the actual disturbance exhibits a small northward displacement, and

vice versa. The statistical regression equation of the form:

$$Cy = m \hat{Cy} + b$$

where $\hat{Cy}$ is the model result, and m and b are regression parameters, can be used to predict the actual phase speed, but one can only be confident of the physical validity of the results for $m \rightarrow 1$ and $b \rightarrow 0$. In that case, there would be a one-to-one correspondence between the model and the real atmosphere.

In the 12 hour forecast, the baroclinic model again underpredicts the observed deepening rates and overpredicts the phase speeds. The CISK model does much better, but the deepening rates are too large, suggesting that the forcing on average has already weakened. The CISK model, when applied for only the period of most rapid deepening, shows an increased reduction of variance over the standard CISK extrapolations, and the mean and standard deviation of the resultant deepening distribution conform more closely to that of the observations; this result lends support to the supposition that the CISK mechanism is operative only for the period of most rapid deepening.

EXPLOSIVE CASES (model results)

T=6h

Model	Ext	DP	σ	R		C	σ	R
QG	LCF	-7.3	4.6	-.06	Cx	19.8	8.1	.26
	LLF	-7.1	4.5	-.07	Cy	11.4	5.0	-.21
					C	23.5	7.4	.08
CISK	LCF	-14.2	5.3	.93	Cx	15.9	10.9	.24
	LLF	-14.0	5.3	.94	Cy	21.7	10.2	-.47
					C	28.7	10.6	.26
OBS		-13.3	5.4		Cx	11.7	5.6	
					Cy	6.7	11.5	
					C	16.4	8.4	

T=12h

Model	Ext	DP	σ	R		C	σ	R
QG	LCF	-14.6	9.3	-.15	Cx	19.8	8.1	.07
	LLF	-13.6	8.7	-.15	Cy	11.4	5.0	-.24
					C	23.5	7.4	.05
CISK	LCF	-28.4	10.7	.67	Cx	15.9	10.9	-.05
	LLF	-27.0	10.1	.67	Cy	21.7	10.2	-.19
					C	28.7	10.6	.04
CISK(cut)	LCF	-24.2	11.8	.81	Cx	16.8	10.5	-.05
	LLF	-22.4	11.3	.82	Cy	18.7	10.3	-.35
					C	27.1	10.2	.04
LFM		-9.3	5.1	.32	Cx	9.3	3.7	.21
					Cy	7.6	10.3	.87
					C	15.2	4.5	.17
OBS		-19.1	9.2		Cx	13.0	4.9	
					Cy	8.0	7.5	
					C	16.8	5.4	

FIGURE 3.19

T=24h

Model	Ext	DP	σ	R		C	C	σ	R
QG	LCF	-29.2	20.1	-.52	Cx	20.1	9.5	-.11	
	LLF	-25.2	17.6	-.52	Cy	11.4	5.3	-.36	
					C	24.1	8.3	-.16	
CISK	LCF	-55.3	21.3	.38	Cx	16.6	12.1	-.26	
	LLF	-49.2	18.7	.35	Cy	18.9	8.2	-.40	
					C	27.1	10.3	-.26	
CISK(cut)	LCF	-36.8	15.7	.19	Cx	18.3	11.0	-.21	
	LLF	-29.3	12.9	.21	Cy	14.8	5.7	-.56	
					C	25.0	8.7	-.28	
LFM		-18.5	5.9	.01	Cx	8.5	3.1	.91	
					Cy	8.8	5.6	.96	
					C	12.9	4.7	.90	
OBS		-31.2	10.1		Cx	11.2	5.6		
					Cy	7.0	7.4		
					C	14.9	5.9		

In the 24 hour extrapolations, there is a dramatic improvement in the baroclinic model performance, as measured by the reduction of variance. This is due to the large negative correlation between the model forecast and the observed data. The continued trend of dry model forecast improvement with time is most likely related to the method of extrapolating instantaneous results rather than any improved forecast skill, particularly if the main deepening period of these storms is less than 24 hours. The model improves, since it develops slowly, and therefore does not come into frictional balance as rapidly as the real atmosphere. It is possible to examine the effectiveness of the linear friction model in producing frictional balance; the maximum pressure fall and the time required to attain 90% of that maximum were computed for the 18 cases and compared to the observed data. The mean maximum computed pressure fall and the average time to 90% of that maximum were greater than that observed, implying that the friction is really of a higher order than in the model (e.g. quadratic). Since the extrapolations are based on a constant forcing, the possibility also exists that the forcing itself weakened and frictional balance was attained somewhat earlier than would otherwise have been the case.

In the case of strong forcing followed by weak forcing

(CISK cut-off), the maximum pressure falls were still too large, and the time required to attain 90% of that maximum was much longer than the time to observed balance. It is not clear from these results that the forcing necessarily weakens before frictional balance is attained; however, these results are also influenced by the linearity and consequent underestimate of the frictional dissipation. The pressure changes following the cut-off of the CISK mechanism are small, and a quadratic frictional force could conceivably reduce substantially the time to frictional balance.

Returning to the 24 hour data, there appears to be a dramatic drop in CISK model performance, another suggestion that this time scale is inappropriately long for extrapolating instantaneous results; the success at a range of 12 hours gives some hope of applying the scheme to the operational forecasting of explosive cyclogenesis, however, and the details of one such study are presented in the next section.

DEEPENING PERIODS (Hours)

Model	Statistics				
	N	$\bar{T}$(h)	σ	$\bar{DP}_{mx}$(mb)	σ
GG	18	183.3	53.3	-98.4	69.5
CISK	18	183.3	53.3	-188.6	67.5
CISK(cut)	15	150.7	87.4	-47.9	20.7
OBS	18	23.8	9.3	-31.8	13.3

FIGURE 3.20

3.5 Operational forecasting of explosive cyclogenesis

The climatological map of the heating intensity parameter, E, provides a means for a general forecast scheme, which would proceed as follows:

1. Evaluate the quasi-geostrophic model parameters in the usual way (Sanders, 1971).
2. Consult satellite coverage of the area in question to look for evidence of convection in the storm region.
3. If evidence of convection is found, assume it is interacting cooperatively with the large scale disturbance, and determine the value of E from the climatological map, based on the position of the storm center.
4. If no evidence of convection is found, set the heating intensity to zero.

There are, of course, some drawbacks to this scheme. Convection is a necessary but not sufficient condition for CISK. There must be a symbiotic relationship between the observed convection and the forcing, that is, convection which would have some meaningful effect on the dynamics of the developing cyclone. Perusal of satellite pictures can tell nothing about this. Furthermore, satellite evidence is often inconclusive; convection may be occurring, but could be obscured by a cirrus shield or else simply does not show up well on the photos.

A second drawback is with the values of E from the climatology of explosive cyclones. Perhaps there are cyclones with operative CISK mechanisms at lower heating intensities that do not result in explosive cyclones; the contours may be biased towards the most intense events, rather than cover a range of development.

Lastly, there are the usual problems with extrapolating diagnostic results. It is necessary to assume the heating intensity, and consequently the CISK forcing is constant in time. In reality, the intensity would likely vary as the storm developed and moved over different geographic areas. The scheme does not consider the thermodynamic properties of the system, and consequently does not automatically cut off the CISK when the boundary layer can no longer support the continued convection.

As a test of the scheme on an operational basis, all lows that formed in or entered the coastal waters adjacent to the eastern U.S. in the period from November 14, 1982 through February 12, 1983 were modeled and a forecast of bomb (1) or no bomb (0) was made for the 24 hour period beginning at 12Z. As a control, the forecast was compared to that of a subjective forecast made prior to the modeling for the same period. Also, the performance of the LFM was

noted.

In all, there were 19 cases in this period, of which 2 were explosive cyclones. The positions within the model area are plotted in figure 3.22. This is about 1/4 the expected bomb frequency for this period, in this area, as computed from the 1980-81 climatology, in which 8 of 17 storms were bombs, as shown in figure 3.21. The 1980-81 season appears to have been fairly representative; in the 1978-79 season, 7 bombs were observed in this period. In the two previous seasons, there were 6 and 10 cases of explosive cyclogenesis in the sector. Thus, the test period represents an anomalously quiet period for explosive cyclogenesis.

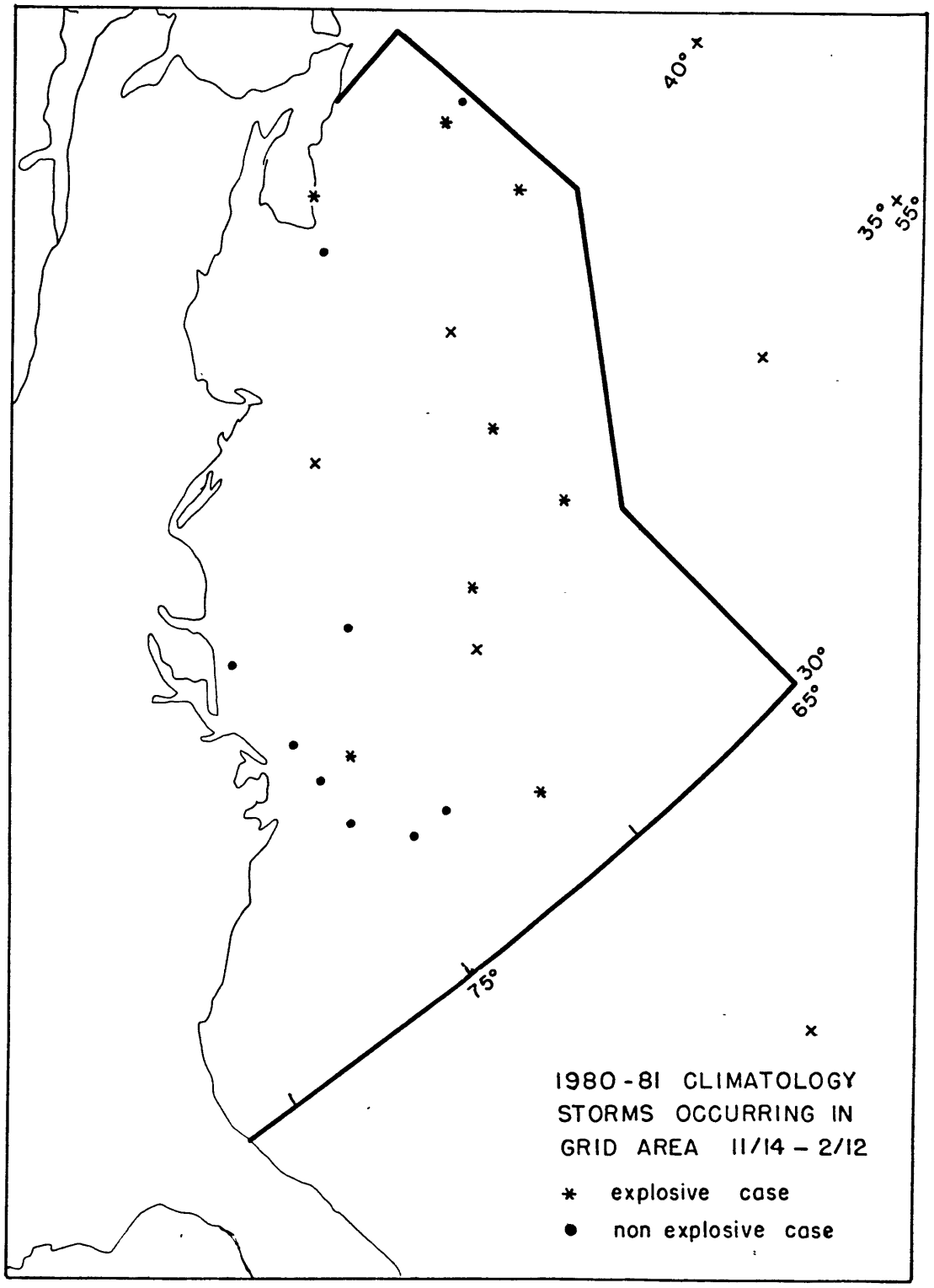
40°
35°
55°
65°
30°
75°
1980-81 CLIMATOLOGY
STORMS OCCURRING IN
GRID AREA 11/14 – 2/12
* explosive case
● non explosive case

FIGURE 3.21

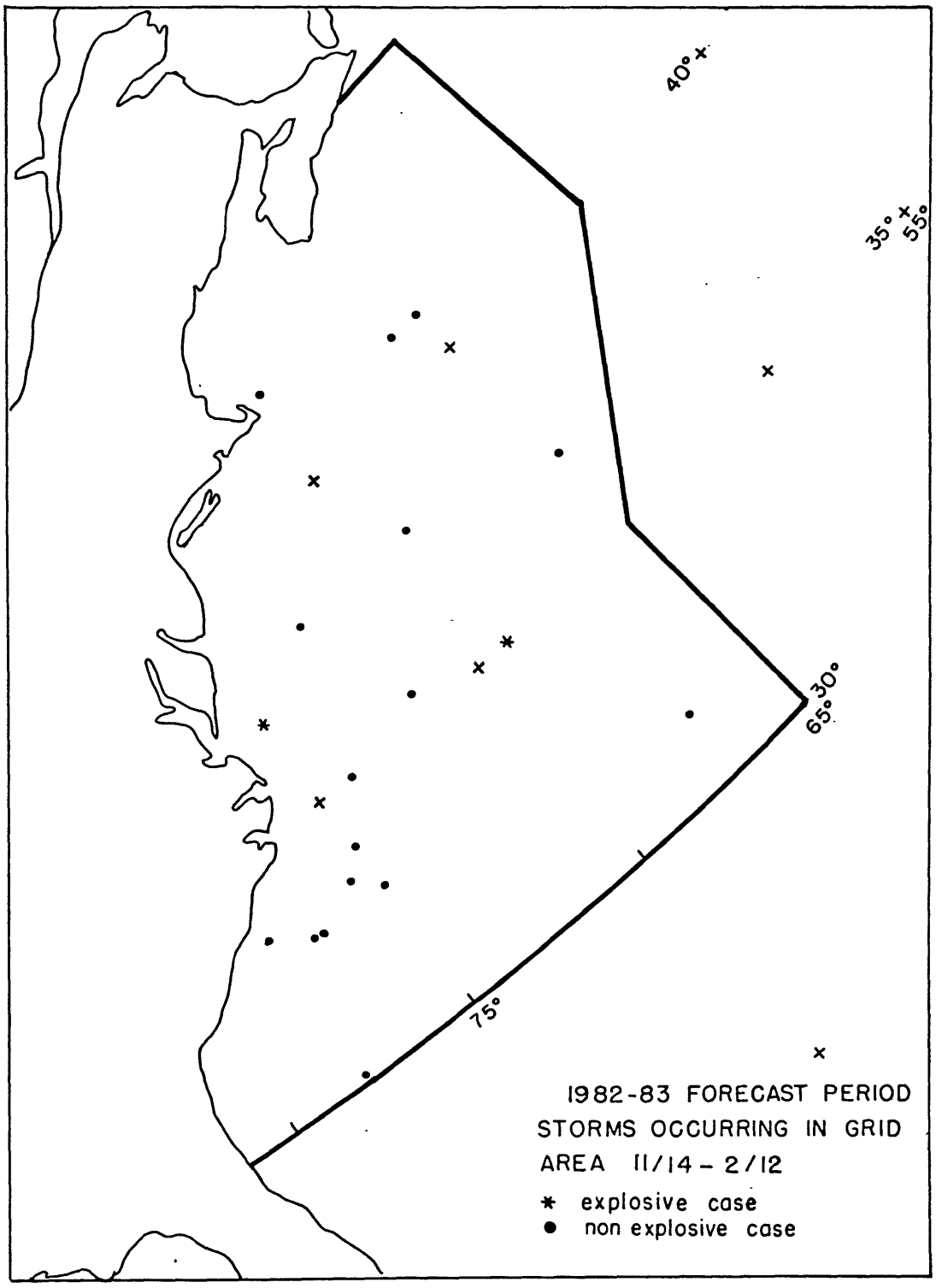
40°
35°
55°
65°30°
75°
1982-83 FORECAST PERIOD
STORMS OCCURRING IN GRID
AREA 11/14 - 2/12
* explosive case
● non explosive case

FIGURE 3.22

Two 24 hour model predictions were made, an extrapolation of the 12Z diagnostic results, and the sum of two 12 hour diagnostic extrapolations, beginning at 12Z and 00Z. The results, summarized in the table (fig. 3.23), indicate generally poor performance. The schemes overforecast the occurrence of explosive cyclogenesis, in marked contrast to the LFM, which in typical fashion, predicted none. The CISK schemes showed a slightly better reduction of variance in the actual deepening rates, but the difference was minimal. The bomb/no bomb forecasts were able, at best, to account for 62% of the variance in the sample. The baroclinic model did better in this respect, reflecting their tendency to develop storms less than the CISK model. The models were generally unable to improve on the subjective forecast, however; thus, the utility of the scheme was minimal. The model average deepening rates were excessive, even in the baroclinic case, indicating that the process or processes responsible for the lack of development were not handled well by the basic model. In particular, two cases on December 12, 1982 merit further examination. The baroclinic forcing in the region was quite strong, with estimated meridional temperature gradients ranging from 1.40 to 1.71 X 10^{-5} K/m and perturbation temperature amplitudes in excess of 10 K. The wavelengths of the disturbances were somewhat large, on the order of 4500 km, but the baroclinic forcing was

sufficiently strong to easily produce model bombs, with 24 hour deepening rates of -25 and -48 mb. The real atmosphere was apparently stable to small perturbations, however, as the surface systems did not develop (-2 mb and +4 mb). If these two cases are removed from the sample, the forecast performance is improved (see table, fig. 3.23), but the schemes still fall short of the subjective forecast. The schemes were able to forecast the actual cases of explosive cyclogenesis; the trouble was rather in predicting too many bombs.

If one accepts the CISK hypothesis as a viable means for explaining the occurrence of explosive cyclogenesis, then it is necessary to understand the mechanism that was inhibiting the observed convection from interacting cooperatively with the large scale flow. The basic problem, then, is to understand the interactions between the mesoscale and the synoptic scale.

OPERATIONAL FORECAST RESULTS

T=12h

Model	Ext	$\overline{DP}$	σ	R
GG	LCF	-6.0	7.7	.34
	LLF	-5.4	6.6	.35
CISK	LCF	-8.1	8.9	.37
	LLF	-7.4	7.9	.39
LFM		-1.5	4.7	.12
OBS		-3.8	6.2	

T=24h

Model	Ext	$\overline{DP}$	σ	R	R(O/1 FCST) All	R(O/1 FCST) w/o 12
GG	LCF	-11.3	12.0	.33	.57	.78
	LLF	-9.3	9.9	.32	.79	.78
CISK	LCF	-15.7	15.4	.24	.56	.78
	LLF	-13.2	12.7	.25	.56	.78
LFM		-3.3	8.3	-.06		
SUBJ					.58	.80
OBS		-8.3	9.6			

T=24h (12+12)

Model	Ext	$\overline{DP}$	σ	R	R(O/1 FCST) All	R(O/1 FCST) w/o 12
GG	LCF	-14.0	14.3	.33	.49	.65
	LLF	-12.4	12.3	.34	.57	.65
CISK	LCF	-16.4	15.2	.35	.49	.55
	LLF	-14.7	13.2	.36	.55	.55
LFM		-3.3	8.3	-.06		
OBS		-8.3	9.6			

FIGURE 3.23

4.0 Conclusions

In the first section, a statistical analysis of deepening rates revealed significant deviations from the normal curve, along the tail of the distributions associated with most rapid deepening. This evidence suggests that the operative process in explosive cyclones is in some way different from that of ordinary baroclinicity. With the climatological distribution of explosive cyclones, which showed a maximum in frequency in the strongly baroclinic areas adjacent to warm ocean currents, the evidence suggests a process in combination with baroclinicity.

In the study of explosive cyclones, the CISK mechanism was able to account for the observed deepening, whereas the baroclinic model fell well short. A logical pattern of heating intensity, a parameter based upon physical and geographic considerations, was established from these cases. The axis of maximum heating intensity was located slightly to the warm side of the mean Gulf Stream position, a prime area for conditionally unstable air with a warm, moist boundary layer. This relationship suggested an explanation for the preference of explosive cyclogenesis for the maximum SST gradients, since such an area represents strong baroclinicity yet is still able to

support conditionally unstable air.

The CISK mechanism provided an explanation for the "left moving" phenomenon, in which some storms move to the left of the instantaneous 500 mb flow, contrary to typical synoptic systems. The evidence was unclear as to whether the explosive forcing weakens before frictional balance can be attained, but the possibility of such an occurrence seems to indicate the advisability of formulating a parameterization that includes an internal check on the thermodynamics, so that an automatic cut off of the convection can be assured when the physics no longer supports its continuance.

In the operational forecasting study, it was found that in an anomalously low bomb frequency period, the baroclinic model was about as able to handle cyclone evolution as the CISK model. This was largely due to the observation of convection associated with storms, since in the presence of convection, a cooperative interaction was assumed. The basic problem, and the solution, of explosive cyclogenesis appears to reside in the better understanding of the interactions between the synoptic and sub-synoptic scales.

ACKNOWLEDGMENTS

I must thank Professor Frederick Sanders for introducing me to the wild world of atmospheric bombs, and to Synoptic meteorology in general. I also thank Isabelle Kole for drafting the figures quickly, and neatly. Lastly, I wish to express my appreciation of my fellow students, whose help and humor made life at M.I.T. not just possible, but probable. This research was supported by the Office of Naval Research, and by the Naval Environmental Prediction Research Facility, under contract N 00014-79-C-0384.

APPENDIX

The following equations describe the model atmosphere. The temperature structure is:

$$T(x,y,p) = Tm(p) - (ay + \hat{T} \cos kx \cos ly)$$

where $Tm(p) = Tm(PO) (p/PO)^{b}$

$$Tm(PO) = (kl/4\pi^2) \iint T(x,y,PO)dxdy$$

$$k = 2\pi / Lx \; ; \; l = 2\pi / Ly$$

and the geopotential structure is:

$$\Phi(x,y,p) = \Phi m(p) + \hat{\Phi}_o \cos k(x+\lambda) \cos ly - R \ln(PO/p) (ay + \hat{T} \cos kx \cos ly)$$

where $\Phi m(p) = R \int_{p}^{\infty} Tm(p)d\ln p = \{R\ Tm(PO)/b\} [\ 1 - (p/PO)^{b}\ ] + \Phi m(PO)$

From the geopotential, we can derive relationships for the geostrophic wind and the geostrophic relative vorticity:

$$u(x,y,p) = \{ l\ \hat{\Phi}_o \cos k(x+\lambda) \sin ly + R \ln(PO/p) [\ a - l\ \hat{T} \cos kx \sin ly\ ] \} / fO$$

$$v(x,y,p) = \{ -k\ \hat{\Phi}_o \sin k(x+\lambda) \cos ly + R \ln(PO/p)\ k\ \hat{T} \sin kx \cos ly \} / fO$$

$$\zeta(x,y,p) = (b_1/fO) [\ R\ \hat{T} \ln(PO/p) \cos kx \cos ly - \hat{\Phi}_o \cos k(x+\lambda) \cos ly\ ]$$

where $b_1 = k^2 + l^2$

The expression for the stability factor, σ, is:

$$\sigma = \{K/p - d\ln Tm/dP\} (R\ Tm / p)$$

$$= \{ \gamma\ R\ \overline{Tm} \} / p^2$$

where $\overline{Tm} = \{Tm(PO)/(PO-PT)(1+b)\} [1 - (PT/PO)^{1+b}]$

The equation to be solved to determine the vertical motion field is:

$$\left(p^2\frac{\partial^2}{\partial p^2} + \frac{\gamma R\overline{Tm}}{f_0\eta_0}\right)\omega = \left\{\frac{\partial R^2\hat{T}ak b_1}{f_0^2\eta_0}p\ln(P0/p) - \frac{R\hat{T}K\beta}{f_0\eta_0}p\right\}\sin kx\cos ly$$

$$-\left\{\frac{RaKb_1\hat{\Phi}_0}{f_0^2\eta_0}p\right\}\sin k(x+\lambda)\cos ly$$

$$+\left\{\frac{R\hat{T}Klb_1\hat{\Phi}_0\sin k\lambda}{f_0^2\eta_0}p\right\}\sin 2ly$$

Let:

$$W = W1 + W2 + W3$$

where $W1 = \hat{W1}(p)\ \text{Sin kx Cos ly}$; $\hat{W1}(p) = \hat{W11}(p) + \hat{W12}(p)$

$W2 = \hat{W2}(p)\ \text{Sin k(x+}\lambda\text{) Cos ly}$

$W3 = \hat{W3}(p)\ \text{Sin 2ly}$

The solutions are:

$$\hat{W11}(p) = \{2R\hat{T}ak/f0\gamma\overline{Tm}\} \{ (a_1/b_1) F1(p, q_1) - \ln(PO/p)$$

$$+ (PT/p)^{1-q_1} [(PO^{1-2q_1} - p^{1-2q_1})/(PO^{1-2q_1} - PT^{1-2q_1})] \ln(PO/PT) \} p$$

$$\hat{W12}(p) = \{kT\beta/b_1\gamma\overline{Tm}\} \{ F1(p, q_1) \} p$$

$$\hat{W}2(p) = \{ak\hat{\Phi}_0/f0\gamma\bar{T}m\}\ \{\ F1(p,q_1)\ \}\ p$$

$$\hat{W}3(p) = \{-k1\hat{T}\hat{\Phi}_0/f0\gamma\bar{T}m\}(b_1/b_2)\,Sin\ k\lambda\ \{\ F1(p,q_2)\ \}\ p$$

where $a_1 = \{\ f0\ \eta_0/\gamma\ R\ \bar{T}m\ \}$

$b_2 = 4l^2$

$q_1 = \{\ 1 + [\ 1 + 4(b_1/a_1)\ ]^{1/2}\ \}\ /\ 2$

$q_2 = \{\ 1 + [\ 1 + 4(b_2/a_1)\ ]^{1/2}\ \}\ /\ 2$

$F1(p,q) = \{\ [PO(p/PT)^{q-1} - PT(p/PO)^{q-1}]$

$-[PO(PT/p)^{q} - PT(PO/p)^{q}]\}\ /\ [PO^{1-q}PT^{q} - PO^{q}PT^{1-q}]$

$+\ 1$

The equation to be solved for the frictionally induced vertical motion is:

$$\left(\rho^2\frac{\partial^2}{\partial\rho^2} + \frac{\gamma R\bar{T}m}{f_0\eta_0}\nabla^2\right)\omega_4 = -\left\{\frac{g\rho C_0|\hat{V}|b_1\hat{\Phi}_0}{f_0\eta_0}\frac{n(n-1)}{\rho_0^n}\right\}\rho^n\,Cos\,k(x+\lambda)\,Cos\,ly$$

Thus, we can write:

$$W4(p) = \hat{W}4(p)\ Cos\ k(x+\lambda)\ Cos\ ly$$

and solving for W4(PO)=W4(PT)=0 yields:

$$\hat{W}4(p) = \{[\ ]/(n-1+q_1)(n-q_1)\}\ \{\{[\ p^{q_1}(\ PO^{1-2q_1}PT^{n-q_1} - PO^{n-q_1}PT^{1-2q_1}\ )$$

$$+\ p^{1-q_1}(\ PO^{n-q_1} - PT^{n-q_1}\ )]\ /\ (\ PO^{1-2q_1} - PT^{1-2q_1}\ )\}$$

$$-\ p^n\ \}$$

where [ ] = { g ρ Cd $|\vec{V}|$ b_1 $\hat{\Phi}_0$ n(n-1) } / f0 η_0 $P0^n$

For including the effects of convective latent heat release on the vertical motion field, the following equation must be solved:

$$\left(p^2\frac{\partial^2}{\partial p^2} - \frac{\gamma R \bar{T}_m bn^*}{f_0\eta_0}\right)\hat{\omega}_d = \Gamma_n H(p) p^2$$

The solutions are of the form:

$\hat{W}dn$ = A2n p^q (p^{1-2q} − $P0^{1-2q}$) ; p>PL

= A3n p^q + A4n p^{1-q} + {a_1 rn / ($2a_1$ − bn*)} p^2 ; PL>p>PU

= A5n p^q (p^{1-2q} − PT^{1-2q}) ; p<PU

where qn*, bn* = q_1 , b_1 for n=1, 2, 4

= q_2 , b_2 for n=3

rn = {− R E $\hat{W}a*n$ bn* / f0 η_0 P0}

In order to solve for the constants A2n, A3n, A4n, A5n, the vertical motion profiles and their first derivatives are matched at p=PL and p=PU. Thus, the constants are:

A2n = An {(2−qn*)PT^{1-2q} (PL^{1+q} − PU^{1+q}) − (1+qn*)(PL^{2-q} − PU^{2-q})}

A3n = An {(2−qn*)$P0^{1-2q}$ PT^{1-2q} (PU^{1+q} − PL^{1+q}) − (1+qn*)($P0^{1-2q}$ PU^{2-q} − PT^{1-2q} PL^{2-q})}

$$A4n = An \{(2-qn^*)(PO^{1-2q}PL^{1+q} - PT^{1-2q}PU^{1+q}) - (1+qn^*)(PL^{2-q} - PU^{2-q})\}$$

$$A5n = An \{(2-qn^*)PO^{1-2q}(PL^{1+q} - PU^{1+q}) - (1+qn^*)(PL^{2-q} - PU^{2-q})\}$$

$$An = (-a_1\, rn) / [\,(2a_1-bn^*)(1-2qn^*)(PO^{1-2q} - PT^{1-2q})\,]$$

From the vorticity equation, the geopotential tendency can be found, if the vertical motion field is known. In the model, the geopotential tendency at the surface center ($x=Lx/2-\lambda$, $y=0$, $p=PO$) can be written:

$$X(\text{sfc center}) = X(\text{dyn/adiab}) + X(\text{diabatic}) + X(\text{friction})$$

where $X(d/a) = \{k\hat{T}\,\eta_0/b_1^2\,\overline{\gamma Tm}\}\sin k\lambda\,\{2Ra\{[b_1(1-2q_1)PT\ln(PO/PT)/(PO^{1-q}PT^{q} - PO^{q}PT^{1-q})] - [\,a_1 F1(q_1,PO) + b_1\,]\} - f0\,\beta\,F^*\}$

$$X(\text{diab}) = \{-A21\,\eta_0 f0\,(1-2q_1)\,/\,b_1\,PO^{q_1}\}\sin k\lambda$$

$$X(\text{fric}) = \{[g\,\rho\,Cd\,|\vec{V}|\,\hat{\xi}_0\,n(n-1)]\,/\,[(n-1+q_1)(n-q_1)PO]\}G^* + \{A24\,\eta_0 f0\,(1-2q_1)\,/\,b_1\,PO^{q_1}\}$$

$$= XF(\text{dyn/adiab}) + XF(\text{diab})$$

where $F^* = \{(1-2q_1)PT + q_1(PO^{1-q_1}PT^{q_1} + PO^{q_1}PT^{1-q_1}) - PO^{q_1}PT^{1-q_1}\}\,/\,\{PO^{1-q_1}PT^{q_1} - PO^{q_1}PT^{1-q_1}\}$

$$G^* = \{(1-2q_1)PO^{1-n-q_1}\,PT^{n-q_1} + q_1\,PT^{1-2q_1} - PO^{1-2q_1}\} / \{PO^{1-2q_1} - PT^{1-2q_1}\}$$

$$+ n$$

The equations for the eastward and northward components of the phase velocity can also be found:

$$Cx(PO) = \{ X(dyn/adiab) + X(diab) \}\, Cot\, k\lambda \,/\, k\,\hat{\xi}_0$$

$$-\{ 2\,\eta_0 a/b_1\,\langle\tilde{T}m\rangle F^*$$

$$-\{ A22\,\eta_0 f0(1-2q_1)/b_1\,k\hat{\xi}_0\,PO^{q_1}\} - \beta/b_1$$

$$Cy(PO) = \{-2\,\eta_0 b_1\,K\hat{T}/b_3^2\,\langle\tilde{T}m\rangle F^{**}\,Sin\,k\lambda$$

$$+\{ 2\,A23\,\eta_0 f0(1-2q_3)/b_3\,I\hat{\xi}_0\,PO^{q_3}\}$$

where $F^{**} = F^*$, q_1 replaced by q_3.

In the expression for the friction, the term $|\vec{V}|$ appears. We can estimate a value of $|\vec{V}|$ based on our equations for the velocity:

$$u(PO) = (\,1\,\hat{\xi}_0 \,/\, f0)\,Cos\,k(x+\lambda)\,Sin\,ly$$

$$v(PO) = (-k\,\hat{\xi}_0 \,/\, f0)\,Sin\,k(x+\lambda)\,Cos\,ly$$

Since $|\vec{V}| = (u^2 + v^2)^{1/2}$, it can be shown from the above that:

$$|\vec{V}|max = b\,\hat{\xi}_0 \,/\, 8\,f0$$

If the assumption is made that the moisture convergence into the column plus the surface evaporation is approximately

equal to the precipitation rate, then the integrated heating due to condensation must also be approximately equal to the rate of precipitation. Thus,

$$P = - \int_{PL}^{PU} \{\dot{q} \; / \; g \; Lc\} \; dP$$

From the model parameterization for $\dot{q}$, it can be shown that:

$$P = - Cp \; E \; Wa^* \; (\; PL^2 - PU^2 \;) \; / \; 2 \; g \; Lc \; PO$$

$$= (-q \; W \; / \; g) + Evap$$

Thus, the mixing ratio q can be related to the heating intensity, E, such that:

$$q(PL) > E \; Cp \; (\; PL^2 - PU^2 \;) \; / \; 2 \; Lc \; PO \; (\; 1 + Wd^*/Wa^* \;)$$

REFERENCES

Arakawa, A., and W. Schubert, 1974: "Interaction of a Cumulus Ensemble with the Large Scale Environment. Part I." Journal of the Atmospheric Sciences. Vol. 31, pp. 674-701.

Bates, J. R., 1973: "A Generalization of the CISK Theory." Journal of the Atmospheric Sciences. Vol. 30, pp. 1509-1519.

Bosart, L. F., 1981: "The Presidents' Day Snowstorm of 18-19 February 1979: A Subsynoptic-scale Event." Monthly Weather Review. Vol. 109, pp. 1542-1566.

Chang, C. B., D. J. Perkey and C. W. Kreitzberg, 1982: "A Numerical Case Study of the Effects of Latent Heating on a Developing Wave Cyclone." Journal of the Atmospheric Sciences. Vol. 39, pp. 1555-1570.

Chang, C. P., 1971: "On the Stability of Low Latitude Quasi-Geostrophic Flow in a Conditionally Unstable Atmosphere." Journal of the Atmospheric Sciences. Vol. 28, pp. 270-274.

----------, and R. T. Williams, 1974: "On the Short-wave Cutoff of CISK." Journal of the Atmospheric Sciences. Vol. 31, pp. 830-832.

Charney, J. G., and A. Eliassen, 1964: "On the Growth of the Hurricane Depression." Journal of the Atmospheric Sciences. Vol. 21, pp. 68-75.

Davies, H. C., and R. A. de Guzman, 1979: "On the Preferred Mode of Ekman CISK." Tellus. Vol. 31, pp. 406-411.

----------, 1979: "Phase-lagged Wave-CISK." Quarterly Journal of the Royal Meteorological Society. Vol. 105, pp. 325-353.

DeGroot, M. H., 1975: "Probability and Statistics." Addison-Wesley, 607 pp.

Gyakum, J. R., 1983b: "On the Evolution of the QE II Storm. II. Dynamic and Thermodynamic Structure. Monthly Weather Review. Accepted.

----------, 1981: "On the Nature of Explosively Developing Cyclones in the Northern Hemisphere Extratropical Atmosphere." Ph.D. thesis, M.I.T., 225 pp.

Haltiner, G. J., 1971: "Numerical Weather Prediction." Wiley, 311 pp.

Krishnamurti, T. N., 1968: "A Study of a Developing Wave Cyclone." Monthly Weather Review. Vol. 96, pp. 208-217.

Kuo, H. L., 1975: "Instability Theory of Large-Scale Disturbances in the Tropics." Journal of Atmospheric Sciences. Vol. 32, pp. 2229-2245.

----------, 1965: "On the Formation and Intensification of Tropical Cyclones through Latent Heat Release by Cumulus Convection." Journal of Atmospheric Sciences. Vol. 22, pp. 40-63.

Lindzen, R. S., 1974: "Wave-CISK in the Tropics." Journal of Atmospheric Sciences. Vol. 31, pp. 156-179.

----------, and D. Stevens, 1978: "Tropical Wave-CISK with a Moisture Budget and Cumulus Friction." Journal of Atmospheric Sciences. Vol. 35, pp. 940-961.

Mak, M., 1981: "An Inquiry on the Nature of CISK. Part I." Journal of Atmospheric Sciences. Vol. 33, pp. 531-537.

-------, 1982: "On Moist Quasi-Geostrophic Baroclinic Instability." Journal of Atmospheric Sciences. Vol. 39, pp. 2028-2037.

Sanders, F., 1971: "Analytic Solutions of the Nonlinear Omega and Vorticity Equations for a Structurally Simple Model of Disturbances in the Baroclinic Westerlies." Monthly Weather Review. Vol. 99, pp. 393-407.

----------, and J. R. Gyakum, 1980: "Synoptic-Dynamic Climatology of the 'Bomb'." Monthly Weather Review. Vol. 108, pp. 1589-1606.

Stark, T. E., 1976: "Wave-CISK and Cumulus Parameterization." Journal of Atmospheric Sciences. Vol. 33, pp. 2383-2391.

Tracton, M. S., 1972: "The Role of Cumulus Convection in the Development of Extratropical Cyclones." Ph.D. thesis, M.I.T., 157 pp.